

6 - 17



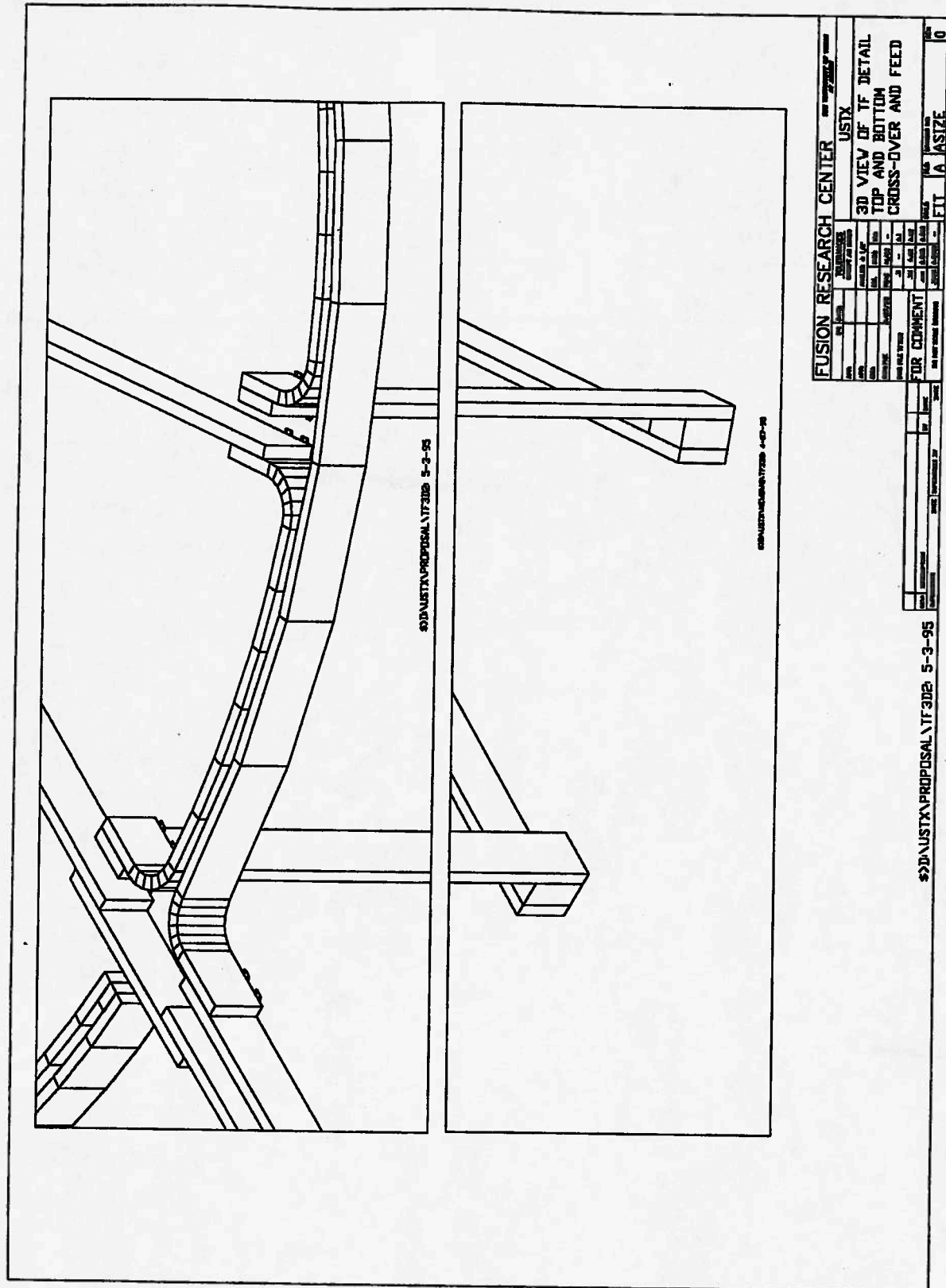


FIG. 6.10. 3-D view of top and bottom TF cross-overs and feeds.

Design work outstanding includes detailing the core and return-leg interfaces to the support structure, detailed load and thermal calculations for the bolted joint concept, and detailed thermal calculations of the temperature rise of the return legs.

OH solenoid

The design of the OH solenoid follows on from the establishment of the outer radius of the TF core assembly. The present plan is for a conventional multi-layer wound coil assembly. Alternate construction techniques, such as either a Bitter coil concept or a helically machined cylinder will be considered if the conventional winding technique appears impractical. An elevation view of the design, including insulation details, is shown in Fig. 6.11. This figure corresponds to the point design solenoid described in Table 6.3, page 6-29. Details of the solenoid ends and weldments are shown in Fig. 6.12. An installation detail of the solenoid end is shown in Fig. 6.13.

A considerable number of studies for a low aspect ratio tokamak solenoid have been made and the present state of the art is summarized in a recent review [3]. A detailed study of both the design and stress issues for solenoid magnet construction is available, this is also applicable to the present problem [4]. A detailed algorithm has been developed for this critical design for the specific USTX requirements. In general, it is desirable to minimize the number of turns in order to maximize the fraction of the available space filled with copper. The mechanical forces are initially calculated using the infinite-solenoid approximation with a multi-layer description of the winding as described in Chapter 5. This preliminary calculation of the coil resistance, temperature rise, and power-supply demand includes the winding-geometry details and a constant multiplier to the electrical resistivity to account for temperature effects. The solenoid self inductance and solenoid-plasma mutual inductance are calculated using a finite length solenoid description, modeling the individual turns with circular filaments. The plasma self inductance is calculated using the Hirshman-Neilson model [5] for the self-inductance of an elongated low inductance plasma. Then, using the time dependent simulation described in chapter 5, the expected performance of the solenoid is derived for various plasma models. Using this performance the solenoid design is then re-optimized to match both the electrical and anticipated plasma performance.

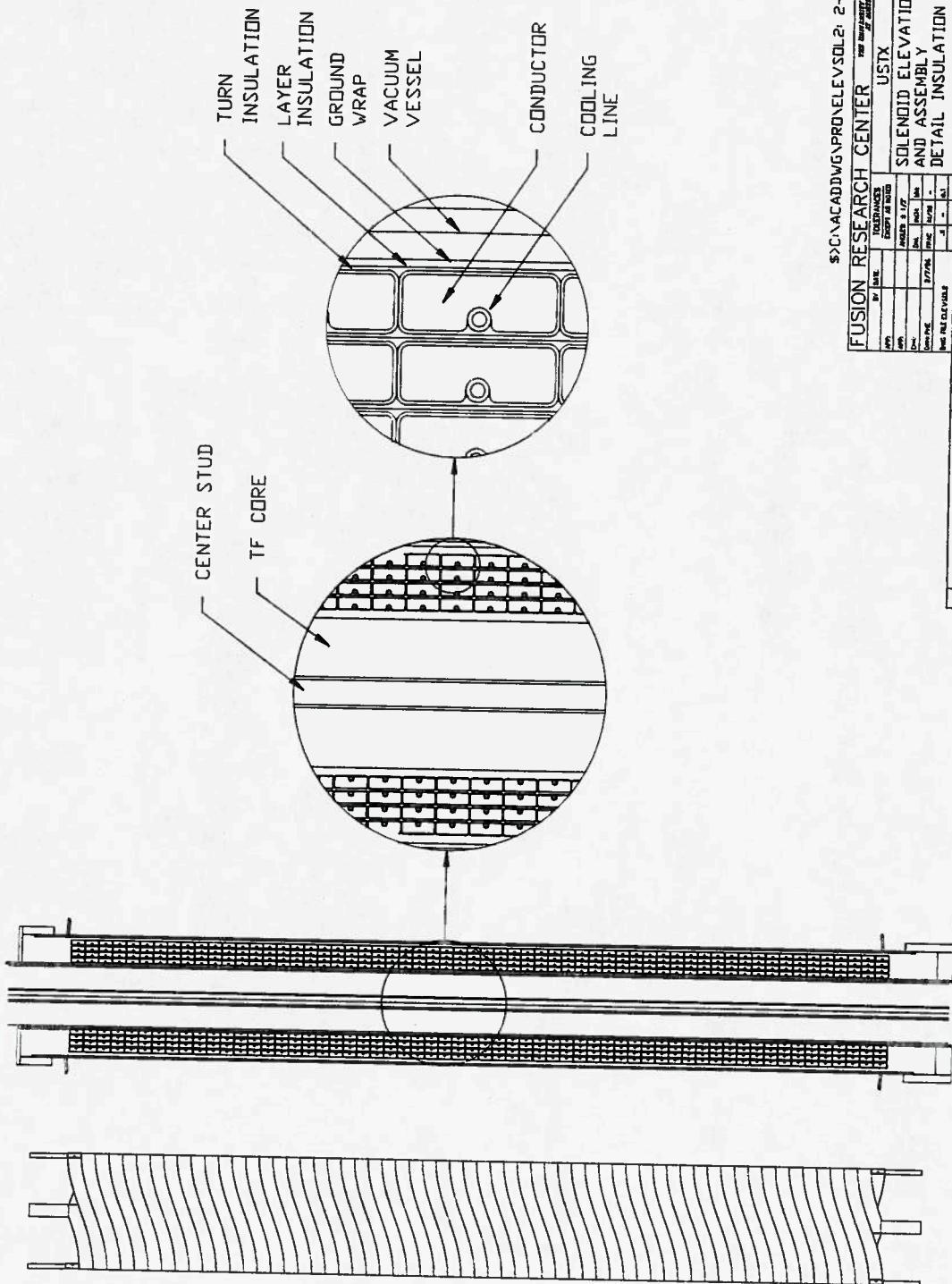
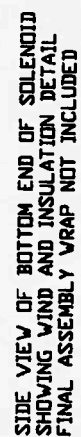
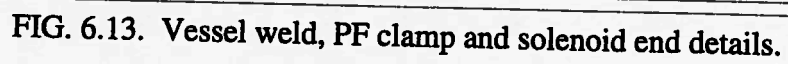


FIG. 6.11. Solenoid elevation and assembly detail.



6 - 22



The present candidate material for the solenoid is chrome copper (C-182). The reason for this choice is that there exists considerable in-house experience with the fabrication and joining of this high-strength material. In particular, chrome copper can be welded with little loss of strength, both by fusion and with chrome copper as a filler material. A major advantage of welding over alternative joining techniques, Sil-fos or equivalent braze, is that the heating can be localized with cooling blocks, and welds can be made in material within a few cm of the epoxy insulation with no damage. This permits making up cross-overs and feeds after the coil has been wound. In addition, non-destructive inspection using both radiographic and ultrasonic techniques allows 100% testing of joints. Considerable experience shows that weld defects can be ground out and repaired. Alternative materials with better strength/resistivity performance may be used in the final design, if appropriate fabrication techniques are demonstrated.

The design procedure, following material selection, is to define a temperature range and calculate the average electrical resistivity. The insulation dimensions for each coil and for each layer are chosen from consideration of both the stand-off voltage and winding technique. The inner and outer radii are constrained by applying suitable assembly and fabrication tolerances to the outer radius of the TF center leg assembly and to the inner radius of the vacuum-vessel sleeve. Another choice is the number of layers and the number of turns wound in-hand. Selection criteria are: 1) that the individual coil length is less than 30 m, required for reasonable cooling performance, and 2) that the conductor cross-section aspect ratio is favorable for winding and minimizing keystoneing.

Conductor current is another variable. Higher currents are desirable as this requires fewer turns, and less of the cross-section is lost to insulation. Large currents also reduce the inductance (fewer turns) and hence the operating voltages required for charge and discharge, and the voltages induced during fault conditions, such as disruptions. Higher currents also reduce the electrical insulation stress and increase reliability. On the other hand, large currents increase the error fields produced by the cross-overs and feeds. For this study the maximum solenoid current has been established at 60 kA in order to match available power supplies. The optimum match occurs when the P/S reaches both the voltage and current limits simultaneously with the material reaching the design stress limit.

The design procedure is then to select the number of layers. A range from two to eight has been studied, with the other constraints such as length, insulation, cooling

requirements and winding difficulty established. A serious limit to the number of layers is the increased stress concentration caused by the cooling line cut-out. As the number of layers is increased the available conductor width decreases and, for a fixed cooling line diameter, the stress concentration rapidly increases. Conversely, large radial widths will make the coil winding very difficult, particularly using the high strength copper. In general, to minimize springback, one desires that the entire cross-section is in tension at the winding radius. This requires a winding tension force of about 10 ksi, which for the design cross-section implies a tension in the winding process of order several tons. The coil needs to be wound under this linear load without, amongst other problems, damaging the Kevlar insulation. The coil winding is regarded as an R&D activity, and a prototype coil will be wound to develop the required technology. For initial development mild steel or a similar low cost material with properties comparable to chrome copper will be used.

The design algorithm is then run with an increasing number of turns, until either the stress limit, presently set at 12 ksi, (which results in a maximum stress of about 24 ksi, due to cross-section reduction, stress concentration and von Mises forces) or the temperature limit, presently set at a 75 °C temperature excursion, is exceeded. Two optimization procedures are possible. In the first, the number of turns per layer is held constant, whereupon the innermost coil establishes the stress limit. Alternatively, the number of turns per layer is separately optimized, keeping the mechanical stress at the maximum value in each layer. It was discovered that this latter optimization procedure produced small increases in performance with large increases in required input power. The design described here uses the same number of turns and conductor cross section for each layer. For the final construction it is likely that different materials will be used for the innermost layer, where the stress is highest, and the outer layers, in order to minimize the resistance. Note that the design algorithm at this stage assumes an infinite solenoid so there is no field outside a given layer from the current in that layer. The coil resistance and power supply requirements, taking into account that the coils are wound four-in-hand, are then calculated. With the coil specifications determined, the finite-solenoid self-inductance and the mutual inductance to the plasma are computed using a filament model for each turn of the solenoid.

The above results are next imported into the time dependent simulation code which predicts power supply currents and material heating for the three plasma models used to date. The results for the present point design, using as the plasma model an Ejima coefficient of 0.67, an internal inductance of 0.7 and a resistive voltage set to either the

resistive term from the Ejima coefficient or the flat top voltage of 1.5 volts, whichever is the larger, are shown in Fig. 6.14. The results obtained using a model assuming Neo-Alcator scaling produce very similar time histories. If Lackner-Gottardi scaling is assumed the flat top duration is extended to about 300 ms (Fig. 5.5). For reference the $A = 1.25$ solenoid using a plasma model based on Neo-Alcator scaling with q defined as $q\psi$ and for a 0.5 MA demand produces the time history shown in Fig. 6.15 with a flat top duration in excess of 400 ms. For the lumped circuit plasma model, with $l_i = 0.3$, and a flat top voltage of 1.5 V, the flat top duration is about 40 ms.

The results of this optimization for the two point-design cases, $A = 1.43$ and $A = 1.25$, are given in the accompanying worksheets, Tables 6.3 and 6.4, it should be noticed that the volt second results are shown for the full double current swing.

Active cooling between shots is required to control the maximum temperature of the coil and will be accomplished with a closed-loop heat exchanger. For full-performance operation the cooling water will be cooled below ambient using a chilled-water supply. The local dew point will be maintained below the condensation temperature. The cooling circuit for the individual turns will be connected in parallel and flow through each circuit will be monitored. A flow rate of one gallon per minute is adequate to lower coil temperature between shots and gives a reasonable pressure drop of less than 100 psig. Differential expansion of adjacent layers during the cool down cycle may pose a problem and flow rates through each layer may need to be individually controlled. The water flow is turbulent, and the interface heat transfer coefficient is of the order of 1 W/cm^2 .

The primary loads on the solenoid are the self loads, additional forces are caused by the alternating vertical current components in each layer and in the vertical and radial current feeds. The primary self load is the "hoop" stress, in addition a vertical compression force is produced by the radial self field components due to the solenoid finite length. A secondary effect of the finite length is that the outermost winding is in a reversed poloidal field, and experiences a net inward force, the entire solenoid is in compression. In the stress analyses that have been carried out no credit has been taken for the sharing of forces between adjacent conductors. A calculation of the magnetic fields produced by both the solenoid and the PF windings has been used to calculate the maximum conductor force, this is experienced by the mid-plane innermost turn. An FEA calculation has then been carried out, using the von Mises criterion, and indicates a stress multiplication of about a factor two over the infinite solenoid hoop stress.

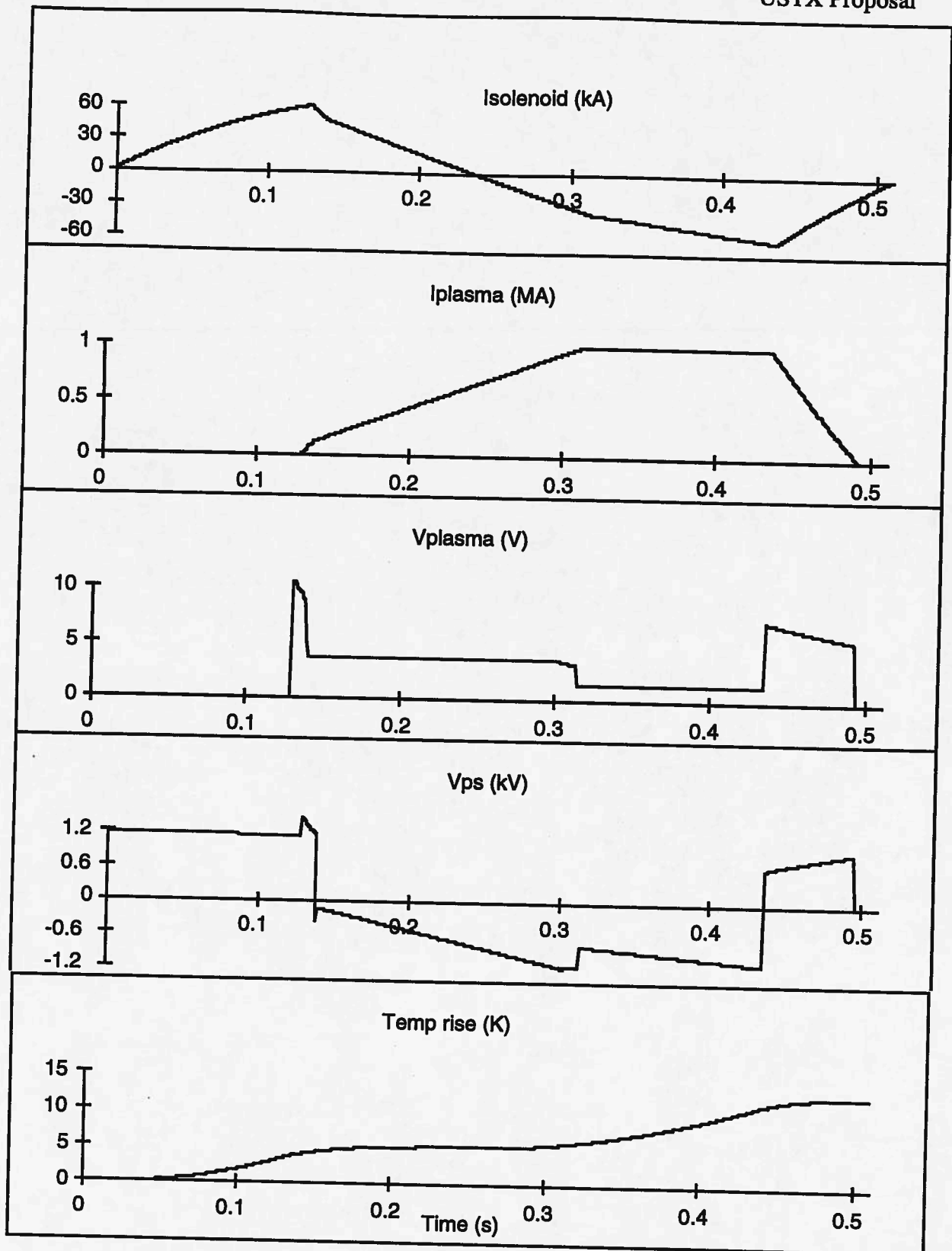


Fig. 6.14 Simulation time history for a 1 MA plasma with an $A = 1.43$ solenoid and a lumped model of the plasma with $l_i = 0.7$ and $\bar{V}(\text{flat top}) = 1.5$ V.

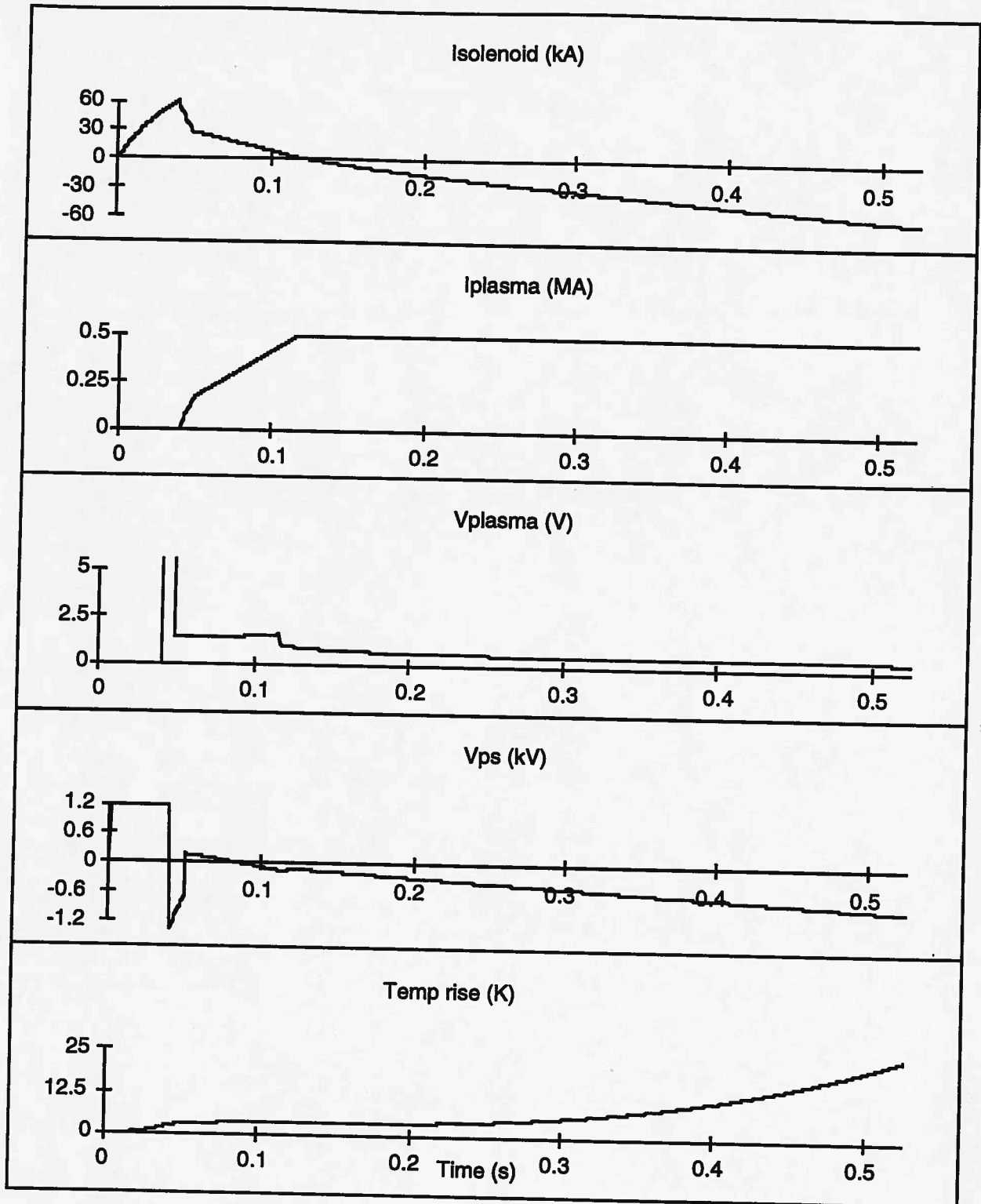


Fig. 6.15 Simulation time history for a 0.5 MA plasma with an $A = 1.25$ solenoid and a Neo-Alcator model for the plasma, with q defined as q_Ψ .

Table 6.3. Excel spreadsheet procedure for core optimization, $A = 1.43$.

Tf Core/Solenoid Parameters			$R_0 = 0.70 \text{ m}$, $A = 1.43$, $I_l = 0.7$, 60 kA			
Input Data			Constants			
B_T	0.5	T	CuDens	8.96	g/cm^3	
R_0	0.7	m	CuThCap	400	J/kg/K	
a_p	0.49	m	CuRes	2	$\mu\Omega\text{-cm}$	
L	2.6	m	CrRes	2	$\mu\Omega\text{-cm}$	
Elongation	1.7					
I_{sol}	60	kA	Plasma-Sol	0.03	m	
I_{ps}	60	kA	Vol	5.64	m^3	
A	1.43		R_{sout}	0.18	m	
Calculate TF out						
B_{TFmax}	0.5	T	I_{TF}	160	kA	
R_{TFmax}	0.70	m	TF_{area}	15.10^{-4}	m^2	
R_{tfout}	0.085	m	ΔT_{TF}	76	$^{\circ}\text{C}$	
R_{tfin}	0.015	m	Curr Dens	9.6	kA/cm^2	
Tf Sol Sep	0.01	m	I^2_t	1.5	sec	
Packing Factor	0.8					
Calculate Solenoid						
# Layers	4		Nlayer	1	2	3
SepLayer	0.002	m	n(m-1)	23.08	23.08	23.08
SepTurn	0.001	m	h(m)	0.043	0.043	0.043
AreaCool	0.0625	in^2	B(j)	1.740	1.740	1.740
AreaCool	$4 \cdot 10^{-5}$	m^2	Flux(j)	0.071	0.097	0.126
			Full area S(j)	7.82	6.92	5.31
R_{sin}	0.105	m	Area(j)	$5.7\text{E-}4$	$5.7\text{E-}4$	$5.7\text{E-}4$
Turn Width	.0188	m	rmid(j)	0.114	0.133	0.152
			Rin(j)	0.105	0.124	0.143
Volt-s ($\pm 60 \text{ kA}$)	0.906	Vs	Curr Dens	10.54	10.54	10.54
# Turns	240		N(j)	60	60	60
B_{max}	7.0	T	S(j)	11.17	9.87	7.58
L_s (Inf&approx)	1.81	mH				
L_p (Hirshman)	0.463	μH	Self inductance and Plasma Current			
M_{sp}	7.90	μH	li	0.7	I_p	1.0
L_{sol}	1.53	mH	Ejima Factor	0.67	$\tau_{\text{Flat top}}$	0.125
			Vloop	1.5	V	
Winding Details, four in hand						
			Layer #	1	2	3
Total Resistance	7.92	$\text{m}\Omega$	Turns/layer	15	15	15
Ohmic Voltage	0.48	kV	Length/layer	11.09	112.81	14.55
Ohmic Power	28.5	MW	Resistance/layer	0.39	0.45	0.51
			T rise	14.5	14.5	14.5
						$^{\circ}\text{C}$

Table 6.4. Excel spreadsheet procedure for core optimization, $A = 1.25$.

TF Core/Solenoid Parameters: $R_0 = 0.70$ m, $A = 1.25$, $I_i = 0.3$, 60 kA									
Input Data					Constants				
B_T	0.5	T			CuDens	8.96	g/cm ³		
R_0	0.75	m			CuThCap	400	J/kg/K		
a_p	0.60	m			CuRes	2	$\mu\Omega$ -cm		
L	2.60	m			CrRes	2	$\mu\Omega$ -cm		
Elongation	2								
I_{sol}	60	kA			Plasma-Sol	0.025	m		
I_{ps}	60	kA			Volume	10.66	m ³		
A	1.25				R_{sout}	0.125	m		
Calculate TF out									
B_{OTFmax}	0.5	T	I_{TF}	150	kA				
R_{OTFmax}	0.75	m	TF_{area}	1510^{-4}	m ²				
R_{tfout}	0.085	m	Curr Dens	10.2	kA/cm ²				
R_{tfin}	0.015	m	ΔT_{TF}	76	°C				
Tf Sol Sep	0.01	m	I^2_t	1.3	sec				
Packing Factor	0.8								
Calculate Solenoid									
# Layers	2		Nlayer	1	2				
SepLayer	0.002	m	$n(m-1)$	30.77	30.77				
SepTurn	0.001	m	$h(m)$	0.033	0.033				
AreaCool	0.0625	in ²	$B(j)$	2.320	2.320	T			
AreaCool	4.10^{-5}	m ²	Flux(j)	0.076	0.100	Vs			
			Full area S(j)	7.87	4.55	ksi			
R_{sin}	0.095	m	Area(j)	$2.95e-4$	$2.95e-4$	m ²			
Turn Width	0.0150	m	$r_{mid}(j)$	0.103	0.118	m			
			$R_{in}(j)$	0.095	0.110	m			
Volt-s (± 60 kA)	0.354	Vs	Curr Dens	20.33	20.33	kA/m ²			
# Turns	160		$N(j)$	80	80	Turns/layer			
B_{max}	5.41	T	$S(j)$	12.99	7.52	ksi			
L_s (Inf&approx)	0.47	mH	Self inductance and Plasma Current						
L_p (Hirshman)	0.215	μ H	l_i	0.3					
M_{sp}	2.56	μ H	Ejima Factor	0.67					
L_{sol}	0.411	mH	$\tau_{flat top}$	40	ms				
V_{loop}	1.5	V	I_p	0.5	MA				
Winding Details, four in hand									
Total Resistance	7.63	m Ω	Layer #	1	2				
Ohmic Voltage	0.46	kV	Turns/layer	20	20				
Ohmic Power	27.5	MW	Length/layer	13.1	15.0				
Temp Rise	53.8	°C	Resistance/layer	.89	1.02	m Ω			

Poloidal field coils

The PF coil design concept is for a fairly complete poloidal coverage by the coils for maximum flexibility. Diagnostic access requirements are then the main consideration for coil location. The PF coil set is required to:

- a) cancel the error fields from the fully charged solenoid in order to allow breakdown with a minimum loop voltage.
- b) supply the necessary shaping fields and return correction fields over the full solenoid current swing to allow the planned limited and diverted plasma configurations.
- c) supply the necessary time-varying fields for plasma position control during the various phases of the discharge and for the various planned operating scenarios.

The location of the PF coils is shown in the elevation view, Fig. 6.5. An isometric view of the vacuum vessel and PF coils is shown in Fig. 6.16. The PF coil parameters are shown in Table 6.5 with preliminary P/S and winding assignments. The coil design is for uncooled rectangular windings; the design allows the assembled coils to be located on the support structure (exoskeleton). The specification is for less than 3°C temperature rise per shot with the total cool down time estimated at less than 1 hour (from the TEXT experiment, where coils of a similar design are in use), allowing a shot repetition rate of 5 minutes between shots. If required, the coils in series with the solenoid will be fitted with cooling lines.

Table 6.5. PF coil locations and dimensions.

Coil	R (m)	Z (m)	ΔR (cm)	ΔZ (cm)	Turns	I (kA)	P/S Allocation
PF1-A	0.25	± 1.550	2.5	9	2	60	Solenoid
PF1-B	0.25	± 1.480	5.0	6	8	0.5	HF
PF2	0.53	± 1.475	7.5	13	10	5	VF1
PF3	1.02	± 1.365	7.5	13	16	10	OH
PF4	1.60	± 1.20	10	10	2	60	Solenoid
PF5	1.77	± 0.55	20	10	16	25	VF2 & Div P/S

See Table 6.9 for P/S assignment details.

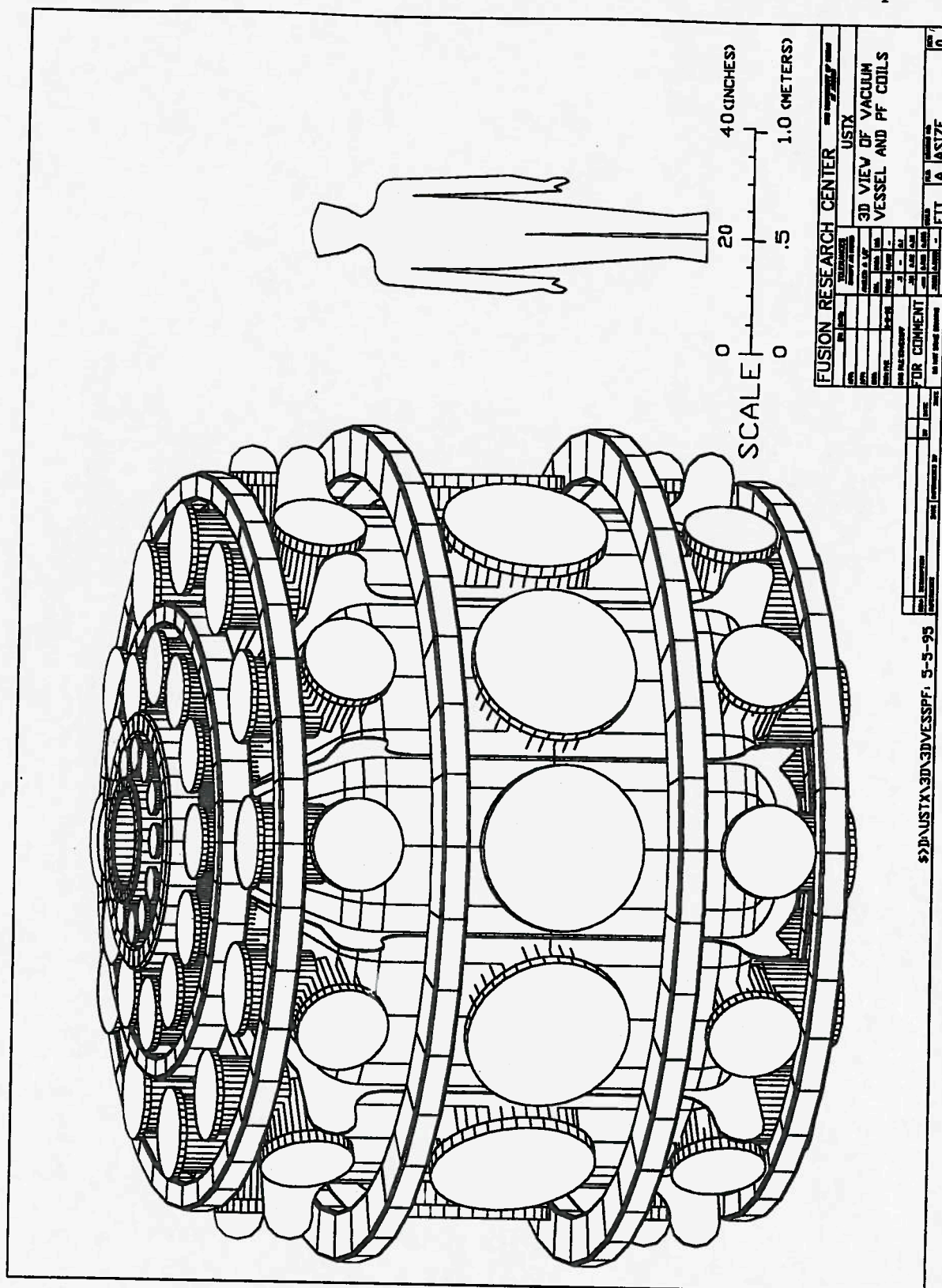


FIG. 6.16. 3-D view of vacuum vessel and poloidal-field coils.

The coils will be wound from half-hard rectangular-cross-section copper bar (OFHC). The coils may include taps in order to increase the flexibility of the coil set for different plasma configurations. Insulation will be fiber-glass epoxy (if necessary Kevlar will be used to minimize damage during the winding process). The coils will be wound and potted in precision mandrels in order to meet dimensional requirements. Coil feeds will be radial and located in the shadow of the exoskeleton components. The coils will be mounted to the exoskeleton with silicon-rubber isolator mounts.

The individual PF coil power-supply requirements have been estimated by running EFIT equilibria for a number of solenoid and plasma currents. These equilibria have then been taken at regular time intervals using the results of the time dependent simulation. Plasma ramp rates are preset at 5 MA/s and plasma and solenoid performance is for the point design. With these results, and calculating current change rates by differentiating forward, the inductive voltages can be included in the P/S demand calculation. The coil set and preliminary PF P/S assignments have been generated using this procedure. The results are shown in Table 6.6.

Table 6.6. Currents (kA) in the PF coils for different times (ms) during the flux swing for the coil set described in Table 6.5.

Time (ms)	0	32	82	184	306
Solenoid	60	36	-12	-37	-60
PF2	0	0	0	0	-13
PF3	0	-43	-57	-66	-84
PF5	-27	-115	-215	-259	-242
I_p	0	250	500	1000	1000

Performance applies to point design parameters described in OH section

6.3 Vacuum vessel and plasma-facing components

The vacuum vessel is an all-welded structure made from thin-walled 316 stainless steel. The major radius is selected to include space outside the plasma for limiters, diagnostics, passive stabilizers, and RF antennas. The height is selected to include space for diagnostics and possible divertor concepts.

The upper and lower caps are made from commercially available domed parts. The cylindrical wall will be supplied by the same manufacturer to match the upper and lower caps. The vessel structure will be reinforced by poloidal, and if necessary, toroidal ribs to provide adequate strength for both dead and live loads. The inner sleeve assembly is designed to be replaceable by a simple grind and weld operation. Details of the joint assembly are shown in Fig. 6.13. This figure also shows preliminary details of the PF coil clamps, the vacuum-vessel ribs and the solenoid feeds. The limiter tiles will be constructed from bare graphite containing resistance heaters and will be attached to water-cooled vertical rails welded to the inner sleeve. Views of the design are shown in Fig. 6.17. This figure also shows a cross section at the machine midplane with details of the TF core. The design must account for the reduction in toroidal resistance of the inner sleeve caused by the tile and rail assembly. An order of magnitude scaling from the C-Mod results for disruption forces [6] indicates that the design is within elastic limits for the membrane forces on the inner sleeve caused by the non-axisymmetric halo-current prediction. Out-of-plane forces caused by non-symmetric loads such as the neutral-beam vacuum load are potentially serious and will be investigated during the detailed design phase of the project.

Vacuum vessel

The inner cylinder and top and bottom sections of the vacuum vessel are constructed of 1/4" thick 316 series stainless steel. The outer cylinder may be constructed from a thicker material. The top and bottom sections are manufactured from standard ASME flanged and dished steel tank heads. Both the dished heads and the outer wall are reinforced with ribs. The upper and lower rib extremities are used for the support links and hydraulic cylinders. The ribs are constructed from 1/4" steel with welded caps 1/4" by 2" in the present design, located in the shadow of the TF coils. A finite-element stress analysis (FEA) of the vacuum vessel has been completed [7]. The vessel is provided with numerous access ports for diagnostics. The mid-plane radial flange is a 75 cm diameter standard size Helicoflex flange. A single 40 cm aperture tangential port and nozzle is included for the NBI system. The remaining flanges are standard ConFlat sizes. We will consider building a prototype corner port structure for testing and bracing as required. This is to complement the multiple-mesh FEA necessary to analyze stress concentrations at the corner weldments. A 3-D isometric view of the vessel is shown in Fig. 6.18. An exploded view of the vessel parts is shown in Fig. 6.19.

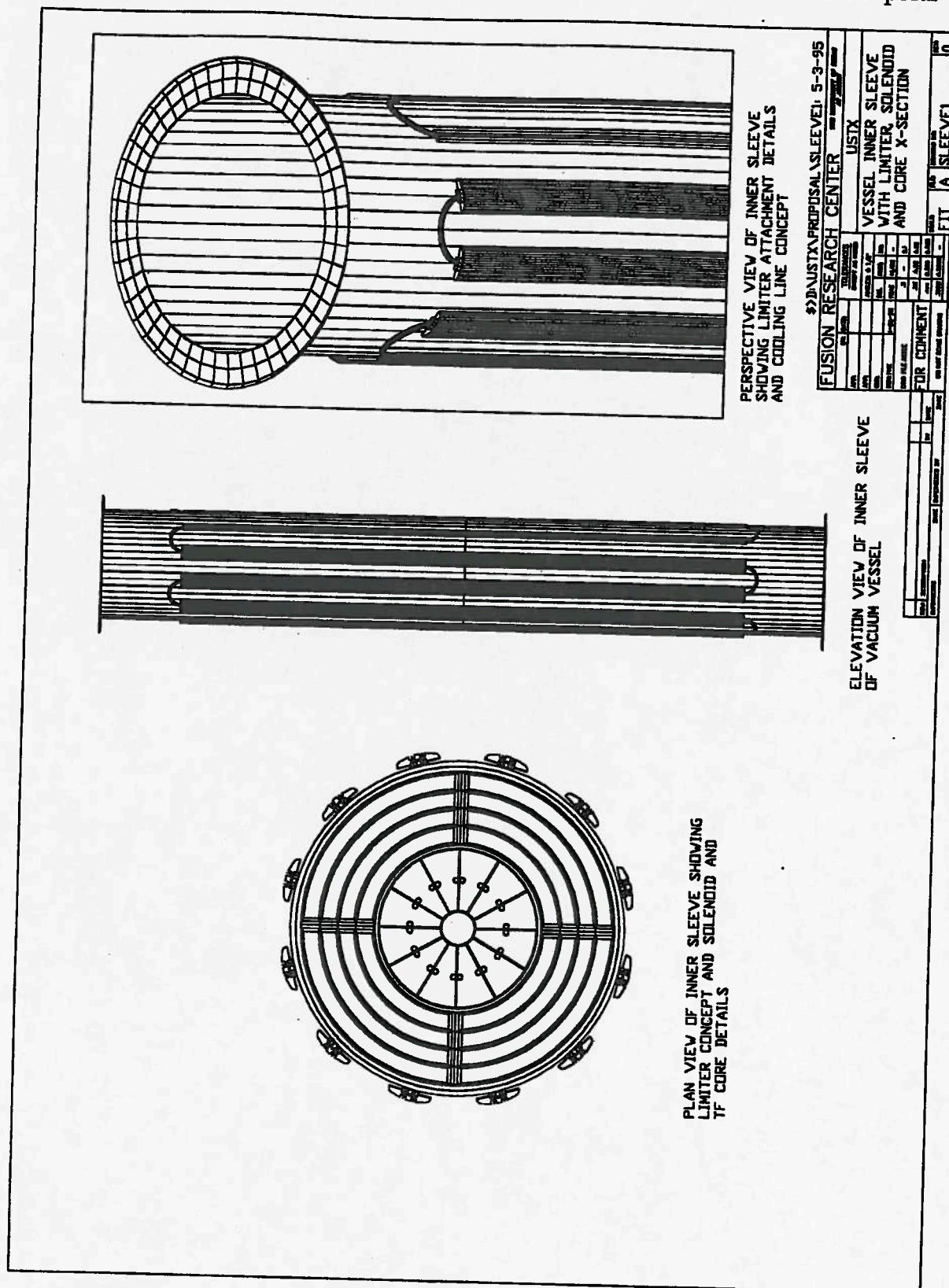
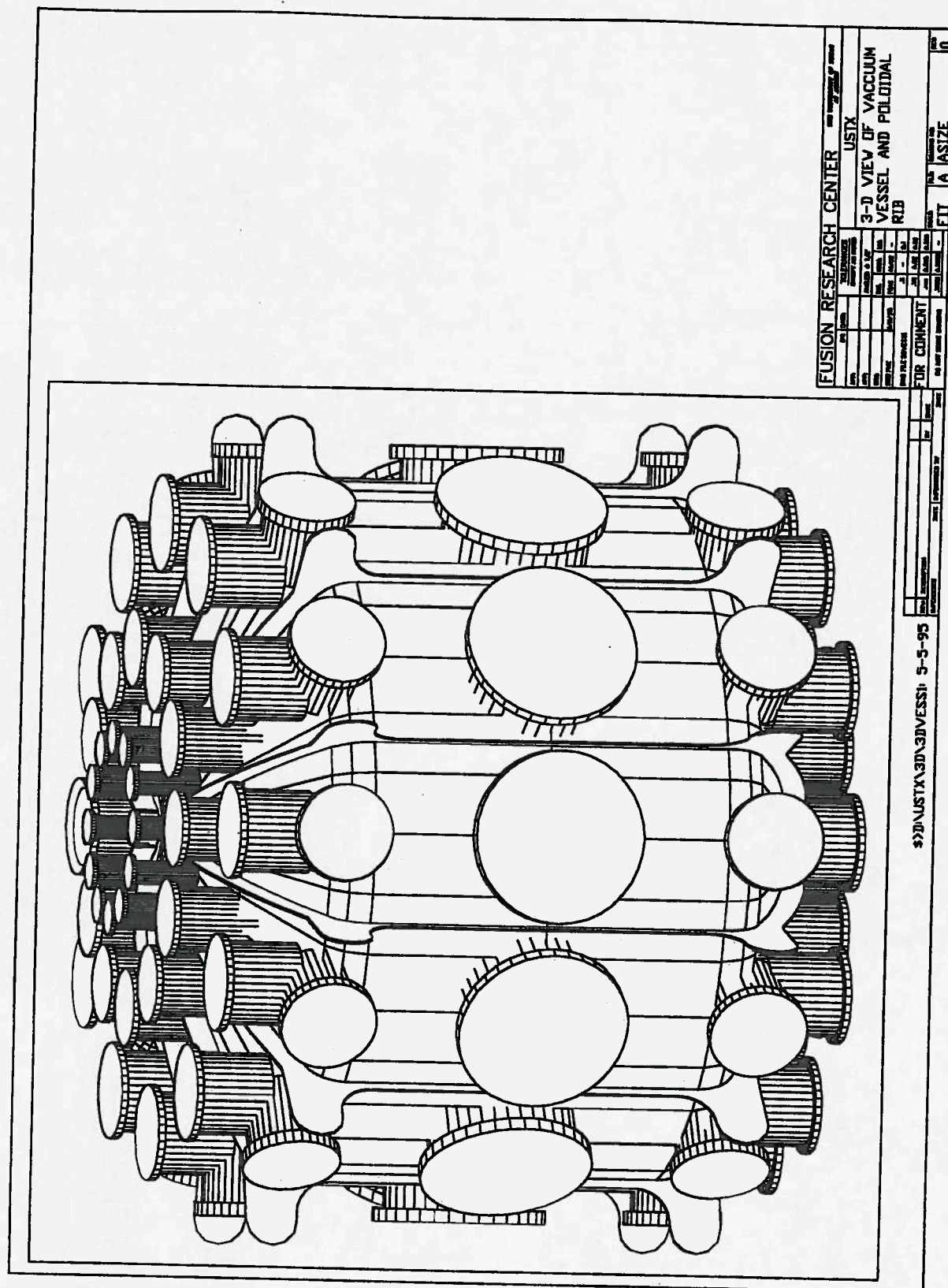


FIG. 6.17. Vessel inner sleeve assembly and conceptual inner limiter design.



6 - 36

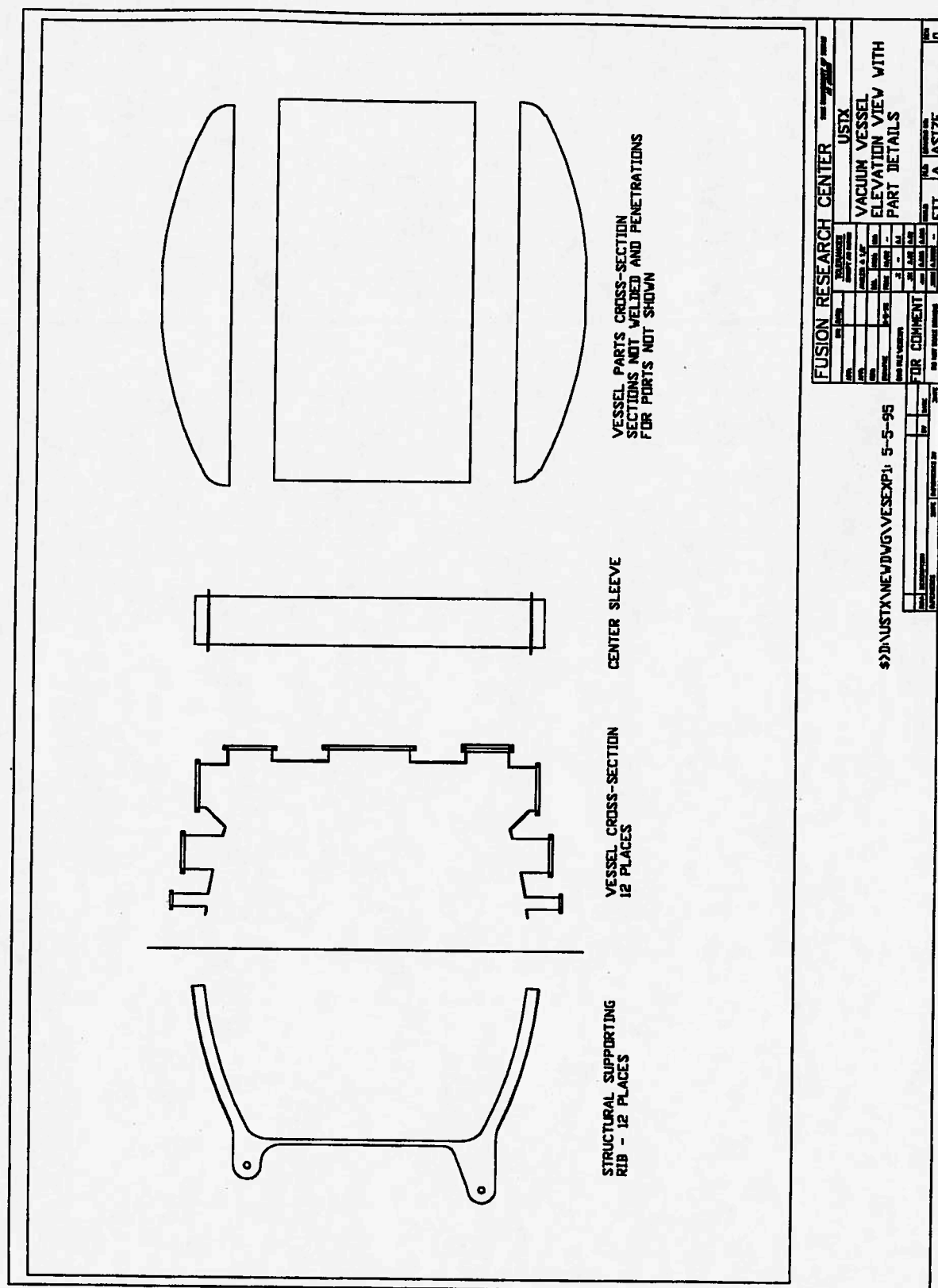


FIG. 6.19. Vacuum vessel elevation view with part details.

Welded to the inner-diameter wall are limiter-tile support rails. They are approximately 1 cm^2 in cross section and are located in groups of two immediately under each TF coil (see Fig 6.17). Between the support rails is a $1/4$ " cooling line. The cooling lines for each of the twelve sections are in series. With a water supply pressure of 100 psi there is adequate water flow (1 gpm) to remove the tile heat load estimated at 0.75 kW. The deposited power calculation is detailed in the worksheet, Table 6.7. The cooling lines will also be available for temperature control during bakeout, using cooling or high temperature gas.

The present design is to support the vessel from a set of twelve swinging links connected between ears attached to the vessel ribs and to structural plates attached to the exoskeleton assembly. These links are located and sized such that for uniform temperature changes, the vessel midplane remains at a constant elevation. The structure is shown in the elevation view, Fig. 6.5. The design only allows freedom of movement for expansion and will hold the vessel concentric with the TF and solenoid assembly. A set of hydraulic cylinders will interconnect matching support ears on the upper half of the vessel. These cylinders will be hydraulically controlled to lock solid during a plasma shot but allow free radial expansion at all other times. The purpose is to supply additional support for protection against disruption and fault loads. The inner sleeve extends past the top and bottom vessel caps. These extensions will be used to provide the base for the solenoid support structure. This support structure will be detailed during the design phase.

Plasma facing components

The inner-cylinder limiter tiles will be constructed from bare graphite. The present concept is to heat the vacuum vessel to about 180°C and to add SS co-axial resistive heating elements to the graphite tile arrays and other plasma facing components for bakeout to about 400°C . These tiles are mounted and cooled as described in the previous subsection, and a preliminary design is shown in Fig. 6.17. A worksheet estimating the tile performance and cooling is given in Table 6.7. For extremely small beam-tangency radii, the inner-cylinder tiles also may intercept a portion of the neutral-beam shine-through. Additional heat loads may be expected from fault conditions, in particular disruption and VDE events.

Table 6.7. Limiter tile heat loading.

Operating conditions: Plasma current 1 MA, loop voltage 1.5 V, shot length 0.3 s
Heat input: $Q_{in} = 10^6 \times 1.5 \times 0.3 = 450 \text{ kJ}$
Of this input power, half is assumed to be radiated and half is assumed to be absorbed by the inner graphite tiles (225 kJ). No benefit is taken for heat transferred vertically by the plasma plume. Toroidal asymmetries are not considered.
The plasma strike area, A_s , is estimated as being in a band 20 cm in height around the center wall of the vacuum chamber.
$A_s = 2\pi r l = 2.4 \times 10^3 \text{ cm}^2$
Assuming the heat profile extends 2 mm deep into the graphite, then
Target volume $= 2.4 \times 10^3 \times 0.2 = 5 \times 10^2 \text{ cm}^3$
Specific heat of graphite $1.8 \text{ J/cm}^3/\text{°C}$
and the temperature rise $T_r = 225 \times 10^3 / (5 \times 10^2 \times 1.8) = 250 \text{ °C}$
(This is more than a factor 4 below the sublimation temperature for graphite)
The water cooling requirement for the 300 second interval between shots is only:
$225 \text{ kJ}/300 \text{ s} = 750 \text{ W}$

The top and bottom of the vacuum vessel will also be provided with graphite tile armor. At present the design is for a set of rail limiters at several toroidal locations. The design will also include the capability to install fairly complete top and bottom coverage to provide protection for the plasma plume and divertor strike area. A possible divertor design would include a divertor baffle at the lower x-point, with the exhaust plenum pumped with titanium or chromium getter balls and the divertor-baffle floor covered with graphite tiles. This design is described in more detail in Chapter 9.

Graphite armor will also be installed on the outer vessel and port walls, where necessary, to protect against neutral-beam shine-through. The present design includes the provision for steering the direction of the NBI system Fig. 6.3, and the outer wall armor will be modified for the different injection tangency radii.

6.4 Support structure

The different elements of the USTX assembly will be interconnected and supported by a stainless steel exoskeleton. The conceptual design is shown in the elevation cross-section shown in Fig. 6.5 and in the plan view, Fig. 6.3. A general view of the complete assembly is shown in the isometric view, Fig. 6.6. The exoskeleton will

primarily be constructed from welded four-inch square-cross-section tube. The primary structure will consist of two wheel-shaped assemblies with the radial spokes or arms directly above the TF coils and the toroidal struts located above the PF coils. The two wheel assemblies will be separated by a cylinder of vertical struts, also in the planes of the TF coils with toroidal struts at the elevations of the PF coils. A 1-1/4" schedule-80 Inconel pipe is inserted through the center of the TF core assembly. This tie-rod will connect the top and bottom exoskeleton assemblies together and will be pre-stressed to about 10,000 lb. (about 25% of yield). The top and bottom wheel-shaped assemblies will be slightly dished outward to absorb this pre-stress. Coolant will be circulated through the rod in order to minimize rod heating during tokamak operation. The final assembly has the shape of a wire-mesh drum.

The present design does not include an electrical toroidal break. The assumption is that the mutual inductance between the structure and the solenoid and plasma is small, and the induced currents will not produce significant error fields. An eddy current model for the exoskeleton will be included in the plasma discharge models to verify this assumption. If required, the design will be modified to include an insulating break at two toroidal locations. Two poloidal breaks will be included; these will be in the vertical cylinder section, located at the elevation of the PF5 coil sets.

The PF coils will be supported from the exoskeleton by a lattice of radial and toroidal structures. The design is at present preliminary as the exact location of the windings depends on further modeling of plasma shape and stability.

The present design includes a matching set of radial arms inboard of the drum head, and the TF coils will be supported between these elements. This set of inboard radial arms is diagonally braced against the vertical members to supply rigidity against vertical loads and the pre-stress force from the center stud tie. These diagonal braces will also react the out-of-plane loads on the PF coils. The bottom end of the TF core will be rigidly attached to the center of the structure. The upper end will be mounted with a set of compliant interconnects to permit vertical and radial expansion.

An inner web structure will provide out-of-plane stiffness and hard points for the vacuum-vessel support links and hydraulics. Toroidal links tangential to the vessel will be connected between the outer drum cylinder and the vessel hard points to prevent vessel rotation and reduce out-of-plane loading on the swinging-link vessel supports.

6.5 Construction and assembly plan

This section describes preliminary outlines of the construction procedures for the machine components and for the base, $A = 1.43$, machine assembly, and of the procedure for the later installation of the $A = 1.25$ modification.

Solenoid construction

The solenoid assembly consists of four nesting single-layer coils, each coil wound four-in-hand. The four layers of the solenoid will be sequentially wound. The conductor will be supplied wound on drums, with the cooling-line cutout included in the cross section used for the drawing die. The cross section may be trapezoidal to compensate for the keystoneing caused during winding.

The only technically difficult activity associated with this project is the fabrication of the TF core and solenoid. The initial project activity will concentrate on the development of a reliable winding technique and construction of a prototype TF core-solenoid assembly. A winding line will be built, relying heavily on the techniques successfully demonstrated during the winding of the STX prototype solenoid [8].

Prior to winding, the conductors will be straightened and the cooling lines soft-soldered into the cooling channel. The first layer will be wound on a 5 mm thick G-10 cylinder, itself mounted on a precision mandrel, designed for removal on completion of fabrication. The coils will be dry-wrapped with a 1-mm thickness of Kevlar insulating tape (two layers 0.01" thick with 50% overlap and reverse-wound) before winding. Kevlar tape will be used to prevent insulation damage during the winding cycle. After winding, the ends and cooling lines will be dressed and a 1-mm thick Kevlar ground wrap (four layers of 0.01" tape) applied to the layer. The coil will then be fixtured in a mold for vacuum/pressure casting and curing, with the G-10 cylinder and the mold defining the inner and outer radius and end support locations. Following epoxy vacuum/pressure fill and high-temperature cure, the layer assembly will be 100% inspected for dimensional and electrical quality. The second layer will then be wound over the first, and the cure and inspection procedures repeated. This cycle will be repeated for each of the four (or two, for the $A = 1.25$ design) layers.

After fabrication the cross-over and feed-stub connections will be welded. Welds will be 100% ultrasonically inspected and repaired as required. A number of completed

welds will be X-ray tested. If faults are found in the X-ray tests, then 100% of the welds will be X-ray tested. Electrical tests will be carried out at this phase of construction.

After inspection the end supports will be mated to the solenoid and G-10 cylinder, and a complete test and dimensional cycle completed.

PF coil construction

The coils will be wound from half-hard rectangular cross-section OFHC copper. Insulation will be fiberglass epoxy. The coils will be wound and potted in precision mandrels in order to meet dimensional requirements. Coil feeds will be radial and located in the shadow of the exoskeleton members. The coils will be mounted to the exoskeleton using silicon rubber isolation to allow for differential movement.

TF core construction

The TF core will be constructed from half-hard OFHC copper. The individual turn segments, including the heel-plate mating surface and threaded holes for the Helicoil inserts, etc., will be machined from plate. A longitudinal slot will be cut for eddy current reduction. The cooling lines will be soft-soldered into the turns, and the 0.5mm G-10 sheets installed in the longitudinal slots. The turns will then be dry wrapped in fiberglass tape. The core will be assembled around the central tie-rod and G-10 dividers installed. The fiber-glass tape will be cut away at the location of the TF radial-leg heel-plate installation, and the machined surfaces coated with release agent. The cylindrical assembly will then be wrapped with glass fiber tape. The end-wrap bands will then be applied; these may be wrapped from roving (fiberglass fabric) and pre-tensioned. The assembly will be installed in a potting mold and epoxy-filled. The fundamental clearance requirement is that the solenoid must be installable over the TF core.

TF return winding fabrication

The TF return conductors will be made from rectangular cross-section OFHC, 3.5 cm (1-1/2") by 15.3 cm (6"). The conductors will be sandwiched between radial and vertical legs of the exoskeleton, and all forces will be reacted to this structure. In general, the only insulation will be insulating epoxy paints. All joints will be overlap bolt jointed. Two sets of parallel slots, one at each end, will be machined into the upper and lower radial legs to supply the compliance required by the 7 mm thermal expansion of the

center column. Teflon bearing pads attached to the exoskeleton will absorb radial and torque loads while permitting movement in the vertical plane.

Vacuum vessel fabrication

The vacuum vessel will be built from thin stainless steel 316 or an equivalent material. The end caps are commercially available domed parts and will be delivered with the outer cylinder, as a single component, with the diagnostic port nipples installed. End-cap wall thickness will be 0.635 mm (1/4"). The outer cylinder wall thickness is to be determined. The reinforcing ribs will be welded with intermittent strength welds to minimize distortion. All welds will be inert-gas shielded. The appropriate tooling and jiggling will be used to locate all flange surfaces to specifications. Stress annealing (such as vibrational stress relieving VSR) should be considered prior to machining.

Support structure fabrication

The exoskeleton will primarily be built from rectangular SS-316 box section. The upper and lower radial elements will be shadowed by the TF coils. The radial arms will be connected by toroidal bars shadowed by the PF coils. Fundamental structure will be welded; a design point will be to make sections flat where practical so they can be laid out and welded accurately. Vertical and radial struts will support the PF coils. Alignment dowels and bolts will be used at assembly where required. The structure supplies all the dimensional control, and considerable precision (≈ 1 mm (0.040")) will be required.

Assembly

This section briefly describes the conceptual plan for the device assembly and for the installation of the $A = 1.25$ inner sleeve and solenoid modification. Details will be developed during the detail design phases of the project.

Initial assembly

A feature of the design is that, as much as practical, all fabrication is in parallel, and assembly is essentially on site. A preliminary assembly procedure outline is as follows:

- a) The site will be cleared of the TEXT tokamak and all electrical and other utilities. The machine-center floor location will be surveyed, and twelve SS support pads grouted to the floor and shimmed to provide a level base for the tokamak assembly. Reference marks for sightings will be placed on the surrounding walls and accurately surveyed.
- b) The lower PF (PF1L - PF4L) coils will be installed on the lower spool piece. This subassembly includes the TF-coil radial legs.
- c) The lower spool piece will be placed on the support pads, and the exoskeleton side panels installed. The vertical TF coil legs are a part of this subassembly.
- d) The vacuum vessel will be installed and attached to the lower spool piece and radial panels.
- e) The outer PF coils (PF5L and PF5U) will be installed on the radial panels.
- f) The central column structure will be assembled. This assembly consists of the TF core and the solenoid. A support spreader will be temporarily attached to the bottom of the center tie-rod to transfer the core and solenoid loads to the lifting device. The lifting device will be attached to the upper end of the center tie-rod.
- g) The center assembly will be installed inside the vacuum vessel and attached to the support and centering structures.
- h) The joint between the lower TF core and the lower radial leg will be made up.
- i) The upper PF (PF1U to 4U) coils will be attached to the upper spool piece, and the upper spool piece attached to the radial panels. The upper radial TF legs are a part of this sub-assembly and will be made up to the core assembly at this stage.
- j) The fundamental assembly will then be complete, and electrical and other utilities will be connected.

Procedure for conversion to 1.25 aspect ratio

- a) Disconnect utilities and all upper-half electrical, as required.
- b) Disconnect diagnostics, as required, to permit disassembly and grind and weld operations.
- c) Remove upper spool piece with PF coils and TF radial legs.
- d) Disconnect lower TF heel assembly from TF core and spread lower radial TF legs.
- e) Remove inner core and solenoid assembly.
- f) Remove internal components from vacuum vessel, as required.
- g) Grind out vessel sleeve weldment, top and bottom, and remove sleeve.
- h) Grind and clean up weldments in vacuum vessel caps.

- i) Install low-aspect-ratio sleeve assembly and weld new insert ring.
- j) Disassemble central structure and install the new solenoid over the TF core.
- k) Complete re-assembly.

6.6 Vessel pumping and bakeout

Vacuum pumping

The vacuum pumping system presently installed on TEXT will be used for USTX. It consists of two 1500 l/s turbo-pumps connected to a conventional oil roughing and backing system. The vessel is 2.6 m high and 3.05 m in diameter. The vessel surface area is approximately 40 m². The diagnostic port extensions add to this, making the total surface area approximately 50 m². The outgassing rate of clean, but unbaked, stainless steel is 10⁻¹⁰ Torr l·s⁻¹·m⁻² [9]. Using two 1500 l/s turbo-molecular pumping systems located diametrically opposite each other, together with their extension plenum, a total useful pumping speed of 1500 l/s is produced. The expected impurity base vacuum will be of order 3×10⁻⁸ Torr.

Vessel bake-out system

The target bakeout temperature for the vacuum vessel is 180°C. Bakeout will be through a mix of inductive heating from the PF and solenoid coil sets, and by direct electric heating using heating tapes and pads. As much of the vessel as is practical will be thermally insulated. The differential temperatures will be fine tuned using the cooling lines installed on the inner vessel sleeve and by varying the mix of heating sources.

Table 6.8. Vessel bakeout worksheet

Assume 80% of the vessel exterior surface is covered with a 1" thick layer of fiberglass insulation. "R" factor = 10 W/m²/°C
 Vessel dimensions are: height = 2.6 m, diameter = 3.1 m, with a 30% addition for diagnostic ports and extensions. Surface area is ~ 50 m².
 Power required to increase the wall temperature to 180°C ($\Delta T = 150^\circ\text{C}$)

$$P = 150 \times 10 \times 50 = 75 \text{ kW}$$

An estimate of the required power suggests that 75 kW would heat the vessel to 180°C. The diagnostics will be attached to the vessel by bellows or similar thermal resistance components, and the isolation gate valve will be maintained at a temperature of

150 °C during bakeout. The details of the calculation of the power required for bakeout are shown in the attached worksheet, Table 6.8.

6.7 Power Systems

Primary power requirements and availability

The Fusion Research Center has available three inertial generators, designated MG0, MG1 and MG2. MG0 is a salient-pole, 100 MVA pulse-rated generator, operating at 600-800 rpm with an energy output of 90 MJ and output voltage of 6.9 kV. MG1 and MG2 are synchronous generators each rated at 18 MVA, operating at 3000-3600 rpm with an energy output of 15 MJ and output voltage of 13.8 kV. The maximum pulse rating is estimated at four times the continuous rating [10].

The TEXT experiment has a large resource of power supplies, including a number on loan or available from other sources. These power supplies are described in Table 6.9, together with their assignments. The power supply assignments are flexible and may be changed, depending on the particular plasma configuration to be produced.

With the addition of a 6.9 kV to 13.8 kV transformer to the MG0 system these power supplies can be connected to the inertial generators in a variety of modes in order to optimize the power and energy available for the USTX coil set. Figure 6.20 illustrates, in a one-line diagram, the power-supply allocation of the three generators for the $A = 1.43$ point design. The present TEXT TF supply will be used for the TF supply on USTX. The two existing 400 V, 25 kA supplies will be used for the vertical field coils, PF5U and PF5L. These three supplies and the existing ADCPS neutral beam supply will be powered by MG0. The OH solenoid power supply will consist of two separate 1183 V, 30 kA power supplies, individually connected to MG1 and MG2. These supplies, identified as the LLNL "A" supplies, are available from LLNL, and were originally used on Alcator-C. An additional candidate supply, also from LLNL, the LLNL "B" supply, may be used in place of the "DIV" supply to increase the vertical field capacity for high current or high beta operation. The ECH pre-ionization supply will be connected to the existing ECH capacitor bank.

Revised 2/19/9

USTX Power Supply Assignment

System	Parameters	Proposed Supply	Status	Power Source	Power Required
OH	1183V / 30kA x 2	LLNL	Mothballed	MG1 and MG2	30MW
TF	200V / 160kA	TEXT TF	TEXT	MG0	32MJ
PF1-A		In series with solenoid		OH	
PF4		In series with solenoid		OH	
PF5-U	400V / 25kA	TEXT Div.	TEXT	MG0	10MJ
PF5-L	400V / 25kA	TEXT VF2	Mothballed	MG0	10MJ
PF3	180V / 10kA	TEXT OH	TEXT	MG0	2MJ
PF2	180V / 10kA	TEXT VF1	TEXT	UT Grid	2MJ
PF1	150V / 500A	TEXT HF1	TEXT	UT Grid	.025MJ
Spare	450V / 10 kA	TEXT HML	TEXT	Cap./Grid	
NB1	80kV / 80A(a)	TEXT ECH	TEXT	MG0	5MJ
"	Mod/Reg / PPM	LLNL / ORNL	Mothballed	UT Grid	10kW
"	Aux. Supplies	LLNL / ORNL	Mothballed	UT Grid	10kW
ECH	100kV Caps.	TEXT ECH	TEXT	UT Grid	Very Small
"	+2 Mod/Regs	TEXT ECH	TEXT	Caps / Grid	Very Small
Hel.Inj.	2kV Caps.	TEXT OH	TEXT	Caps / Grid	0.4MJ

Unless otherwise noted, supplies are to be located in TEXT Main Hall.

Pulsed Power available from generators: MG0 (100MW), MG1 (50MW), MG2 (50MW).

TEXT primary facilities include adequate deionized and chilled water, LHe, and LN2.

(a) The accelerating DC supply (ADCPS) is located in Areaaway B.

Table 6.9. Power Supply availability and Assignment Table.

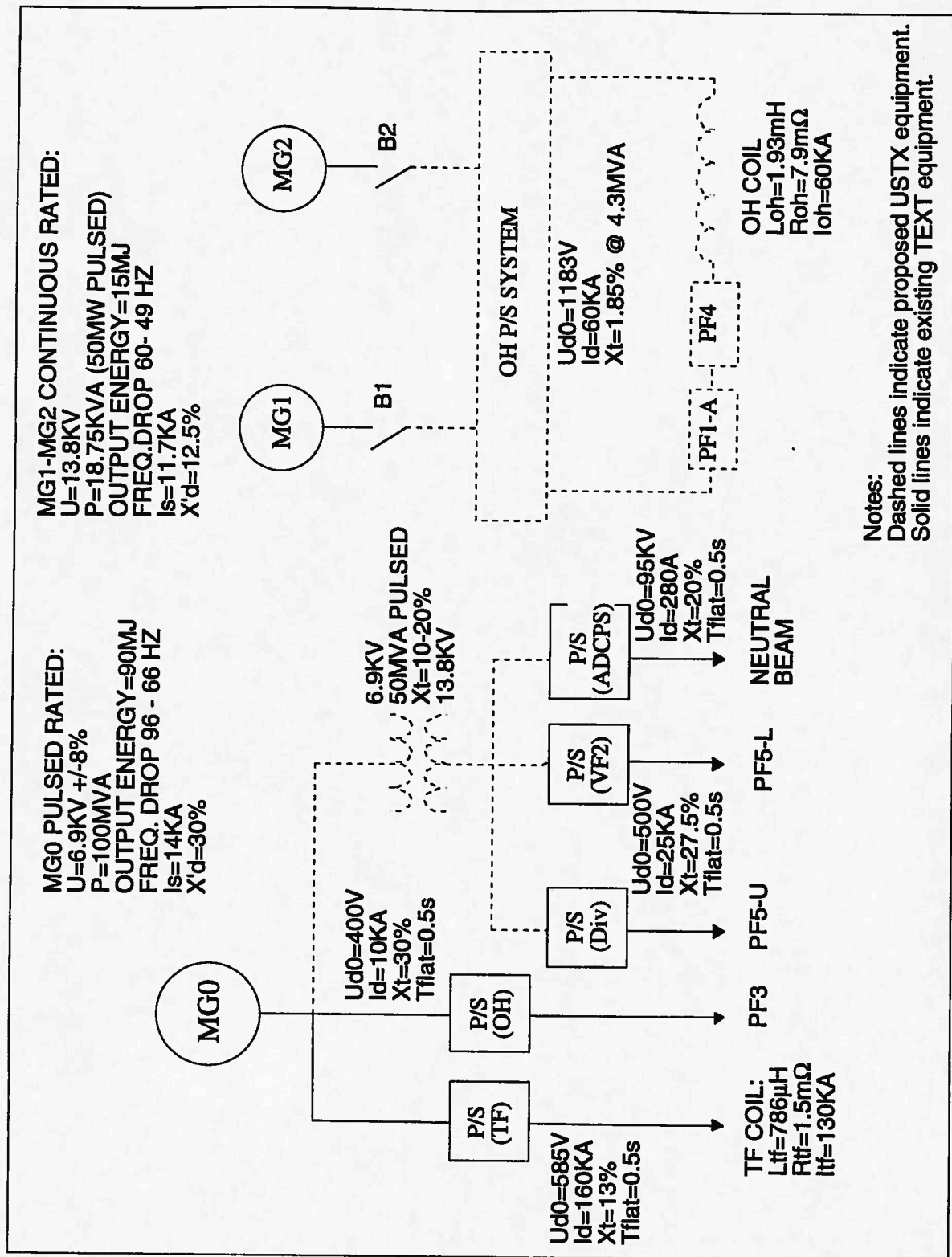


FIG. 6.20. 1-line diagram of power supply allocation of generators for A=1.43 design.

OH power supply

The basic OH power-supply circuit is shown in Fig. 6.21 (a). The main power supply consists of two 1183 V, 30 kA, two-quadrant six-phase SCR controlled supplies, the LLNL "A" supplies. The two supplies will be parallel connected to supply 60 kA to the solenoid through a reversing switch. Nominal power supply rating is 50 kA 1223 V but will be derated for improved reliability and to supply a margin against increased circuit resistance. The present intent is to use the reverse voltage, available at full forward current, to supply the plasma breakdown voltage. This reverse voltage is estimated at 67% of full no-load voltage, the voltage degradation is due to commutation lag because of the inductive load. (Breakdown will be assisted by ECH; refer to chapters 5.2 and 7.3 for a complete discussion of this subject). At current reversal an SCR reversing bridge will be used to reverse the P/S polarity in order to drive the solenoid to full reverse current. A full study of the system performance using the EMTP circuit simulation program is in progress. In the event that the voltage available for breakdown is inadequate the circuit will be modified to include a series resistor and associated switching SCRs. This circuit is shown in Fig. 6.21 (b). The plasma loop voltage is expected to be about 15V for a 75 mohm series resistor. The SCR reversing switch is rated at 3 kV to permit this increased terminal voltage.

TF power supply

The TEXT toroidal-field power supply will be used as the USTX TF supply. It is a two quadrant, twelve-pulse, line-commutated SCR-controlled power supply. It is rated at 160 kA, 500 V DC for 0.5 seconds flat-top pulse with an interpulse period of 3 minutes. The supply is fed from MG0.

PF power supplies

The PF-coil power allocation is shown in Table 6.9. The largest field coils, P5, are fed from two identical supplies, DIV and VF2. These are two-quadrant, twelve-pulse, line-commutated, SCR-controlled power converters. Specifications for these supplies are 450 V no-load and 25 kA full-current, with an I^2t rectangular-pulse-equivalent 0.6-second capability with a repetition rate of three minutes. Supply requirements are 10 MW at 13.8 kV. The two supplies will be fed from MG0 (with a rated terminal voltage of 6.9 kV) via a step up transformer, as shown in Fig. 6.20.

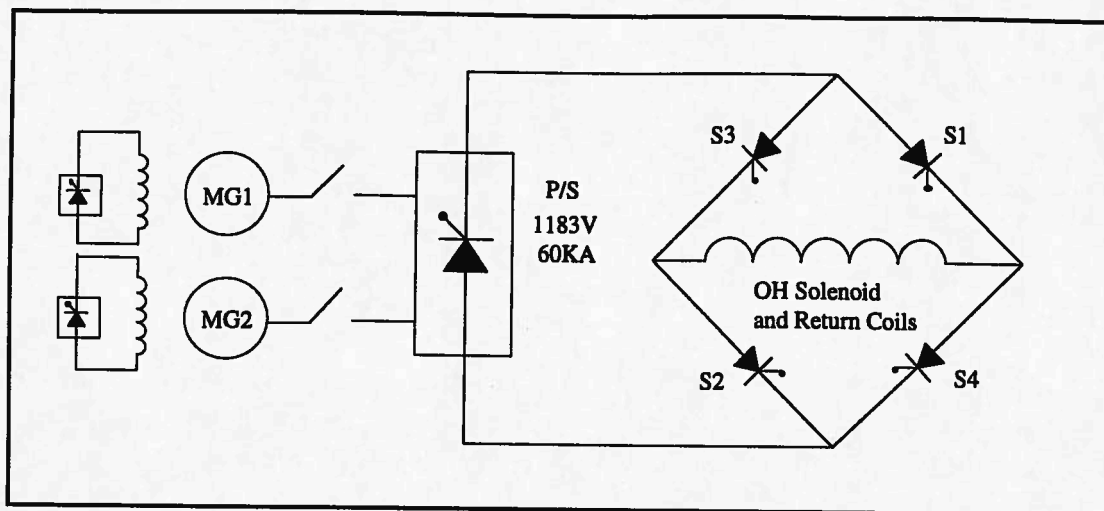


FIG. 6.21 (a). OH power supply schematic with P/S reversal for breakdown.

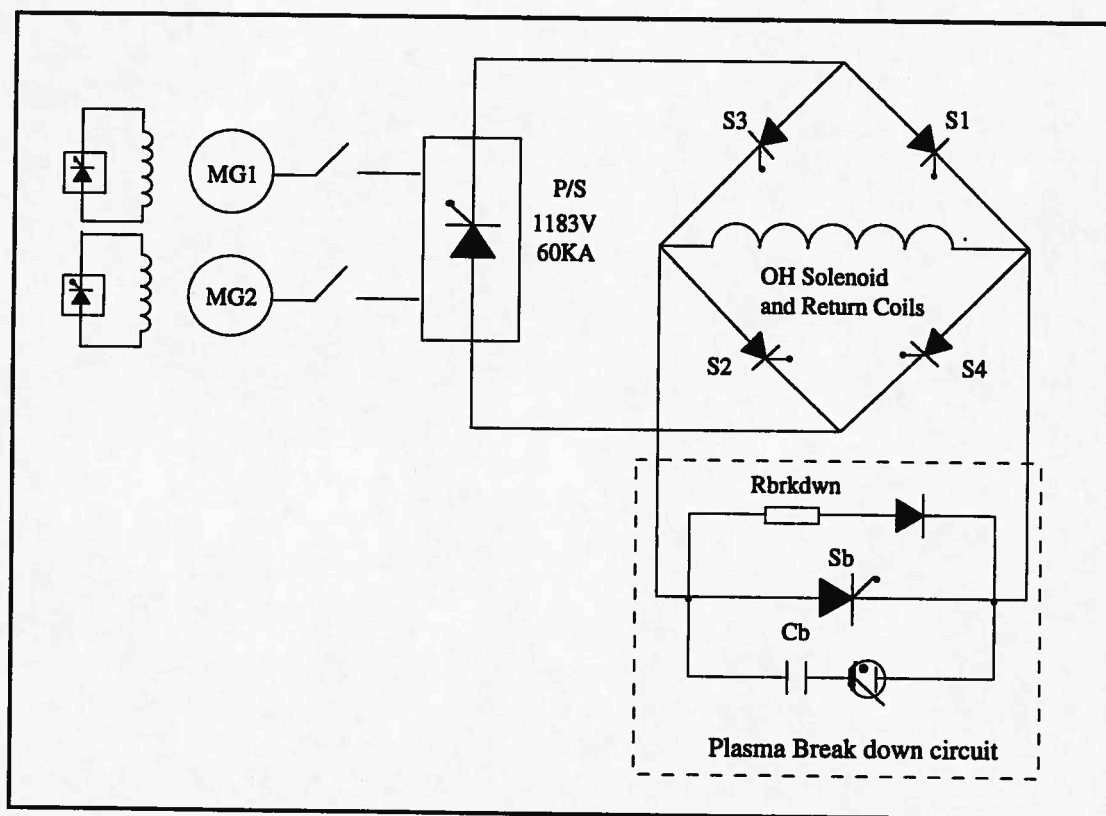


FIG. 6.21 (b). OH power supply schematic with resistive enhanced breakdown voltage.

Coils PF1-A and PF4 are both two-turn coils connected in series with the OH solenoid. Coil PF1-B, located directly adjacent to PF1-A, consists of 8 turns and will be driven by the 4 quadrant TEXT HF supply for position, shape and improved breakdown null control. Coil PF3 is connected to the present TEXT OH supply, coil PF2 is connected to the present TEXT VF1 supply. Also available is the TEXT EML supply, a capacitor-driven chopper-stabilized supply with a 450-V, 10-kA, 0.5-s capability. This supply may be used to provide enhanced position control and shaping.

Neutral-beam power supply

This existing supply consists of both the accelerating DC supply and pulsed power modulator/regulator. The accelerating DC power supply (ADCPS) was originally installed in the MFTF Sustaining Neutral Beam Power Supply System. The ADCPS power supply includes switch gear, step voltage regulator (50-100% voltage range), rectifier transformer (about 20% impedance), rectifier assembly, and control and protection circuitry. The power supply is designed to convert a 13.8 kV AC input into 35 to 80 kV DC output (45-95 kV unloaded output voltage) and deliver 10 to 88 A DC to a pulsed power modulator/regulator circuit.

The pulsed power modulator/regulator circuit is designed to provide the 0.5-s 80-kV pulses at 80 A required for the neutral beam accelerating potential. It utilizes a power tetrode in a series pass tube configuration.

The filament, plasma arc, and beam deflection magnet requirements will be provided by a number of power supplies, using both MG0 and the university 440-V systems. The beamline will be a standard ORNL/ISX beamline, with a source current of about 80 A at 45 kV, delivering about 1 MW of neutral beam power into the plasma.

Long-pulse operation

The discharge pulse length is limited by a complex matrix of constraints. Primary to an evaluation of pulse capability is the selection of plasma current and the identification of the appropriate plasma model. There are two basic cases. In the first case the entire inductive volt-sec capability is available for plasma drive. In the second case the inductive drive is terminated at the zero crossing in the solenoid, and the current is sustained by non-inductive drive techniques. Intermediate conditions exist where

instance bootstrap, current sources. For the first case, the flat top duration is a compromise with the plasma current; at the maximum current the flat top duration is zero. After a plasma current has been selected, the performance is established by a) the solenoid design and charging current, b) the mutual inductance of the solenoid and PF coil set to the plasma, and c) the plasma self inductance and resistance. The flat-top duration is then established by either the P/S reaching full voltage or current, or the solenoid reaching maximum stress or temperature. The maximum temperature is a function of the repetition rate, and higher temperatures can be used at the expense of a lower shot rate. For the solenoid described here the limiting term is generally the solenoid reaching peak current; for low plasma currents, ~0.5 MA, the temperature limit sets the shot length.

For the second case, where the solenoid current is left at zero and the plasma current is non-inductively sustained, the flat-top duration is then established by one of the following:

- a) The TF core reaches maximum temperature. This I^2t limit is $(160 \text{ kA})^2 \times (1.5 \text{ s})$.
- b) The TF power supply reaches the I^2t limit. This is $(160 \text{ kA})^2 \times (1.0 \text{ s})$. Table 6.10 shows the flat-top limit for both the TF core and the TF power supply. It is assumed that the current ramp times are 0.25 s each, and are independent of peak current, to give an indication of the pulse length gain obtained by operating at reduced toroidal field.

Table 6.10. TF flat top duration.

B_{T0} (T)	TF core limit (s)	TF P/S limit (s)
0.5	1.6	1.1
0.4	3	1.75
0.3	5	3.2
0.2	12	7.4
0.1	47	30.1

*Assumed current ramps are 0.250 s each.

*TF field is measured at 0.7 m radius.

*TF core dimensions for $A = 1.43$ and $A = 1.25$ point designs.

- c) One or more of the PF coils reaches the I^2t limit. For the PF5 coil power supplies this is $(25 \text{ kA})^2 \times (0.6 \text{ s})$. For the PF3 or PF2 coil power supply this is $(10 \text{ kA})^2 \times (0.5 \text{ s})$. As the PF1-A and PF4 coils are in series with the solenoid they no longer carry current. The actual value of the PF coil currents is very dependent on the plasma model, current distribution, etc., assumed in the equilibrium calculation. Because of these uncertainties it is rather difficult to predict the limiting times. For full performance, the power supplies are run at about 70% full current to allow for both headroom for control and general design uncertainties. For the predicted currents the full performance flat top is thus about one second. For lower plasma currents and less stringent equilibria, the pulse length would be appropriately longer.
- d) One or more of the PF coils reaches the maximum operating temperature. This is not likely to be a limit, as the coils are sized such that the temperature rise for the standard $A = 1.43$ point design is only 3° C per shot. It could be run for 20 s once per hour for a 60° C temperature rise.
- e) One of the M/G sets supplying energy to the electrical system reaches its available stored energy limit. These limits are very dependent on the details of the discharge conditions and power distribution system. In general the M/G sets are matched to the P/S loads, and the limiting pulse duration is set by the P/S I^2t limits. For non-inductive current drive the reverse swing P/S is no longer used, and this M/G set energy will be available for the other electrical systems.
- f) One of the auxiliary systems reaches a time limit; for example, the NBI system is designed for about 0.3 MJ per pulse, or 1.5 MW for 0.2 s. Longer heating pulses can only be obtained for lower-power operation or by installing two beams and operating them sequentially. If the current drive systems include heating capability, the pulse length will be less affected by the NBI limit. Another possible pulse-length limiting factor is the temperature limit of the limiter or divertor tiles. The cooling time constant for these tiles is of order minutes and, depending on the heat loads, the tiles may have limited full-power pulse capability. Moving the energy strike point during a shot can alleviate this limit.

The above discussion applies to the $A = 1.43$ point design. Pulse lengths are somewhat shorter for the $A = 1.25$ design as the 0.5 T toroidal field is at a radius of 0.75

m. On the other hand, plasma edge- q limitations will probably require operating the $A = 1.25$ plasma at reduced toroidal field ($B_{T0} \approx 0.25$ T).

In summary, by running at both reduced toroidal fields and lower plasma currents, the device should be capable of long pulse operation. As an example, for a plasma current of 0.5 MA and a toroidal field at a radius of 0.7 m of 0.25 T, and with a current-drive-assisted loop voltage during flat top of 0.14 volts, the inductively current-driven, ohmically heated, flat-top pulse length (with no modification to the coil set, power supplies or power system) should be two or more seconds.

References to Chapter 6

- [1] Songtao Wu "Stress Analysis of USTX Solenoid Design", IPP-Hefei, Private communication.
- [2] R. J. Colchin, "Eddy Currents in the Core of the Low Aspect Ratio Tokamak START", accepted for Fusion Technology, 1996.
- [3] R. J. Colchin, J. D. Galambos, P. L. Goranson, S. P. Hirshman, P. H. Edmonds and J. R. Uglum, "The design of the Center Core of a Spherical Tokamak, to be published in Fusion Technology, *Proceedings of the Symposium on Fusion Engineering*, Sept. 30 - Oct. 5, 1995.
- [4] D. B. Montgomery, *Solenoid Magnet Design*, Wiley-Interscience, John Wiley and Sons, 1969.
- [5] S. P. Hirshman and G. H. Neilson, *Phys. Fluids* **29** (1986) 790.
- [6] R. Granetz, D. Gwin, and J. Irby, in *Proceedings of the ITER disruption Expert Group Workshop*, Feb. 1995 (1995).
- [7] Chen Siyue, Cheng Xingqian, Wu Songtao, Zhang Young, Shi Jia Biao, Liou Baohua and Huo Yuping, "The ETG Design Review", FRC Report #476, July, 1995.
- [8] T. J. McManamy, R. D. Benson, R. L. Brown, G. H. Henkel, E. A. Lazarus, and D. E. Williamson, "Design and Fabrication of a Prototype Solenoid for the Spherical Torus Experiment", *Proceedings of the 12th Symposium on Fusion Engineering*, Monterey CA, October 12 - 16, 1987, Vol. 1, p. 350.
- [9] A. Roth, *Vacuum Technology*, North-Holland Publishing Company, Amsterdam (1982).
- [10] C. G. Adams, *Pulsed Motor Generator Sets*, Jackson and Moreland, Boston, MA.

CHAPTER 7

AUXILIARY PLASMA HEATING AND CURRENT DRIVE

Auxiliary plasma heating and non-inductive current drive are important elements of a small-aspect-ratio tokamak program. Auxiliary heating is probably needed to study high- β regimes with $\beta_N \approx 5$, although we fully expect $\beta_N \approx 3$ with ohmic heating alone. Due to the small space available for the ohmic heating solenoid at very low aspect ratio ($A \approx 1.25$), non-inductive current drive may be necessary to reach $I_p > 0.5$ MA and is probably required to provide the necessary hollow current-density profiles over long times. In this section we discuss both bootstrap current and auxiliary-heating and current-drive options envisioned for USTX. These auxiliary options include neutral-beam injection heating (NBI), neutral-beam current drive (NBCD), electron cyclotron heating (ECH), Alfvén and fast-wave (AW and FW) heating and current drive, and coaxial helicity injection (CHI). Of these, only NBI, NBCD, and ECH are well established techniques. In Phase I, we will implement ECH, which we expect to be useful mainly during current startup. We will also start low power studies of the promising but less established AW/FW CD in Phase I. In Phase II, we expect to implement NBI, NBCD, full power ECH and AW/FWCD, and possibly CHI, if the HIT results prove promising. We expect the bootstrap current to be $\leq 50\%$ of the total current (significantly less in most cases), NBCD to be $\leq 12\%$ of the total current. The contributions of AWCD, FWCD, and CHI can be significant, but they cannot be accurately estimated at low A with the current experimental and theoretical knowledge.

We intend to provide USTX as a facility for interested groups to investigate these current-drive techniques at low A . Our initial goal will be to provide a well-diagnosed flexible target plasma in Phase I, in preparation for implementing one or more of these methods in Phase II. We also intend, subject to available funding, to carry out theoretical Alfvén current drive studies, and are prepared to perform low power diagnostic experiments on wave propagation and mode structure, should the theoretical studies prove as encouraging as expected. We have already discussed the foreseen conceptual problems in Sec. 3.6.

The University of Wisconsin group, in particular Tom Intrator, has expressed interest in implementing RF current drive (AWCD, FWCD) and heating (AWH, FWH) on USTX, following their successes on Phaedrus-T [1, 2]. These methods could potentially drive 60 to 120 kA with AWCD and 300 to 500 kA with FWCD, for 2 MW of RF power at $n_e = 0.2 \times 10^{20} \text{ m}^{-3}$ [3]. They have, however, never been tried at low aspect ratios and are not well understood theoretically. At high densities the current-drive efficiency may be low.

The University of Washington group, in particular Brian Nelson, has expressed interest in adapting coaxial helicity injection (CHI) for USTX following their success on HIT [4]. To date, however, all CHI experiments have required a solid flux-conserver in the form of a copper shell around the whole plasma. This cannot be implemented on USTX without seriously interfering with the low-aspect-ratio design. A design without the solid flux-conserver is being pursued on HIT. If these experiments are successful and uncertainties in scaling the results to USTX are reduced to acceptable levels, CHI could be implemented on USTX. This would be done during the transition from the $A = 1.43$ phase to the $A = 1.25$ phase.

7.1 Bootstrap-current estimates

We have noted in Sec. 4.3 that the calculation of neoclassical transport coefficients at all aspect ratios and collisionalities, underway at ORNL [5, 6], is very complicated and has not been fully completed. Therefore, to estimate bootstrap current for USTX equilibria we use the small- A collisionless formula of Hirshman [7], corrected by the finite collisionality factors of Hinton and Hazeltine [8]. The argument of Shaing [9] suggests that this may be an underestimate. This model is implemented in the SUPERCODE [10] studies described in Sec. 3.5 [11] and in a profile spreadsheet based on the geometry of Sec. 3.1 [12]. These agree with each other reasonably well.

The bootstrap fraction is extremely sensitive to plasma pressure, magnetic configuration, and current profile. For ohmic cases, our spreadsheet finds bootstrap fractions $\leq 10\%$, for β ranging from 6-35%, depending on the toroidal field and other factors such as plasma shape and profiles.

For beam-heated cases, SUPERCODE calculations show that under the most optimistic assumptions of confinement and profile control, which require $q(0) \cong 4$ and a

hollow current distribution, it might be possible to achieve a bootstrap fraction $f_{bs} \equiv I_{bs}/I_p \geq 50\%$ (including the diamagnetic term). Table 7.1 gives two examples. ITER-89P scaling was used with $H = 2$. The spreadsheet model approximately reproduces these bootstrap-plus-diamagnetic fractions, with $\beta = 15\%$ and $\beta = 9\%$, respectively, *not* including the beam energy.

Table 7.1. Bootstrap fractions for USTX simulations

A	1.25	1.4
B_{T0} (T)	0.24	0.56
I_p (MA)	0.64	0.91
β	24%	14%
P_{NBI} (MW)	1.25	4.0
f_{bs}	50%	45%

The above cases represent extreme profiles of current or q . For similar conditions of β , T_e , T_i , etc., but with $q(0) \approx 1$ and a centrally peaked current profile, our spreadsheet finds $f_{bs} \approx 17\%$ for both aspect ratios.

Thus, we expect our ability to study bootstrap current to increase rapidly with auxiliary heating, current drive, and current-profile control. Of course, the bootstrap current itself can contribute to the hollowness of the current profile. This can, in turn, affect MHD stability. High levels of synergism become important here.

7.2 Neutral-beam injection

Neutral-beam injection (NBI) is a reliable and well-established technique for plasma heating [13] and the FRC has considerable experience with neutral beams due in part to its diagnostic neutral beam which was routinely operated on TEXT. NBI is well suited to the high-density operation of a 1-MA-class device such as USTX. A neutral-beam injection system consists of a beam line, vacuum pumps, cooling-water plumbing, power supplies, instrumentation, control electronics, and safety interlocks. The beam-line hardware includes an ion source, magnetic shields, beam tanks, neutralizer, deflecting magnet, ion dump, and calorimeter. The basic requirements of the injector system are supporting utilities and floor space for the injectors and power supplies.

At ORNL, 1.25 MW NBI systems were constructed for ISX-B, and modified for ATF. High current ion sources [14, 15] for these injectors were developed for plasma heating on PDX and ISX-B [16-19], and used on ISX-B and ATF plasmas [19, 20]. Two of the injectors were operated on ATF through 1991 for both heating and testing alpha-particle diagnostics. The ORNL team can furnish up to two NBI systems for USTX, each capable of delivering 1.25 - 1.5 MW of neutral power for < 300 ms.

As an alternative, we have investigated the possibility of obtaining one of the neutral-beam systems from Lawrence Livermore National Laboratory (LLNL) [21]. The LLNL NBI system is one of 22 built for MFTF-B [22], of which sixteen were designed for 0.5-s pulse length and six for 30-s pulse length. A short-pulse unit would be appropriate for USTX. The modulator/regulator system designed to drive this unit is presently at the FRC (see Sec. 6.7) and is used for ECH on TEXT-U. Typical operating parameters of the ORNL and LLNL short-pulse systems are essentially identical and are listed in Table 7.2.

Table 7.2. Neutral-beam characteristics

Accelerating Voltage, (kV)	40 - 60
Accelerating Current, (A)	100
Pulse Width, (ms)	300
Ion Beam Power (MW) / module	1.25 MW @ 40 kV, 1.5 MW @ 60 kV

For USTX applications an injection port of 30 cm by 50 cm is large enough to minimize interception and re-ionization loss of energetic neutrals. Each of the neutral-beam injectors is capable of injecting approximately 1.5 MW of energetic hydrogen neutrals at energies adjustable from 40 to 60 keV (by re-gapping the source) for heating and current drive experiments on USTX. The primary difference between the two sources is the space requirement. Figure 6.1 shows USTX with two of the beam lines and the LLNL power-supply locations (Table 6.9). This layout allows access to all the beam components for installation and service. The conceptual design allows for the capability of swinging the beam line to select a tangency radius between 0.7 and 0.9 m. For plasma heating purposes, the neutral-beam system will be configured to inject neutrals of 40 to 45 keV at 1.25 MW for less than 300 ms. For current drive the injector can be configured to inject neutrals at 60 keV. The estimated effects of NBI on plasma performance were discussed in section 3.

In an ST with high β and low net magnetic field, an important factor to consider is that the true orbits of fast ions depart significantly from their guiding center orbits. The true ion trajectories were computed [23] with an orbit code for a typical USTX plasma. Due to the low magnetic field in a low- A tokamak the particle orbits can make considerable excursions around their guiding centers, as is shown in Fig. 7.1. The first orbit shown is for a circulating ion, which is barely perturbed by gyro-motion. The second one is for a deeply trapped ion, for which the effect of gyro-motion is to produce large departures from the average orbit. These orbit considerations limit the minimum B_T for a given beam energy.

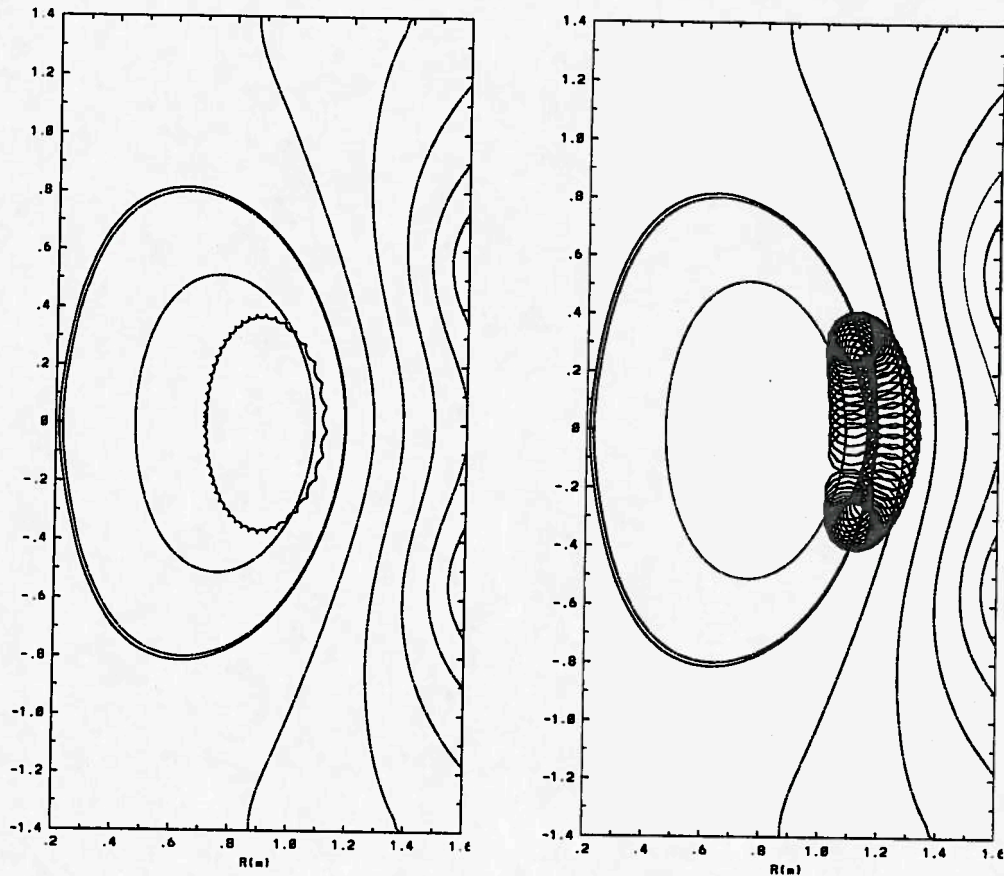


FIG. 7.1. Orbits of 40 keV H ions in a 1 MA, 0.5 T USTX plasma . a) initial position $R = 0.7$ m, $z = 0$; purely toroidal initial velocity, co-injection, passing. b) initial position $R = 1.1$ m, $z = 0$, radially inward initial velocity, trapped.

Neutral-beam injection can also drive plasma current (≈ 120 kA) in a high temperature, low density ($T_e \geq 1$ keV, $n_e \approx 10^{19} \text{ m}^{-3}$) target plasma. Neutral-beam current-drive allows some measure of current-profile control so that the net profiles may be

tailored to match those required to reach very high β and low q . The choice of neutral-beam energy is based upon considerations of beam penetration, loss rate of injected fast ions, and current-drive efficiency. We can approximate the plasma current driven by neutral beams as

$$I_b \text{ (kA)} = 6.73 \times 10^{+20} \frac{P_b \text{ (MW)} T_e \text{ (keV)}}{\bar{n}_e \text{ (m}^{-3}) R_0 \text{ (m)}}, \quad (7.1)$$

which agrees with the results from a calculation reported by Counsell and Cox [24] for parameters similar to USTX. We have also compared the expression (7.1) with results of SUPERCODE [10]. This is a 1-1/2 D code, which has been benchmarked against ACCOME [25] calculations for the ITER conceptual design activity [26]. It calculates profiles of neutral-beam deposition, fast-ion pressure, beam-heating power, and beam-driven current density. It also yields global values of current-drive efficiency, fast-ion beta, beam shine-through, and fusion power from beam-ion interactions. We have further checked the neutral-beam penetration results against the results of a 3-D neutral transport code NUT [27], which had previously been validated against DEGAS [28]. Our calculations indicate an energy window of 40 to 60 keV for adequate beam penetration with less than 10% shine-through for all USTX plasma scenarios. The higher energy of 60 keV is better suited for neutral-beam current drive.

7.3 ECH startup assist scenarios

To reduce volt-second consumption and allow operation at very low toroidal field, the use of ECH to initiate breakdown is planned. Three ECH systems were routinely used for heating on TEXT. Results from DIII-D [29] suggest that the use of ECH-assisted breakdown minimizes the effects of error fields such as those produced by the OH solenoid. With ECH assist the pre-fill pressure can also be increased without quenching plasma formation, and runaway electron production is reduced, eliminating hard X-ray interference with diagnostics. In addition, ECH has the potential to significantly reduce volt-second consumption during the current-ramp phase. Recently, efficiencies of order 0.1 mV-s/kA have been obtained in START [30] where the current ramp reached 50 MA/s ($V_{\text{loop}} = 3 - 4 \text{ V}$, $I_p < 160 \text{ kA}$).

ECH may also be useful for current-density profile control to help produce the hollow profiles necessary for stability with low- A high- β plasmas. In CDX-U [31-33]

both poloidal and toroidal fields define the initial geometry for plasmas that are initiated and sustained using ECH alone. The field lines are initially open, but the poloidal component leads to strong particle trapping through the gradient along field lines. The initial toroidal current, due mainly to the diamagnetism of the trapped particles, enhances the applied poloidal field, yielding closed flux surfaces. The strong bootstrap current then sustains the topology during the ramp and steady state. Note that refraction and cut-off place severe limits on the effectiveness of ECH for high density applications at low toroidal field, and large, unabsorbed amounts of ECH power could nullify any benefits because of the associated impurity influx from direct wall heating or other ECH interaction in the scrape-off layer.

Electron cyclotron (EC) pre-ionization will be employed on USTX to provide reliable breakdown at low loop voltage. This method is the one used successfully in START [34]. A 14 GHz source capable of providing a several kilowatt pulse for a few milliseconds is required. This will be provided by two klystron sources (20 kW/tube).

The use of EC current-ramp assist for $I_p < 50$ kA is also being considered for USTX. Several studies in larger-aspect-ratio tokamaks have shown that a $\approx 50\%$ savings in the ohmic volt-second consumption can be achieved up to this current level, mainly through the reduction in the plasma resistance by ECH [29, 35]. Although this is probably a small saving for a 1 MA device, the main benefit could be for shaping the initial current profile. We have considered three sources and heating options for this method.

1. A 14 GHz, 100 to 200 kW, 50 ms pulse for central heating at the electron cyclotron frequency $f = f_{ce}$. This has been successfully demonstrated in many tokamaks [29, 34-36]. The wave cutoff is at $n_e = 2.5 \times 10^{18} \text{ m}^{-3}$ if we use the low-field-side (LFS) O-mode launch, and at $n_e = 5 \times 10^{18} \text{ m}^{-3}$ if we use the high-field-side (HFS) X-mode launch. The RF power can be provided by a group (10-20) of conventional 20 kW tubes, since high unit power sources are not readily available in the 10-20 GHz frequency range.

2. A 28 GHz, 200 kW, 50 ms pulse for central heating at $f = 2f_{ce}$. Calculations show that at this frequency the heating is not as efficient as fundamental heating at the low densities and temperatures of startup. This concept has not yet been demonstrated. The RF power can be provided by existing 28 GHz, 200 kW gyrotrons using a vertical launch to maximize the absorption path length. The wave cutoff is at $n_e = 5 \times 10^{18} \text{ m}^{-3}$.

3. A 56/60 GHz, 200 kW pulse for HFS edge heating at $f = 2f_{ce}$. This is also an untested idea. We propose using our existing 56/60 GHz gyrotrons with a vertical launch to maximize the absorption path length. The wave cutoff is at $n_e = 2.25 \times 10^{19} \text{ m}^{-3}$ for LFS launch. The most promising scenario is heating the extreme HFS edge using the existing 56/60 GHz system since the density may remain below cutoff there throughout the I_p ramp.

Previous studies in DIII-D [29] showed that a 10% savings in the ohmic volt-second consumption was achieved with optimally 300 to 400 kW ($P_{ech} = P_{oh}$) over the entire current ramp to 1 MA. Most of the savings were accumulated at low current where ECH provided a large initial reduction in the plasma resistance relative to that provided by I_p resistive heating. This may become more important for the $A = 1.25$ solenoid where the inductive I_p capability becomes severely restricted and a relatively modest P_{ech} can supplement the reduced P_{oh} .

7.4 Fast-wave and Alfvén-wave current-drive system

We propose to provide USTX as a facility for studying RF techniques such as Alfvén-wave current drive (AWCD) below ω_{ci} [37] and fast-magnetosonic (FM) wave current drive (FWCD) above ω_{ci} [1, 38-40]. The high-phase-velocity compressional waves have desirable features needed for efficient current drive in USTX as well as in fusion-reactor-like conditions. The high electron β in USTX may lead to high damping on the thermal electron populations for the FM waves [41-46]. Judging from recent results on Phaedrus-T [2], we may drive 60 to 120 kA with AWCD and 0.3 to 0.5 MA with FWCD with 2 MW of RF power at $n_e = 0.2 \times 10^{20} \text{ m}^{-3}$. As explained in Sec. 3.6, however, these promising CD methods have not been fully developed even on conventional machines where the large poloidal asymmetry inherent at small aspect ratio can be neglected. The problem has not yet been fully solved at low aspect ratio, and it is not yet clear whether energy deposition in the plasma periphery due to side-band harmonics can be avoided. Theoretical work is planned by staff at the Fusion Research Center and the Institute for Fusion Studies.

While the pioneering Alfvén wave experiments on Phaedrus-T demonstrated a driven current, they did not include direct observation of the mode structure of the driving waves or the resultant current-profile modification. Since theoretical studies of the rich Alfvén mode structure indicate that both current drive and heating efficiencies are very sensitive to frequency and mode selection, a detailed study of the modes is essential for the

optimum, or even successful, use of RF power and for confident extrapolation of the results to reactor scenarios. These questions become very much more complicated at low aspect ratio, as indicated in Sec. 3.6.

USTX proposal outline

At USTX, we will provide a steady-state target plasma suitable for Alfvén and fast-wave current-drive investigations. We will also bring to this work our own interest and experience in the study of the experimental, theoretical, and numerical aspects of Alfvén waves, as outlined in Sec. 3.6. Guided by new theoretical and numerical work on AW and FW CD at low A , we will start low power studies in the first year of the machine operation, mostly with existing diagnostics and RF equipment at the Fusion Research Center. With these, we can measure, and compare with new theory at low A , the precise frequencies and spatial structures of the RF modes necessary to drive currents. Although we will not be able to measure the small amount of driven current at this stage, a good agreement with predictions of the theory will give us confidence that the current drive predictions will also come true. We believe that this small investment in effort at low power would be of substantial benefit as a precursor to a more expensive effort at high power.

We can use either of the two interferometer systems (FIR and PCI) which are planned for fluctuation measurements on USTX. These will allow direct observation of driven mode profiles, even at low RF power in the range from 1 to 10 kW, provided lock-in techniques are employed. Our proposed FIR interferometer can be used for the detection of RF-driven density fluctuations. The sensitivity of the FIR will also allow us to study the onset of any non-linear power scaling effects even if they appear at these low power levels. The proposed (but not costed) phase contrast imaging system (PCI) can also provide precise measurements of the RF mode structure. The existing system design will permit measurements to the level of $\tilde{n}/n \approx 10^{-5}$. Wavenumbers can be detected in the range between 12 cm^{-1} and a low k determined by the beam width of 0.62 cm^{-1} for a 10 cm beam. If either of the two interferometers can detect RF-driven mode structures, we can also use kinetic Alfvén modes for measuring the q profile. We will also have a reciprocating probe drive on USTX on which a magnetic probe can be mounted to measure radial mode structure near the edge. These diagnostics, used in conjunction with theoretical and numerical studies will greatly facilitate the search for the optimum antenna configuration, frequency, and phasing for efficient RF current drive.

Wisconsin proposal outline

The following is a summary [3] of the Wisconsin proposal for USTX submitted separately to the Department of Energy in 1995. These high power RF experiments are not funded in this proposal.

Antenna requirements and features

A possible antenna system would consist of multiple-antenna arrays at four toroidal locations with two poloidal strap assemblies per array to allow some control over the wave-number spectrum. Each element is a very low-voltage, large-bandwidth, high-power-density antenna with insulating limiters that will not require Faraday shields. The lack of Faraday shields results in a more compact and more closely coupled antenna. The large bandwidth allows the same antenna array to be used for both AWCD and FWCD. The antenna conceptual design is a variation on the stacked stripline (SSL) concept [47] that allows low-voltage (< 1 kV RMS) operation with large power density. Each SSL unit is capable of handling $P_{RF} > 1$ MW / 0.3 m²). The low-voltage aspect reduces the usual RF sheath-impurity and high-voltage arcing problems, as has been shown on PRETEXT [48, 49], TCA [50], and Phaedrus-T [1, 2]. Each SSL strap will be approximately 1.5 m in length, will have two "hot" feeds and two returns, allowing dipole or monopole phasing of each strap. The large vessel allows radial travel of 10 cm for adjustment of antenna plasma coupling via gap spacing between plasma and antenna limiter. It also allows antennas to be oriented at large angles to the poloidal direction for optimum mode coupling. Inductive decoupling of the straps in each array will be required to enable traveling-wave phasing of the array. Novel inductive strap decouplers will be used, so that arbitrary strap phasing can be achieved. The hardware characteristics are shown in Table 7.3.

Transmitter requirements

The goal of high power AWCD experiments on USTX will be to drive 300 to 400 kA for pulse lengths of 100 to 200 ms; longer pulses require more robust and expensive transmitters. Two channels of 1 MW minimum each will be required, preferably with a phase-splitter output for dipole drives on antenna arrays. The frequency bandwidth of available hardware will most likely need to be extended down to 3 MHz. The desired range of 3 to 13 MHz allows operation below ω_{ci} (AWCD, FWCD) to above ω_{ci} (FWCD).

Table 7.3. RF antennas, decoupler, & matching circuits

GENERAL		
frequency	13 MHz	
R_{load}	10Ω	Equivalent R_L @ $30\Omega/m$
I_{circ}	316 A	per straplet
I_{circ}	1.89 kA	total
STRAP, SSL		
total poloidal length of strap	0.3 m	
toroidal width	0.15 m	
radial straplet depth	0.1 m	
sections per strap	2	
straplets per section	3	per straplet $R=0.62 m\Omega$
feed pairs per section	1	pair = 1 hot, 1 return
inductance per straplet	50 nH	per straplet $\omega L= 4.08\Omega$
total L per section	16.7 nH	per feed pair $\omega L= 1.36\Omega$
voltage drop on SSL section	988 Volt	
DECOUPLER		1 pair per section - if needed
inductance	20 nH	
mutual inductance	20 nH	
feed inductance	15.7 nH	per feed pair = 1.31Ω
voltage on line	1.81 kV	
voltage drop on feed	0.82 kV	per feed pair
R_{strap}	$2.34 m\Omega$	feed pair+straplets = $2.54m\Omega$
inductive reactance $\omega L_{ssl+feed}$	2.67Ω	per feed pair
EFFICIENCY		
total power	1.0 MW	2 (SSL sections + feed) pairs
plasma power	1.0 MW	
copper losses	4.4 kW	
efficiency	99.6%	
MATCHBOX		
tank capacitance	4.62 nF	per feed pair
variable capacitance required	85 nF	tune from 3-20 MHz
total L per section	32.4 nH	1 (SSL section + feed) pair
total L for tank	16.2 nH	all sections in parallel
total C for resonance	9.24 nF	all sections in parallel

Plate power-supply pulse line, capacitors, inductors

Any planned experiments will require a stiff plate-voltage power supply for two channels of RF transmitters. For a 200 ms pulse length at 1 MW of coupled RF power, each channel will dissipate approximately 0.2 MJ, requiring 0.8 MJ energy storage in the pulse line. The plate DC power supply will need to be a pulse line with an intrinsic impedance of 9Ω ($= 3\text{ kV} / 330\text{ A}$) terminated in 9Ω . The bank voltage needs to be 6 to 8

kV with capacitor ratings in excess of 15 kV. The duty cycle is 4% for a 5 minute shot cycle. The trickle charging supply will need to source 1 to 2 A at 8 kV. The delay time is 40 ms per section with five resonant sections each at $C = 2200 \mu\text{F}$ and $L = 180 \text{ mH}$. The aggregate pulse length for five sections will be 200 ms. The DC resistance of the inductors will need to be held to a small fraction of 9Ω , e.g., $100 \text{ m}\Omega$. These specifications are shown in Table 7.4.

Matchbox capacitors for tuned tank

With four SSL sections per strap we will require a large capacitance (240 nF, 8 kV) for tuning the tank circuit. Although the circulating current of 13 kA is over the CW ratings of the capacitors, the duty cycle and pulse length is well below thermal welding time. Some vacuum variable capacitors will be required. Methods for attaching capacitors in a hard-vacuum match box are being explored by the University of Wisconsin group.

Table 7.4. RF power transmission specifications

PULSE LINE	NOMINAL	MAXIMUM
pulse length	50 ms	500 ms
R	50Ω	
V_{bank}	20 kV	30 kV
stored energy total	0.2 MJ	total stored energy = 0.4 MJ
number sections	2	
RF pulse energy	0.05 MJ / strap	
Capacitance / section	$500 \mu\text{F}$	
inductance / section	1.25 H	
delay time / section	25 ms	

7.5 Coaxial helicity injection

The results of coaxial-helicity-injection (CHI) current drive on the Helicity Injected Tokamak (HIT) [4] and on CDX [51] have been encouraging. However, the solid flux-conserver in the form of a copper shell around the whole plasma seriously interferes with the low-aspect-ratio design. If experiments without a solid flux-conserver on HIT are successful, and if uncertainties in scaling the results to USTX are reduced to acceptable levels, CHI could be implemented (e.g., by the University of Washington group) on USTX during the transition from the $A = 1.43$ phase to the $A = 1.25$ phase. CHI is not costed in this proposal.

CHI current drive

Magnetic helicity K , proportional to the arithmetic product of linked fluxes, is the best constant-of-motion for magnetized plasmas with helicity barriers [52-54]. In a tokamak, K is approximately equal to the product of toroidal and poloidal fluxes, $K \approx \Phi_T \psi_p$, and for a given current profile, is approximately proportional to the plasma current I_p . Current-drive transformers sustain I_p by producing a loop voltage V_{loop} , 'injecting' helicity through additional ψ_p linking Φ_T , at the rate $\dot{K} = 2V_{loop}\Phi_T$, until the transformer saturates. Coaxial helicity injection (CHI) can sustain I_p in steady-state by applying a voltage V_{inj} to the magnetic flux ψ_{inj} penetrating two divertor electrodes. This voltage continuously injects primarily toroidal flux linking ψ_{inj} , injecting helicity at the rate $\dot{K} = 2V_{inj}\psi_{inj}$. The edge-driven current relaxes toward a constant J_T/B_T profile, driving current throughout the plasma volume.

HIT results

HIT has recently used CHI (only) to sustain currents of 225 kA for about 2 ms. The experiment is being modified to add an ohmic heating transformer and several actively-driven field-shaping coils. These additions will allow tests of CHI at higher temperatures, allow comparison of confinement with CHI plasmas to that of ohmically driven plasmas, and allow operation with a thin helicity barrier. All of these results will have direct bearing on the possible addition of CHI current drive to USTX.

Present scaling of CHI

Because of the following uncertainties, general scaling relations from the HIT results are preliminary: the size of HIT has not been varied; the distribution of helicity dissipation between the injector, the open flux, and the tokamak is unknown; and the detailed injector physics is not fully understood. However, constraining these uncertainties to be fixed at the present HIT values, some simple and reasonably reliable scaling relations can be obtained. At present we would, therefore, build the same injector that is used on HIT for the $A = 1.25$ configuration of USTX. The injector voltage ($V_{inj} \approx 700$ V) and current ($I_{inj} \approx 20$ kA) used for scaling, would be the same as those on HIT. As the location of the helicity dissipation is not known, we assume that the distribution of helicity dissipation between the injector, the open flux, and the tokamak would be the same on USTX as in HIT.

From these assumptions, where f is the linear size increase, Table 7.5 shows the scalings of various parameters with f , their values on HIT, their values for a 500 kA and a 1 MA tokamak, and compares this simple scaling with USTX-2 design parameters. This scaling shows that USTX parameters are near to or exceed the required simple scaling values outlined here, and should lend themselves to successful CHI operation. To sustain a long-pulse discharge with a practical power supply, the injector power would need to be reduced by about a factor of three, using the present HIT scaling. Such a reduction is being pursued on HIT by adding additional ohmic heating and designing a new injector geometry that should improve the performance of the starting point used for this scaling.

Table 7.5. Scaling of HIT parameters to approximately 1 MA

Parameter	Scaling	HIT	≈ 0.5 MA	≈ 1 MA	USTX	units
I_p	f^2	250	500	1000	1000	kA
R_0	f	0.3	0.42	0.6	0.8	m
a	f	0.2	0.28	0.4	0.5	m
B_T	f	0.5	0.71	1.0	0.5	T
Φ_T	f^3	112	316	896	840	mWb
ψ_p	f^3	15.7	44.4	125.6	570	mWb
K	f^6	0.0027	0.022	0.173	0.568	Wb ²
ψ_{inj}	f	5	7.1	10	up to 92	mWb
\dot{K}_{inj}	f	7	9.9	14	2.84	Wb ² /s
V_{eff}	f^2	30	15	7	1.5	V
I_p / I_{inj}	f^2	8	16	32	32	
τ_K	f^5	0.4	3.9	10	200	ms
T_e	f^2	80	160	400	500	eV

Application of CHI to USTX

The addition of the ohmic transformer, feedback coils, and thin shell to HIT will answer many of the scaling and efficiency uncertainties, and provide solutions to implementation on USTX. The new design should also reduce the injector power requirements by opening up the injector geometry.

To incorporate CHI on USTX the design must maintain compatibility with a divertor electrode and have a helicity barrier, utilizing future HIT results for the final injector design. This would be best met by adding toroidal insulators to the USTX vacuum chamber, and using the resistive wall that may be added for beta-limit studies.

References to Chapter 7

- [1] S. Wukitch, M. Vukovic, R. Breun, *et al.*, Phys. Rev. Lett. **74** (1995) 2240.
- [2] T. Intrator, P. Probert, S. Wukitch, *et al.*, Phys. Plasmas **2** (1995) 2263.
- [3] T. Intrator, personal communication (1995).
- [4] B. A. Nelson, T. R. Jarboe, D. J. Orvis, *et al.*, Phys. Rev. Lett. **72** (1994) 3666.
- [5] W. Houlberg, in *Proceedings of the U. S. - Japan Workshop on Bootstrap Current in Tokamaks and Stellarators*, Lake Lanier Islands, GA, (1994).
- [6] W. A. Houlberg, K. C. Shaing, and S. P. Hirshman, in *Proceedings of the Sherwood Theory Conference*, Lake Tahoe, NV, (1995).
- [7] S. P. Hirshman, Phys. Fluids **31** (1988) 3150.
- [8] F. L. Hinton and R. D. Hazeltine, Rev. Mod. Phys. **48** (1976) 239.
- [9] K. C. Shaing, C. T. Hsu, M. Yokoyama, *et al.*, Phys. Plasmas **2** (1994) 349.
- [10] S. W. Haney, W. L. Barr, J. A. Crotinger, *et al.*, Fusion Tech. **21** (1992) 1749.
- [11] J. Galambos and Y.-K. M. Peng, *Probabalistic Analysis of a Proposed Low A Tokamak Experiment*, Report ORNL-TM 12998, Oak Ridge National Laboratory (1995).
- [12] D. W. Ross and J. C. Wiley, Bull. Am. Phys. Soc. **40** (1995).
- [13] K. Okano, J. Nucl. Sci. and Tech. **27** (1990) 689.
- [14] C. C. Tsai, W. L. Sterling, H. H. Haselton, *et al.*, in *Proceedings of the 7th Symp. Engineering Problems of Fusion Research* (1977), p. 278.
- [15] M. M. Menon, C. C. Tsai, W. L. Gardner, *et al.*, in *Proceedings of the 8th Symposium on Engineering Problems of Fusion Research* (1979), p. 656.
- [16] W. L. Gardner, G. C. Barber, C. W. Blue, *et al.*, in *Proceedings of the 8th Symposium on Engineering Problems of Fusion Research* (1979), p. 972.
- [17] W. L. Gardner, G. C. Barber, C. W. Blue, *et al.*, Rev. Sci. Instrum. **52** (1981) 1625.
- [18] W. L. Gardner, G. C. Barber, C. W. Blue, *et al.*, Rev. Sci. Instrum. **53** (1982) 424.
- [19] S. C. Bates, C. E. Bush, P. H. Edmonds, *et al.*, *ISX-B Neutral Beams and the Beam Target Experiment*, Report ORNL/TM-7452, Oak Ridge National Laboratory (1980).
- [20] M. M. Menon, R. N. Morris, and P. H. Edmonds, in *Proceedings of the 11th Symp. Fusion Engineering*, IEEE CAT# CH2251-7 (1985), p. 1269.
- [21] J. A. Paterson, C. F. Chan, M. Y. Fong, *et al.*, *LLNL Beam*, Report No. CH2251-7/86/0000-0153, pg. 153, IEEE (1986).
- [22] A. Molvik, in *Proceedings of the 8th Symposium on Engineering Problems of Fusion Research*, Pub. No. 79CHH1441-5 NPS (IEEE, 1981), p. 661.
- [23] E. R. Solano, Phys. Plasmas (to be published) (1995).
- [24] G. Counsell and M. Cox, personal communication (1995).
- [25] M. E. Fenstermacher, personal communication (1991).

- [26] N. A. Uckan, *ITER -Physics Design Guidelines*, Report ITER Document Series No. 10, IAEA, Vienna (1990).
- [27] P. M. Valanju, J. Comp. Phys. **88** (1990) 114.
- [28] D. Heifetz, D. Post, M. Petravic, *et al.*, J. Comp. Phys. **46** (1982) 309.
- [29] B. Lloyd, G. L. Jackson, T. S. Taylor, *et al.*, Nucl. Fusion **31** (1991) 2031.
- [30] A. Sykes, M. Bevir, R. A. Bamford, *et al.*, in *Plasma Physics and Controlled Nuclear Fusion Research 1994*, (International Atomic Energy Agency, Vienna, 1995), Vol. 1, p. 719.
- [31] C. B. Forest, *Pressure Driven Currents in CDX-U Trapped Particle Configuration*, Ph. D. Dissertation, Princeton University (1992).
- [32] C. B. Forest, Y. S. Hwang, M. Ono, *et al.*, Phys. Rev. Lett. **68** (1992) 3559.
- [33] C. B. Forest, Y. S. Hwang, M. Ono, *et al.*, Phys. Plasmas **1** (1994) 1568.
- [34] A. Sykes, Y.-K. M. Peng, J. W. Connor, *et al.*, in *Plasma Physics and Controlled Nuclear Fusion Research 1994*, (International Atomic Energy Agency, Vienna, 1995).
- [35] B. Lloyd and T. Edlington, Plasma Phys. Controlled Fusion **28** (1986) 909.
- [36] D. R. Whaley, T. P. Goodman, A. Pochelon, *et al.*, Nucl. Fusion **32** (1992) 757.
- [37] Y. M. Li, S. M. Mahajan, and D. W. Ross, Phys. Fluids **30** (1987) 2101.
- [38] R. I. Pinsker, F. W. Baity, S. C. Chiu, *et al.*, in *Proceedings of the 21st European Phys. Soc. Conf. on Controlled Fusion and Plasma Physics*, Montpellier, (European Physical Society, 1994), Vol. 18B, Part III, p. 1118.
- [39] R. Majeski, C. K. Phillips, and R. Wilson, Phys. Rev. Lett. **73** (1994) 2204.
- [40] M. Porkolab, in *Proceedings of the AIP Topical Conference on Radio Frequency Power in Plasmas*, edited by D. B. Batchelor, Charleston SC, (American Institute of Physics, 1992), p. 197.
- [41] V. P. Bhatnagar, J. Jacquinet, and J. team, *Fast Wave Heating and Current Drive Scenarios for JET and ITER*, Report JET-P(94)23, submitted to Fusion Engin. & Design, JET (1994).
- [42] S. Puri and R. Wilhelm, in *Proceedings of the 8th Topical Conf on Radio Frequency Power in Plasmas, 1989*, edited by R. McWilliams, Irvine, (AIP Conf Proc 190, 1989), p. 458.
- [43] S. C. Chiu, V. S. Chan, R. W. Harvey, *et al.*, Nucl. Fusion **29** (1989) 2175.
- [44] A. Jaun, K. Appert, J. Vaclavik, *et al.*, in *Proceedings of the Sherwood Theory Conference*, Lake Tahoe, NV, (1995).
- [45] A. Jaun, *Linear Wave Propagation in a Hot Axisymmetric Toroidal Plasma*, Report LRP 513/95, École Polytechnique Fédérale de Lausanne - Suisse (1995).
- [46] E. F. Jaeger, D. B. Batchelor, and D. C. Stallings, Nucl. Fusion **33** (1993) 179.
- [47] P. H. Probert, S. Oliva, G. R. Winz, *et al.*, submitted to Nucl Fusion (1995).
- [48] T. E. Evans, P. M. Valanju, J. F. Benesch, *et al.*, Phys. Rev. Lett. **53** (1984) 1743.
- [49] W. D. Booth, M. E. Oakes, and P. M. Valanju, Phys. Fluids B **2** (1990) 2024.
- [50] G. G. Borg and B. Joye, Nucl. Fusion **32** (1992) 801.
- [51] M. Ono, G. J. Greene, D. Darrow, *et al.*, Phys. Rev. Lett. **59** (1987) 2165.
- [52] J. B. Taylor, Phys. Rev. Lett. **33** (1974) 1139.

- [53] R. R. Mett and J. B. Taylor, Phys. Fluids B 4 (1992) 73.
- [54] R. R. Mett, Phys. Fluids B 1 (1992) 225.

CHAPTER 8

DIAGNOSTICS, CONTROL, AND DATA ANALYSIS

8.1 Overview

We have specified the USTX diagnostics set with the following four goals in mind:

- It must provide the necessary machine-control functions and, where feasible, measure all relevant plasma parameters. Diagnostics necessary for control of the machine and power supplies must be available for first operation.
- Diagnostics that are necessary for plasma control and characterization must be reliable and available daily. When possible, we attempt to measure profiles rather than single point measurements, but severe financial constraints are a limitation. We will use digital feedback systems whenever possible, which were successfully employed in TEXT-U operation.
- Where possible, the diagnostics will exploit the unique features of the machine design. For example, the small central-core size allows a Thomson scattering view of virtually the whole plasma using a laser beam injected horizontally .
- To be economical, both in terms of manpower and hardware costs, it should, as far as possible, use the diagnostic facilities from TEXT-U.

8.2 Proposed diagnostics set

Table 8.1 lists the proposed diagnostics for USTX, grouped by the parameter being measured. We divide the diagnostic set into *baseline diagnostics* and *special-application diagnostics*. The baseline diagnostic set is comprised of those which constitute the control diagnostics, e.g., position control, and provide the basic plasma characterization, e.g., plasma current, density, and temperature. These baseline diagnostics will be available within one year of beginning operation. The special application diagnostics are desired, but not funded in this proposal. Several of the diagnostics in the baseline set are further

designated *day-one diagnostics*. These must be available for the first discharges at machine startup, and they diagnose a minimum set of physics and engineering parameters necessary for routine machine operation. In most cases, more than one diagnostic has been listed for a parameter to ensure reliability, particularly in the case of the day-one set. In the table, "Category" indicates whether the diagnostic is to be considered *day one* (D1), *baseline within first year* (Y1), or *special application* (SA). "Status" represents the status of an equivalent diagnostic on TEXT-U: *in normal use* (N), *available upon request* (A), or *will require modification* (M) for use on USTX.

Table 8.1. Proposed USTX diagnostics grouped by the parameter measured.

Plasma Parameter	Category	Status	Proposed Diagnostic
Plasma Current, Position, and Shape Control	D1	N	Magnetics
	D1	N	CCD Camera
	D1	N	H α Detectors
	D1	N	Soft X-ray Arrays
n_e	D1	N	2 mm Interferometer
	D1		Reflectometry
	Y1	M	Far-infrared Interferometry
MHD Activity	D1	N	Magnetics
	Y1	N	Soft X-ray Arrays
	SA	A	Heavy Ion Beam Probe
Hard X-rays	D1	N	Hard X-ray Detector
Limiter Heating	D1	N	Infrared Camera
	D1	N	Thermocouples
n_i	Y1	N	Spectroscopy
	SA	A	Charge-exchange (Neutral Particle)
n_Z	Y1	N	Spectroscopy
	SA	A	Charge-exchange Recombination Spectroscopy
T_e	Y1	N	Thomson Scattering
	Y1	N	Soft X-ray PHA
	Y1	N	Soft X-ray Diode Array
T_i	SA	A	Charge-exchange Recombination Spectroscopy
	Y1	N	VUV/UV Spectroscopy
Plasma potential ϕ	SA	A	Heavy Ion Beam Probe

Table 8.1. (continued)

Plasma Parameter	Category	Status	Proposed Diagnostic
Current density $J(r)$	SA	A,M	Faraday rotation
	SA	A	Charge-exchange q diagnostic
	SA		Magnetic reconstruction
	SA	A	Heavy Ion Beam Probe
Energy Content, β	D1	N	Diamagnetic Loop
	Y1	N	Thomson Scattering + magnetics
P_{rad}	Y1	N	Bolometers
	Y1	N	Spectroscopy
	SA	N	X-UV Photodiodes
Core fluctuations \tilde{n}_e	SA	A,M	Far-infrared Scattering
	Y1		Microwave Reflectometry
	SA	A	Beam Emission Spectroscopy
	SA	A	Heavy Ion Beam Probe
	SA	M	Phase Contrast Imaging
Core fluctuations $\tilde{\phi}$	SA	A	Heavy Ion Beam Probe
Core fluctuations \tilde{T}_e	SA	D	Dual-laser Thomson Scattering
Edge fluctuations \tilde{n}_e	Y1	N	Electrostatic probes (also for \tilde{T}_e)
	Y1	A	H α diagnostics
	SA	A	FIR Scattering
Edge fluctuations $\tilde{\phi}$	Y1	N	Electrostatic probes
Rotation velocity	Y1	A	Spectroscopy
	Y1	A	Mach Probes
	Y1	A	Electrostatic probes
	SA	A	Charge-exchange Recombination Spectroscopy
	SA	A	Heavy Ion Beam Probe
	SA	A	FIR Scattering
Divertor & Edge	Y1	N	Electrostatic Probes
	Y1	A	Tile Probes
	Y1	N	Spectroscopy
	SA	A	Retarding Field Energy Analyzer
	D1	N	H α monitors
	D1	N	CCD Camera
	D1	N	Fast neutral pressure gauge
	D1		Thermocouples
	SA	N	Divertor Thomson Scattering
	D1	N	Bolometers

Figures 8.1 and 8.2 show the port allocations presently envisioned for the principal diagnostics. Figure 8.1 shows a top view of USTX with the neutral-beam injector, the location of the major diagnostics, and the proposed fast-wave current-drive antennas.

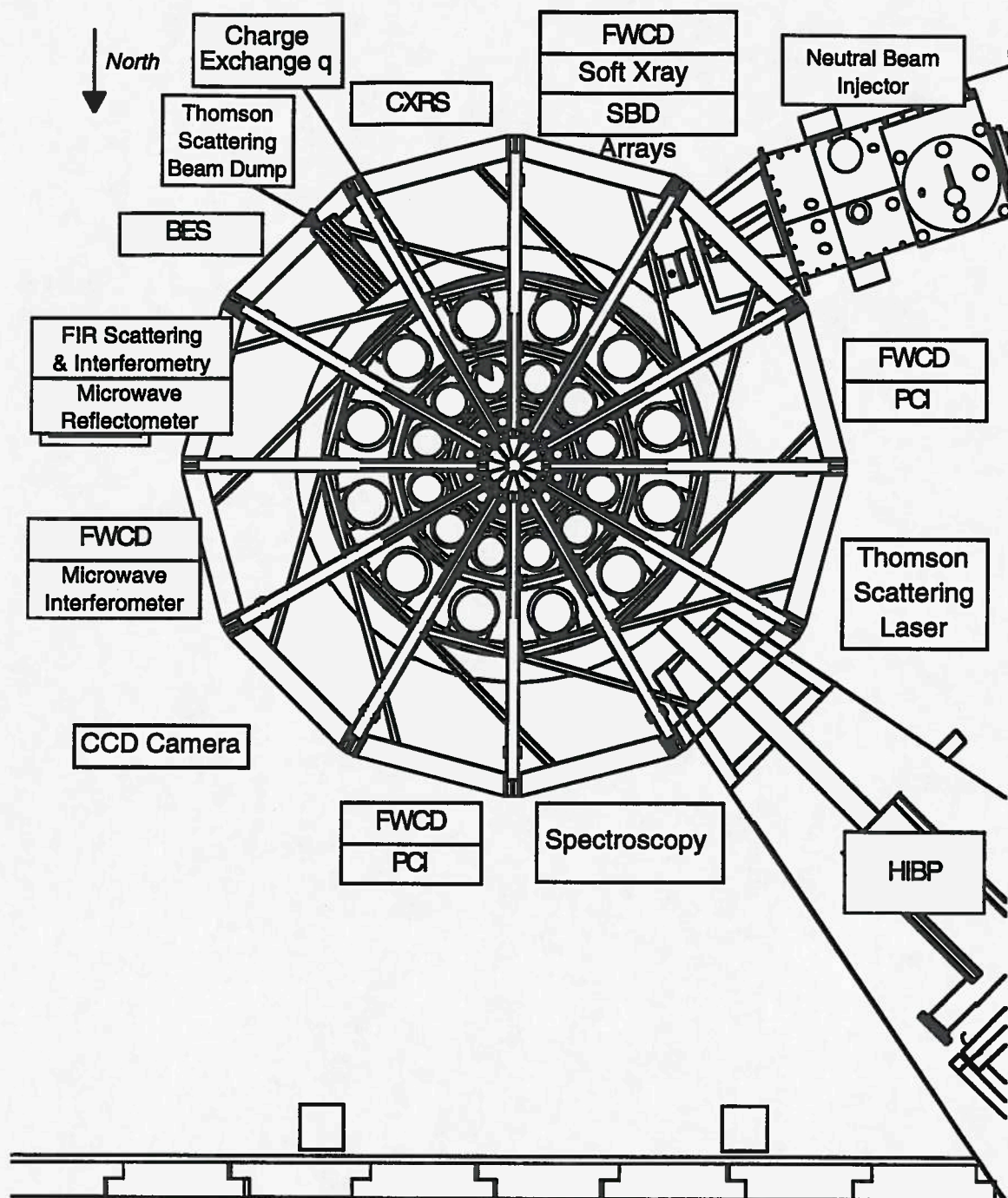


FIG. 8.1. Plan view of USTX showing layout of largest diagnostics.

Figure 8.2 is a combination projection of the USTX ports in θ - ϕ space, showing simultaneously the top, side, and bottom ports. The north half of USTX is shown above the south half. Again, only the principal diagnostic locations are indicated.

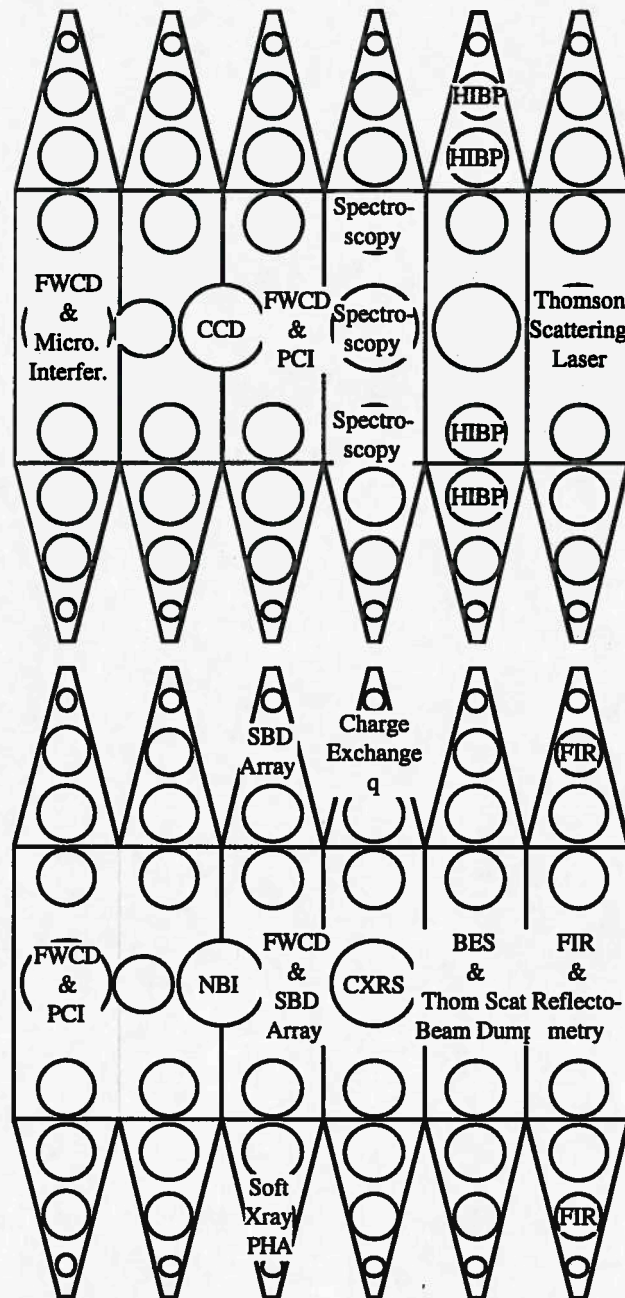


FIG. 8.2. Exploded view of the 12 segments with diagnostic port assignments.

8.3 Selected diagnostics and the needs of USTX

Magnetics and control

The signals necessary for feedback control of plasma position and shaping will be derived primarily from a set of magnetic pickup coils located inside the vacuum vessel. The coils, which will sample the radial and poloidal fields at many locations, will be mounted inside a set of thin protective stainless-steel tubes at the vessel wall. On the inside wall, near the solenoid, the tubes will be further protected by the limiter tiles. The tubes will be thin enough to allow a frequency response of 200 kHz, which, coupled with newly designed drivers, will allow the position and shaping coils to also function as MHD coils.

A similar mounting and stainless-tubing protection scheme will be used for the plasma-current Rogowski coils and diamagnetic loops. Due to the difficulty of repairing the coils in case of failure, duplicate sets of position, Rogowski, and diamagnetic coils will be installed inside the vacuum vessel. Loop voltage "flux loops" will be installed inside the vacuum vessel at the corners and additional locations. For MHD studies locked-mode detection coils will be installed. Additional position monitoring systems will be based on a soft X-ray array and/or H_{α} monitors.

Density

For initial USTX operation for densities less than $5 \times 10^{19} \text{ m}^{-3}$, a 2 mm microwave interferometer, using parts already in-house, will provide routine line-averaged density and perhaps density-feedback control. A reflectometry system will measure the electron-density profile and provide density feedback control. Presently operating reflectometry systems on DIII-D have demonstrated sub-centimeter spatial resolution. The wide range of density and toroidal-field spatial variation on USTX will require systems operating over multiple frequency bands. In addition, reflectometry can provide localized information on the fluctuation distribution in the plasma edge and core. This will be especially useful for later RF current-drive experiments. Horizontal launch for reflectometry and 2 mm interferometry will make these systems relatively insensitive to plasma in-out movements.

A multi-channel heterodyne FIR polarimeter/interferometer will be used to measure the electron and current-density profiles. Only the FIR interferometer is funded in this proposal. Both vertical and horizontal views are desirable because of the asymmetric plasma configurations and the limited port access. Due to the large plasma size and high

density, it is likely that the FIR laser source frequency will need to be increased from that of the TEXT-U system to minimize the effects of long path length and refraction. It is anticipated, and desired that the polarimeter/interferometer be provided by a collaboration, as was done on the TEXT and TEXT-U tokomaks in collaboration with Dr. David Brower of UCLA. The costs of polarimetry are not included in this proposal.

Other baseline diagnostics

The small size of the transformer core provides an opportunity for horizontal-viewing diagnostics to view nearly all of the plasma. A two-dimensional tomographic reconstruction technique should be particularly well-suited to these views. To the greatest extent possible, plasma emission diagnostics, including spectroscopy, bolometry, soft x-ray arrays, and soft x-ray pulse-height analysis, will be adapted to take advantage of these views.

For Thomson scattering, a minimum-cost system will be constructed using the laser and detector from the existing TEXT-U system, with some new optics. The new system will use horizontal launch with the beam entering almost radially, passing near the center column and exiting through a port to a beam dump. A five-channel scannable detector array mounted on the top or bottom would provide good plasma coverage and yield high-spatial-resolution n_e and T_e profiles. A second system is planned with the laser intercepting the divertor region and output optics coupled to a high resolution spectrometer. This will allow measurements of T_e and n_e in the edge and divertor regions.

Langmuir probes will be used on USTX to measure $T_e(r)$, $n_e(r)$ and $\phi(r)$, and fluctuations in the plasma edge and scrape-off layer. Langmuir probes will also be mounted permanently in the "natural limiter" at the top and bottom near the center post. Note: measuring turbulence wave number or turbulently driven particle flux using standard two-probe techniques may be problematic in an ST, because the relatively large ion Larmor radius sets a minimum probe separation which is comparable to the expected characteristic wavelengths. Plasma flow diagnostics including Mach probes will also be necessary on USTX for experiments related to divertor concept development.

Neutral-beam injection, not costed in this proposal, but important for heating or current drive, will also provide a source of neutrals for charge-exchange diagnostics (a role presently filled by the TEXT-U diagnostic neutral beam). We expect the TEXT-U diagnostic neutral beam will be used at MIT while the spherical tokamak is under

construction but will be available for use on USTX. This is important for T_i measurements from charge-exchange neutral analysis, and impurity ion-temperature T_Z ($\approx T_i$) and toroidal-rotation measurements via charge-exchange recombination spectroscopy (CXRS). It may also be possible that the TEXT-U diagnostic neutral beam can be used to drive TAE modes to study threshold characteristics and non linear behavior. The funding requested in this proposal is only for the diagnostics in the baseline set. Additional diagnostics will require additional funding.

Core-fluctuation diagnostics

Since turbulent fluctuations have been considered a leading candidate to explain core particle and energy transport [1-3], it is important to have several techniques for measuring fluctuations on USTX. This is especially true since the various diagnostics, listed below, cover different regions of physical and wave number space. Diagnosing turbulent plasma fluctuations is an area of specialization of the FRC. All of the following diagnostics are available, but their implementation is not costed in this proposal.

- Far-infrared scattering (FIR) measures the frequency spectrum, and wave-number characteristics of density fluctuations in the plasma core and edge. It can measure fluctuations with wave number $k > 1 \text{ cm}^{-1}$, although it has restricted spatial resolution for $k < 5 \text{ cm}^{-1}$. Shifts in the frequency spectrum can also be used to estimate the radial electric field.
- The heavy-ion beam probe (HIBP) measures plasma electric-potential profiles, as well as density and potential fluctuations and their correlations, from which the resulting particle flux can be inferred. It can measure fluctuations with wave numbers $0.1 < k < 2 \text{ cm}^{-1}$. The HIBP is also unique in that it can measure the low m,n structure of \tilde{B} for the internal MHD modes [4]. Most of the present 2 MeV HIBP hardware on TEXT-U will be used on USTX; however, the use of lower mass ions, such as rubidium or potassium will be advantageous. (Cesium and thallium are currently used.) In addition, the large ratio of poloidal to toroidal magnetic field and the size of the region outside the vacuum vessel (but inside the toroidal-field returns) will require a new beam line with additional magnetic shielding and possibly additional beam steering.
- Beam-emission spectroscopy (BES) measures density fluctuations at the intersection of its field-of-view with the diagnostic neutral beam, with a

resolution as low as 0.2%. The wave number range of the fluctuations observable by BES, as determined by multi-point correlation techniques is $k < 5 \text{ cm}^{-1}$. Background rejection will be improved for USTX over TEXT-U, as we expect to be able to resolve a beam-induced Doppler shift at all plasma radii.

- Phase-contrast imaging (PCI), demonstrated on TEXT-U, provides a direct spatial representation of the plasma waves. It should be an excellent diagnostic for low m,n modes and will also be important in studying driven RF waves on USTX. It is sensitive only to waves perpendicular to the beam, and measurements are integrated along the beam path. However, it has a large wave-number range, typically $0.5 \text{ cm}^{-1} < k < 12 \text{ cm}^{-1}$, and a high sensitivity, typically 10^{14} m^{-3} . The TEXT-U PCI system should be usable on USTX with little modification.
- Thomson scattering is used to measure electron temperature and density profiles. Advances in high-sensitivity optical imaging techniques [5] allow one to obtain very high spatial resolution, of the order of 1 mm, which is comparable to, or better than, that of Langmuir probes. This resolution is sufficient to diagnose the turbulence responsible for transport in the tokamak edge. We propose to apply these high-resolution techniques to the USTX Thomson scattering diagnostic. The high-resolution time history of fluctuations is important in identifying the unstable plasma oscillations which may be responsible for transport. Conventional Thomson scattering has very good time resolution (about 50 ns) but with a very slow repetition rate. We propose to overcome this drawback in USTX with a two-laser system capable of firing pulses with arbitrary relative delay. This flexibility would allow us to construct a time correlation function of the temperature and density fluctuations on a shot-to-shot basis from a large number of similar discharges. The proposed technique would be applicable to in-depth studies of specific and reproducible plasma conditions.

Current-Density Profile

As has been mentioned in previous sections, diagnosing the current profile obtained in USTX is of crucial importance in exploring plasma stability, determining pulse-length capability, and studying bootstrap and non-inductive current drive. Of the techniques that

have been developed on TEXT-U to measure current-density profiles, at least two could be transferred to USTX: FIR polarimetry and the charge-exchange q diagnostic.

The TEXT-U FIR polarimetry system presently produces current-density profiles (Fig 8.3). With the conversion of the present polarimetry system to higher frequency and multiple views (e.g. horizontal and vertical) will also come the possibility of producing 2-D current-density profiles. It is anticipated that polarimetry diagnostic will be done by a collaboration with an external user and is not costed in this proposal.

In addition to polarimetry, a novel approach to measuring the poloidal field was recently developed on TEXT-U [6]. This technique allows inference of the poloidal field by measuring the trajectory of ions created from charge-exchanged neutral-beam particles. Results and progress so far have been encouraging. Due to beam attenuation by the plasma, the charge-exchange q diagnostic will be most useful in obtaining q profiles in the large-major-radius portion of the plasma.

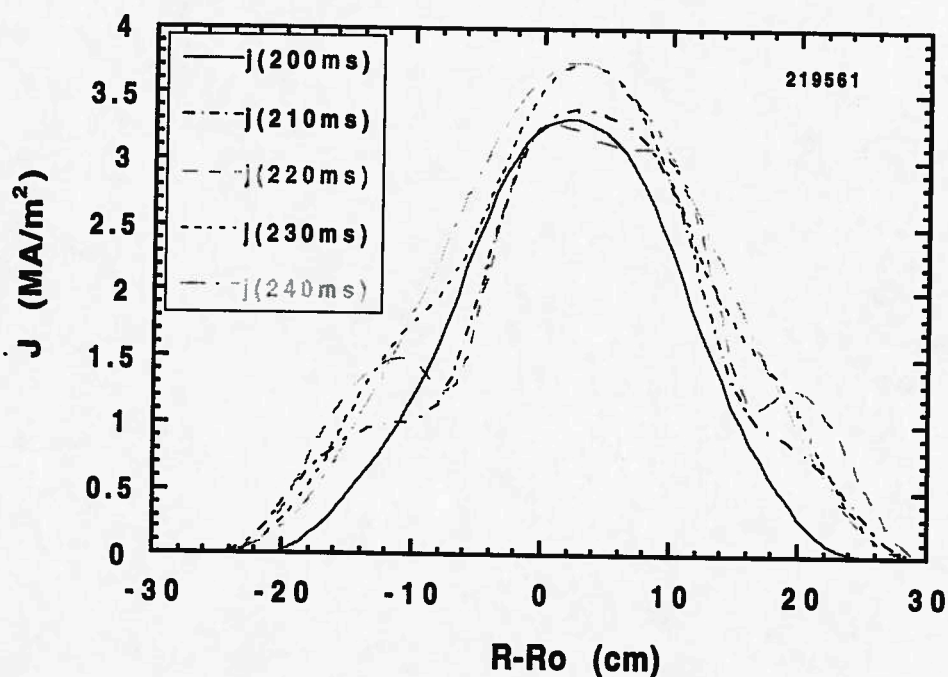


Figure 8.3. Current-density profiles inferred from FIR polarimetry data during a fast current ramp-up experiment, showing current diffusion from the edge to the plasma core.

8.4 Data acquisition and analysis

The TEXT computer system consists of a three-computer VAX cluster with 10 GBytes of disk storage and two IBM RS-6000 (RISC) computers with 2.5 GBytes of disk storage. All computers are members of an Internet Ethernet network. Cross-platform access is provided by remote login, network file system remote mounting, and remote procedure calls (RPC's). Local user access to the TEXT computer system is provided by about 70 Macintosh personal computers running terminal-emulation software. Remote access is available over Internet or by using the UT Computation Center's SLIP dial-up connection.

The TEXT data system is based on byte-serial fiber-optic CAMAC hardware that is accessed using the Oak Ridge CAMAC device driver interface software. Data can be read from the CAMAC modules at a rate of about 2.5 MBytes/min. The data system provides a unified diagnostic support facility. The data program automatically obtains data from the CAMAC modules on each shot and writes it to an archive shot file. Utility programs and subroutines facilitate user control of the CAMAC modules and provide user access to the archived data. A graphics utility program allows any user to view the data from any channel in the disk archive. User-written data analysis programs may access the disk archive by using a number of subroutines contained in libraries. Programs running on the VAX cluster may access the archive files directly. Programs running on an IBM RS-6000 may access the archive files using RPC's. The following commercial software packages are available on the VAX cluster: IDL, IMSL, Template, and INGRES. Access to data by external users is provided either by remote logon to the VAX cluster or through RPC's.

Experimental profile analysis is presently performed using the in-house 1-D, time-independent code TEXTRAN run on a local VAX 8350. The input is extracted from the INGRES database TEXTDB [7] and transformed into flux coordinates using transformation grids provided by an equilibrium code (PSICONT, EFIT) run earlier. The outputs (input profiles transformed into flux coordinates, particle and heat fluxes, etc.) are in turn written into the INGRES database on a fixed r/a grid.

TEXTRAN presently has no capability to compute auxiliary-heating deposition profiles and must read them as input. Likewise, there is no modeling of the plasma scrape-off layer for diverted plasmas. These deficiencies must be addressed for USTX, either by integrating external code "modules" performing individual tasks (NBI deposition profiles,

etc.), or by replacing TEXTTRAN in favor of one of the larger transport analysis codes (e.g. SNAP), retaining perhaps only the database interfaces.

For comparison of profile data between devices, the Magnetic Fusion Energy Database (MFEDB) is a profile-oriented database for storing experimental data from a variety of toroidal magnetic confinement devices. It was developed at the Fusion Research Center to provide the MFE community with complete sets of experimental data from a variety of machines and discharge conditions. The expertise obtained during the development of this database will be a direct benefit to the USTX effort. Tools that have been developed for the MFEDB such as the Mathematica Database Interface MDI [8] can be used to store and analyze experimental data from USTX.

References to Chapter 8

- [1] P. C. Liewer, Nucl. Fusion **25** (1985) 543.
- [2] R. V. Bravenec, K. W. Gentle, B. Richards, *et al.*, Phys. Fluids B **4** (1992) 2127.
- [3] B. Richards, M. E. Austin, R. V. Bravenec, *et al.*, Nucl. Fusion **32** (1992) 567.
- [4] V. J. Simcic, T. P. Crowley, P. M. Schoch, *et al.*, Phys. Fluids B **5** (1993) 1576.
- [5] N. Lopes Cardozo, Phys. Rev. Lett. **73** (1994) 256.
- [6] P. M. Valanju, L. Duraiappah, R. D. Bengtson, *et al.*, Rev. Sci. Instrum. **66** (1995) 369. **66** (1995) 369.
- [7] J. C. Wiley, W. H. Miner, Jr., R. V. Bravenec, *et al.*, Rev. Sci. Instrum. **60** (1989) 1286.
- [8] J. C. Wiley, W. H. Miner, Jr., and D. W. Ross, *MDI: Mathematica Database Interface for the MFEDB*, Report FRCR #411, The University of Texas (1992).

CHAPTER 9

USTX RESEARCH PROGRAM

Here we outline the research program for USTX. It is determined by the mission statement (see Executive Summary) and implied by the experimental program and 'deliverables' found in chapter 1. First various alternative schedules are discussed. Then details are given of some of the more important parts of the experimental program. Note that while the device is designed to allow modifications including an $A = 1.25$ option, neutral beam injection heating and radio frequency current drive, we concentrate here on the ohmic heated plasma capabilities with a nominal $A = 1.43$.

9.1 Experimental schedule and alternatives

We recognize that there is a diversity of opinion as to what is the optimum strategy for experimentally testing low-aspect-ratio tokamaks, and what are the optimum machine sizes to achieve the desired goals. In particular, it has been suggested that the most exciting regimes are at $A \approx 1.25$, and that USTX should immediately address this value, ignoring the $A = 1.43$ point. Alternatively, it has been suggested [1] that $A \approx 2$ is the optimum value to explore.

Concerning an $A = 1.25$ option, the best machine to build (i.e., the optimum ohmic core, inner toroidal-field leg and vacuum-vessel inner cylinder) depends on many as yet unknown parameters. These unknowns include the maximum inductive plasma current which can be driven, the operational limits (especially the density limit), the optimum neutral-beam energy, the pulse length required (longer pulses require a larger inner toroidal-field leg and ohmic core), the TF required (larger fields require larger TF legs), the confinement and impurity properties (will the plasma suffer radiation induced disruptions?), the possible current rise times (which determine the initial internal inductance, and thus the ohmic current itself), and the volts per turn (which partly determines plasma current and pulse length).

In consideration of these many unknown parameters, our plan is to initially complete the design, and construct and operate the $A = 1.43$, $I_p = 1$ MA option, which can

operate in the range $1.33 < A < 2$. A part of the experimental program will then be to determine the parameters necessary to design the optimum $A = 1.25$ (or lower) case.

9.2 Experimental Studies

Here we describe some of the experiments we wish to perform with the $A = 1.43$ point design. Many of these experiments will be performed as functions of the parameter A itself, which can be modified by moving the plasma onto either the inner or outer wall (see Fig. 4.3, the R_0 - A space), or by re-deploying the rail limiters presently on TEXT. Table 9.1 summarizes the important physics issues, together with the capabilities of USTX. These issues and capabilities are expanded on in what follows.

Preparatory studies

These include commissioning diagnostics, commissioning wall preparation techniques (baking, boronization, glow cleaning, Taylor pulsed-discharge cleaning), and commissioning the plasma shape and position control systems. We expect to utilize soft X-ray arrays to assist in plasma position measurements and control; the required techniques were successfully developed on TEXT. The large vessel volume, necessary to maintain flexibility, implies that careful vessel preparation will be necessary. All the proposed wall preparation techniques were employed on TEXT.

Operational regime studies

One of the first objectives is to determine and compare with models those parameters which were assumed in the machine design, and which would be needed for the design of any other low- A tokamak (e.g. an $A = 1.25$ option). They include

- the ohmic primary to plasma coupling coefficients,
- the range of achievable plasma-current rise times,
- plasma current-density profiles and associated internal inductances,
- volts per turn,
- density limits,
- safety factor limits,
- the minimum operable toroidal field consistent with reliable plasma breakdown, and
- the range of shapes (κ and δ) available and their influence on the above items.

The experiments to study some of the parameters tabulated above require a plasma current-density profile, $j_\phi(r)$, diagnostic. Until the relevant diagnostic is working routinely, preliminary information on $j_\phi(r)$ will be obtained by imposing constraints on equilibrium reconstructions. Such constraints include assuming neoclassical resistivity, locating the position of rational surfaces from sawtooth or tearing mode activity (if either are present), and any limited polarimetry data available.

Table 9.1. The physics issues which can be studied with USTX, assuming only ohmic heating.

Physics Issues	USTX capability (OH only)
Plasma initiation and ramp-up	Yes
Plasma control and operational space	Yes
MHD (reconnection events, sawteeth, tearing modes, disruptions)	Yes
Confinement	Yes. Scaling with dimensional and dimensionless parameters. Expect OH - H mode and reversed magnetic shear regimes. ($\tau_E = 20 - 90$ ms).
Turbulence	Yes (existing diagnostics)
High β , β_N	Yes. $\langle\beta\rangle_{\max} \approx 30\%$, $\beta_{N\max} \approx 4$
Low collisionality	Yes. $v_{*min} \approx 0.1$
Bootstrap current	Partial. $f_{bs\max} \approx 0.1$
Advanced Tokamak Scenarios (high bootstrap fraction, high β and β_N , high confinement, divertor)	Partial. Highest values not available simultaneously. This requires upgrade to neutral beam.
SOL and divertor physics.	Yes
RF current drive	Partial. Basic wave penetration and absorption studies.

"Yes": definitive information will be available with the ohmic heated device (but excluding any specific auxiliary heating effects)

"Partial": limited information available, \Rightarrow complete with available upgrades.

Concerning the operational space, Figure 9.1 illustrates the predicted variation in plasma current with plasma major radius. The aspect ratio varies as the plasma major radius R_0 is varied because the plasma is restricted by either inner or outer wall contact. No account has been taken of any current-drive or heating antennas occupying space at the outer equator. For comparison, results are shown for both the $A = 1.43$ point design structure under consideration here, and the possible $A = 1.25$ case. The maximum design toroidal field $B_{T0} = 0.5$ T and $q > 3.2$ are applied. The specific calculations shown assume a plasma internal inductance $l_i \approx 0.7$ for the $A = 1.43$ point design and $l_i \approx 0.3$ for the $A = 1.25$ upgrade case. Figure 9.2 shows the calculated Greenwald density limits [2] for the two cases, again as R_0 (and hence A) is varied. Verification of the large density values shown is important because the Greenwald limit partly determines the design of any future $A = 1.25$, neutral beam heated upgrade (because density determines neutral beam penetration).

Our second objective, closely related to the first, is to categorize at low A the phenomena which limit operation of a normal-aspect-ratio tokamak, e.g., disruptions, axisymmetric instabilities, carbon blooms, tearing modes, locked modes, and sawteeth). All these phenomena except carbon blooms have been studied on TEXT. A large part of this work involves MHD studies, requiring complete magnetic diagnostics and locked-mode coils.

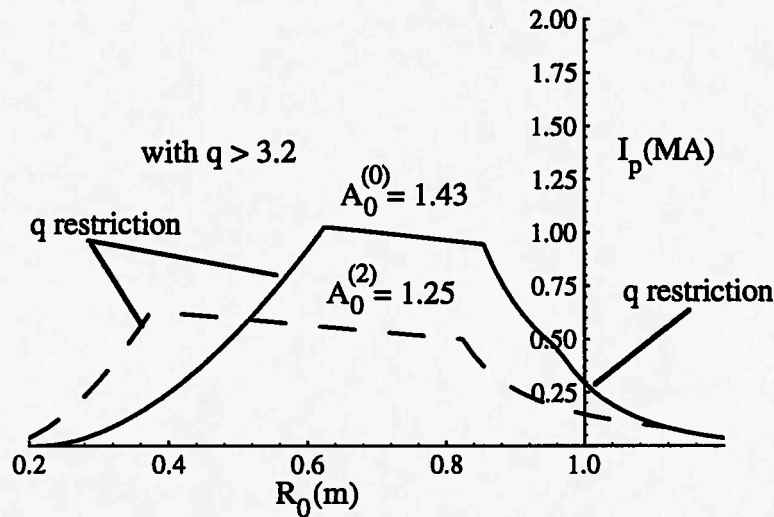


FIG. 9.1. The maximum plasma current with $q > 3.2$ applied as a function of R_0 for the nominal $A = 1.43$ point design (solid line) and an $A = 1.25$ upgrade (broken line).

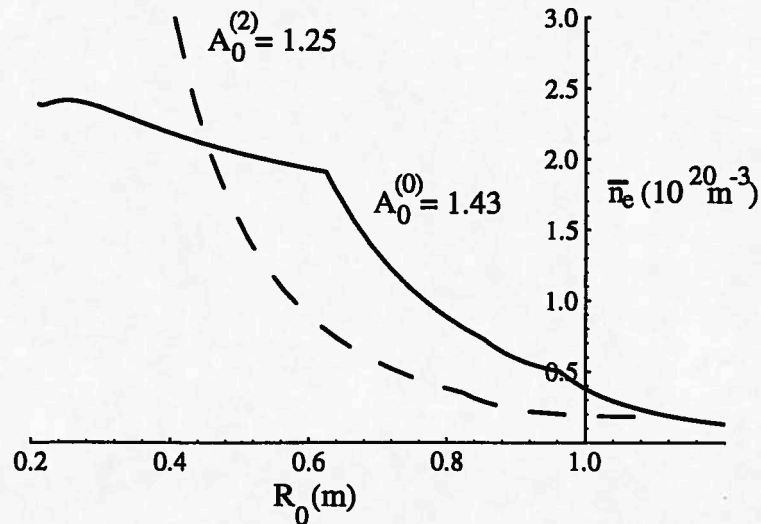


FIG. 9.2. The Greenwald density limit for the nominal $A = 1.43$ point design (solid line) and a nominal $A = 1.25$ upgrade (broken line), both operating at maximum current, as R_0 (and thus A) is varied.

Our third objective is to explore whether the many different but distinct operational regimes found in ohmic heated plasmas at normal aspect ratio exist at low aspect ratio, e.g.,

- improved ohmic confinement (IOC),
- ohmic H mode (in particular, to study the L-H transition threshold power),
- biased-electrode H mode,
- detached plasmas, and
- ELM's.

All of these except ohmic H mode have been studied on TEXT. Detailed profile diagnostics, including one of the plasma potential, are required to monitor any changing gradients. The plasma potential profiles can be measured by Langmuir probes at the edge, and by either spectroscopy (rotation) or the existing heavy-ion beam probe (HIBP) in the interior. However, the HIBP is not available during the first year of operation, and is not included in the costing.

MHD studies

The MHD experimental program includes the following studies:

Magnetic Islands

This includes monitoring tearing and locked modes, and investigating any islands introduced by the primary windings, feeds, joints and crossovers.

Current ramp-up

Because it is intended to utilize fast inductive current ramp-ups to create hollow current profiles (with low I_i), and because it is desirable to reach maximum current as soon as possible to conserve power supply energy for the current flat top, we will investigate this phase in detail. We will repeat the experiments performed on TEXT, namely seeking correlations between the rate of rise of plasma current, the resulting current profile, and the presence of tearing modes. When the HIBP is available, we will apply its unique capability to monitor internal magnetic mode structures [3]. The phase contrast imaging (PCI) system (not available in the first year of operation, not costed) is also suitable for identifying the density perturbations associated with the (long wavelength) tearing modes. Preparatory experiments were performed on TEXT to understand how ECH could be used for heating to modify the conductivity. Current-density and electron-temperature profiles, and any MHD instability phenomena (e.g., tearing modes) will be compared with code predictions which include both neoclassical and anomalous resistivity. The data will provide the engineering parameters (e.g., the Ejima factor) necessary to design future low-A machines.

Sawteeth

The plasma current profiles are expected to be constrained by sawteeth. Preliminary theoretical data suggest that low A can decrease the growth rate of modes at the $q = 1$ surface (Sec. 3.3 and Ref. [4]). The effects of neoclassical resistivity are expected to be important. It has been speculated that sawteeth may help to maintain hollow profiles, and this will be explored, and the effects of bootstrap current and current profile control will be investigated.

The sawteeth will also be used as a source of temperature variations for heat-pulse studies, and of temperature gradient changes for determining the sensitivity of any measured turbulence to the temperature gradient itself. In this way we hope to determine whether the turbulence responds linearly to a drive, or if the concept of a critical gradient is applicable. Preliminary experiments on TEXT [5] indicated that a critical gradient

model is applicable to a turbulence feature that has many of the expected characteristics of dissipative trapped-electron drift waves.

Internal Reconnection Events

These events, which expel current from the center of the plasma and reduce total current, will be investigated.

Disruptions

The START experimental result that no disruptions occur at low A will be tested. The data should determine whether the START result is specific to low aspect ratio (because of different stability properties, for example) or is a result of the particular combination of the magnetic and material structural geometry in START. It is known that certain geometries are more resilient to current perturbations than others [6].

Beta limits

The predictions for USTX show that $\beta_T \approx 30\%$ and $\beta_N \geq 3 - 4$ may be accessible with ohmic heating alone. Whether or not these values can be accessed depends first on the confinement properties which occur, secondly on whether the required current-density profiles can be produced, and thirdly on whether a conducting wall (with a rotating plasma) is necessary. The results from DIII-D emphasize the importance of controlling shape, and we will attempt to repeat their experiments but at the low- A values accessible in USTX. A partial wall inside the vessel will be installed if necessary. We expect to make use of soft X-ray arrays for mode identification in this study.

By measuring the maximum beta as a function of shape, aspect ratio, and plasma current density profile we hope to be able to provide a test of the Troyon model. The experiments would first quantify the effects of reducing A at a fixed shape, then determine the effects of changing shape at fixed low A .

Confinement studies

Global confinement

Here the objective is to determine the characteristics (i.e., *scaling relations*) for energy, particle, impurity, and possibly momentum confinement (the latter using a biased

electrode to apply a driving force), in terms of both machine parameters and dimensionless variables. Initially we intend to deploy a diamagnetic loop and magnetic coils; these will then be supplemented by a multi-point Thomson scattering system (for $T_e(r)$) and spectroscopy (for $T_i(r)$).

Engineering or machine parameters

It is important to compare the experimental results obtained at low A with those at normal aspect ratio, because the assumed scaling of, for example, the energy confinement time τ_E with machine parameters partly determines whether or not a low- A machine is useful as a reactor. Therefore, one of the objectives of USTX is to determine which of many assumed scaling relations, if any, best describes the observations. An upgrade to neutral beam heating would allow us to extend this study to a wider parameter range.

Dimensionless parameters

We have analyzed the capability of USTX to provide information in dimensionless parameter space β , q , A , $\rho_* = m_i v_{Ti}(0) / (Z_i e B_T a)$, and $\nu_* = \nu_e(0) \nu_{Te}^{-1}(0) R^{5/2} a^{-3/2} q$ with ν_e the electron collision frequency. Using the scaling relations outlined in chapter 4, with realistic machine parameter variations, we find for USTX that $0.05 < \beta < 0.3$, $0.005 < \rho_* < 0.015$, and $0.1 < \nu_* < 1$, where these values refer to volume averages. We have compared these values with those obtained in JT-60, DIII-D, TFTR, START, and a prototypical low- A reactor, and conclude that USTX will operate in a completely different range of ρ_* from other high-performance machines, thus allowing access to a previously unexplored regime in parameter space.

Whether it is possible within USTX itself to perform dimensionless-variable scans, for example in ρ_* , holding ν_* , q , β and A constant, depends on the actual confinement properties found in the experiment. Such experiments would best be performed after an upgrade to include auxiliary heating, and would be done by carefully varying I_p , n_e and P_{aux} according to a precise prescription which is determined once the machine-parameter scaling relation is known. We predict that in this way, ρ_* can be varied by a factor of 2, sufficient to distinguish between Bohm and gyro-Bohm scaling, and allow extrapolation to reactor conditions. Further discussion of dimensionless parameters is found in Section 4.3.

Comparing the expected dimensionless parameters in USTX with those of JT-60, TFTR, and DIII-D it should be possible to arrange for the most significant difference to be in the aspect ratio A , thus allowing a between-machine determination of the relevant A scaling.

Local confinement

The usual profile analysis will be performed to measure kinetic electron and ion thermal diffusivities over a subset of the discharges used to obtain global confinement data. The data will be used both to verify the diamagnetic loop measurements of confinement time (the loop-derived energy contains rotational and (in an upgrade) beam components not measured by the kinetic technique), and for comparison of local thermal diffusivities with transport model predictions from ion neoclassical and ion and electron turbulence theory.

The calculation of neoclassical transport coefficients at all aspect ratios and collisionalities, underway at ORNL [7, 8] is very complicated. It is not yet clear in detail how much they will be affected at small A . Apart from this, however, and other shape factors (e.g., $\chi_i \sim 1/\kappa^2$ in an ellipse [9]), we may draw some conclusions from the basic scaling

$$\chi_{i,nc} \sim \frac{(\rho_i q)^2 v_{ii}}{\epsilon^{3/2}} \sim \frac{n_i q^2}{B_T^2 T_i^{1/2} \epsilon^{3/2}}.$$

This scaling implies that we may be able to test neoclassical theory in USTX. Although the ϵ dependence by itself indicates a smaller value for low A , we will be operating at very low B_T and moderate temperature T_i in order to achieve our β goal with modest power. Although we will try to run at low q , the probability is high that we will also explore higher q , enhanced by the small aspect ratio. Thus, very large values of $\chi_{i,nc}$ exceeding 1-2 m²/s are possible, approaching the anomalous values expected.

The negative side of this argument is two-fold. First, the containment may be degraded from what we have estimated in chapter 4, reducing our probability of reaching high β . Second, neoclassical ion transport may be irrelevant in the reactor regime at much higher temperatures and magnetic fields.

As on TEXT, the radial dependence of the total particle flux will be compared with that measured by the HIBP (when available). The electron heat flux profile will be compared with an upper limit of that driven by fluctuations (see next subsection).

Transient transport

Perturbation techniques, employing sawteeth, cold waves from impurity ablation, and modulated heating, will be utilized to evaluate transport coefficients, and evidence for and against non-local transport phenomena.

Turbulence studies

Plasma core

Here the objective is to seek correlations, and hopefully explanations, for the global and local confinement properties found. The diagnostics, experimental methods and analysis techniques already developed on TEXT will be used; that is, incorporating measured fluctuation parameters such as amplitudes, wave vectors, correlation lengths, etc. into theoretical formulae. The existing HIBP, Beam Emission Spectroscopy (BES), PCI, and scattering systems will permit density and potential fluctuations to be measured. A modified Thomson scattering system will be used to measure the T_e fluctuations. (ECE is inapplicable at the fields and densities of USTX.) The HIBP will provide direct measurements of turbulence driven particle fluxes. It will also provide measurements of the radial electric field. Particular attention will be paid to poloidal asymmetries, which have been found to be very important in TEXT. The HIBP is designed to provide full coverage of a poloidal cross-section at one toroidal location. Note however that none of these fluctuation diagnostics will be available during the first year of operation, and that their implementation is not funded in the costing presented in Chapter 10.

Existing experimental turbulence data show that $k \propto 1/\rho_s$ [10], and therefore USTX may be expected to have small wave numbers ($k \approx 0.5 \text{ cm}^{-1}$). Such long wavelength turbulence will be readily measured with the diagnostics discussed above. The low aspect ratio and consequent high trapped-particle content suggest that trapped-particle modes may become dominant, allowing verification (or otherwise) of theoretical models (e.g., the dissipative trapped-electron drift wave). Some calculations, on the other hand, suggest that good curvature regions may dominate, leading to greater stability [11], as noted in chapter 3.

It has not yet been determined how to measure core magnetic turbulent fluctuations, which may be important at high β . It is not expected that any of the methods used on TEXT at low density will be appropriate for the expected high-density discharges required to obtain high beta. At low densities any X-rays produced can be analyzed for energy and flux time dependencies, and then these parameters can be interpreted in terms of a magnetic fluctuation level [12]. With the large minor radius of USTX we expect longer runaway electron confinement times, and thus higher energies, than on TEXT. Therefore corrections to the model will have to be applied to incorporate orbit averaging effects.

Edge regions

Reciprocating Langmuir probes, Mach probes and H_α/D_α arrays will be used to monitor equilibrium and fluctuating quantities. Where probes can be used, we expect to make direct comparisons between fluctuating and total particle and energy fluxes, thus directly determining the importance of turbulence. Poloidally distributed arrays will be used to monitor asymmetries and possible direct convective effects. The H_α/D_α arrays, employing three-point correlation techniques, recently developed on TEXT [13], have the advantage of allowing density fluctuations to be measured in regions inaccessible to probes, such as at the inner equator.

Advanced Tokamak Scenarios

We understand advanced tokamak scenarios to mean conditions with high confinement, high normalized beta, and high bootstrap fraction, with a magnetic configuration which allows for particle and impurity control. In addition such configurations should be maintained for times longer than plasma current density rearrangement times.

The ohmic heated stage of USTX should attain conditions suitable for studying all of the above conditions individually except high bootstrap fraction, but not simultaneously. Concerning confinement, the ohmic input power exceeds that predicted to access H mode. Reversed magnetic shear configurations, found to exhibit improved confinement, can be transiently achieved and controlled by varying the plasma current ramp rate and how any ECRH is applied during the current ramp. Table 9.2 summarizes the predicted parameters required to maximize β_N . All of the above conditions can be achieved in magnetic geometry suitable for poloidal divertor studies (see below).

However, in order to achieve these conditions simultaneously, and for long times, and to study high bootstrap fraction, the planned upgrades (neutral beam heating, radio frequency current drive) must be implemented.

Table 9.2. The optimized plasma parameters to achieve high normalized beta

Optimized Parameter	I_p (MA)	A	R_0 (m)	$\langle n_{e20} \rangle$ (m ⁻³)	τ_E (ms)	β_N	$\langle \beta \rangle$ (%)
Value	1.05	1.49	0.64	1.16	68.8	4.32	35.3

Non-inductive start-up and current-drive studies

It is clear from the preceding discussions (see e.g., chapter 2) that the plasma current profile is expected to broadly impact USTX performance and research objectives. It is thus also a general objective on USTX to develop efficient non-inductive methods for shaping the profile at a variety of stages throughout the evolution of the discharge. Some of these methods are already well established in tokamaks. However, at low aspect ratio there will be new physics to explore; particularly with regard to the enhanced roles of pressure-driven currents and particle trapping [14]. Because there is general interest in investigating ultra-low aspect ratios which preclude the use of inductive startup, time will be devoted to understanding how to create plasma currents, starting from zero current, completely non-inductively.

Experiments on electron-cyclotron resonance heating (ECRH) and current initiation are planned as described in chapter 7. It is our goal to develop a scenario for completely non-inductive start-up and current-ramp. Flat top maintenance, using for example radio-frequency current drive or helicity injection, remain possibilities for upgrades. Before any radio frequency current drive scheme is implemented, low power tests of wave propagation and absorption will be performed.

Divertor and scrape-off layer experiments

In all fusion reactor concepts based on magnetic toroidal confinement, the removal of heat is a key issue. This was emphasized in chapter 2, where it was pointed out that USTX can provide a high flux divertor test facility. Thus any divertor and scrape-off-layer (SOL) studies on USTX are relevant to proposed tokamak reactors.

For most operation the USTX plasmas will have a double scrape off layer. The first, or innermost, part will be a region which is limited by the inner vacuum-vessel cylinder (effectively a toroidal belt limiter). The second, or outermost, part will be a poloidally diverted region, or "plume", with diverted field lines striking the armor on the vessel top and bottom covers. On START the perpendicular diffusion in the edge is so large that most of the particles and power cross the limited region and flow into the diverted field lines before striking the inner wall. This is consistent with existing TEXT data, in which it is found that the perpendicular fluxes are proportional to $B^{-1.5}$, so that low fields should produce large SOL widths.

No separate divertor chamber is planned on the initial $A = 1.43$ USTX device. A simple chamber will be added later in the machine life. We will measure equilibrium SOL parameters and their variations under different magnetic geometries in both scrape-off-layer regions (limited and diverted), as well as in the region of the divertor strike point. The objective is to provide sufficient data to allow modeling of the SOL; such modeling will be necessary to determine particle confinement times.

We will repeat the experiments and analysis pioneered on TEXT, in which the SOL characteristic lengths could be predicted once the turbulence-driven fluxes were determined. We will also use the natural field geometry to simulate divertor magnetic field line incidence on material surfaces to help design a diverted machine. This information is essential in designing a next-step low- A tokamak. Figure 9.3 shows preliminary modeling of the neutral particle sources computed using EFIT equilibria and the code EIRENE [15-17]. The large neutral source regions, shown as the lightest regions (peaking at ≈ 55 amp cm $^{-2}$) are found at the inner post and in annular regions 15 cm wide at the top and bottom at $R \approx 0.5$ m. The peak heat flux with a total (upgrade) heating power (OH + NBI + RF) of 4.5 MW is estimated at about 3 kW cm $^{-2}$, for which TiC coated graphite is suitable.

We will undertake a complete study of divertor options at low A , based on the USTX data. We will utilize mapping techniques to follow the magnetic geometry [18], as were developed for the TEXT ergodic magnetic limiter studies. Using the measured fluctuating electrostatic fields we will then use a Monte-Carlo technique to predict SOL widths and energy deposition patterns; these tools have already been developed for TEXT.

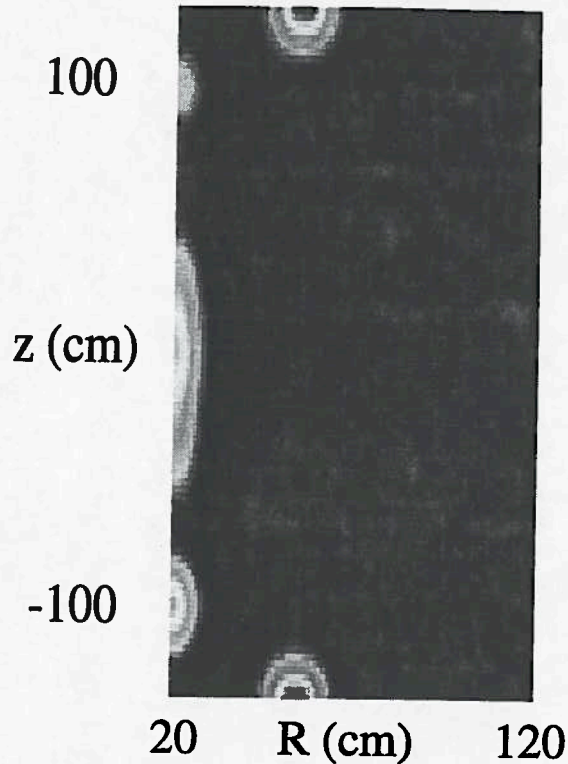


FIG. 9.3. Modeled contours of neutral particle source in USTX. The scale ranges from 0 to 55 amp cm⁻² for darkest to lightest.

We have included an option for a simple divertor chamber (with pumping), and here we present the concepts. Figure 9.4 shows a flux contour plot for an USTX plasma. This shape was obtained for the case where the ohmic solenoid current is near zero; this condition was chosen because it can be maintained in any upgrade which includes current drive. There are two SOL's, the first (innermost) is a result of contact with the inner wall, and the second (outermost) is diverted. Shown schematically is the proposed addition of a false lower floor, at $Z \approx -0.1$ m, with a toroidal slot, initially to collect particles (measure the pressure rise) and if this is successful to pump beneath with titanium getters. Only a lower floor is considered, so that any Ti flaking will be contained. All power supplies and retractable getter drives exist. An up-down asymmetric plasma can also be produced in USTX to allow SOL studies with one or two X-points.

Figure 9.5 shows the radial dependence of the parallel connection length L , calculated at the outer midplane, for the equilibrium of Figure 9.4. The innermost SOL has a width of about 1 cm, in which the connection length $L_1 \approx 15$ m. The outermost SOL has a variable connection length L_2 which is lower than L_1 .

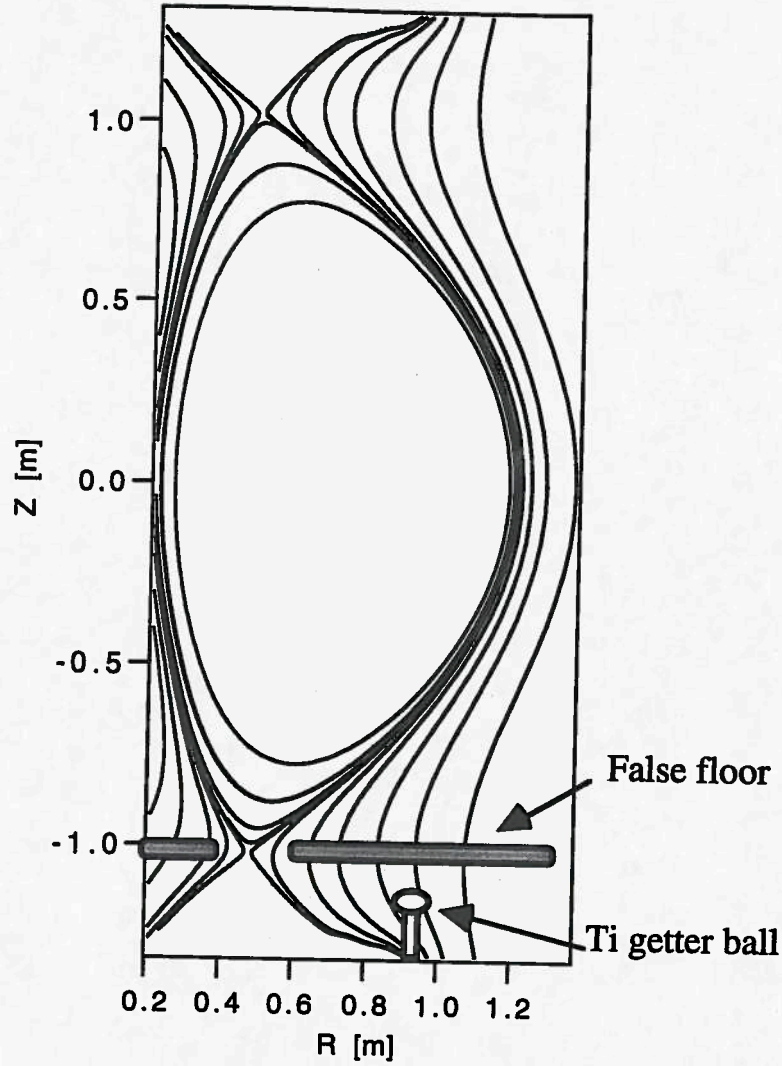


FIG. 9.4. Flux contours for a USTX plasma, with a schematic lower false floor added for a divertor chamber, together with a Ti getter ball.

Consider the simplest model of a two-stage SOL, in which the connection lengths L_1 and L_2 are different but spatially constant. Let ρ be the distance outward from the last closed flux surface at the outer equator, and let the particle diffusivity D be constant in the SOL ($\rho > 0$). Let the parallel connection length L be L_1 from $\rho = 0$ to w_1 , and L_2 from w_1 to infinity. Then the density profiles in the SOL are given by the continuity equation $D \partial^2 n / \partial \rho^2 = n v_{\parallel} / L$, assuming no sources. Suppose that the parallel velocity v_{\parallel} (typically $0.3c_s$) is spatially uniform. Then, n is of the form $A \exp(\rho / \lambda) + B \exp(-\rho / \lambda)$, with $\lambda^2 = DL / v_{\parallel}$. Specifically, for region 1, we obtain

$$n = n_0 \frac{\lambda_1 \sinh[(w_1 - \rho)/\lambda_1] + \lambda_2 \cosh[(w_1 - \rho)/\lambda_1]}{\lambda_1 \sinh(w_1/\lambda_1) + \lambda_2 \cosh(w_1/\lambda_1)}$$

with

$$\lambda_1 = \left(\frac{DL_1}{v_{\parallel}} \right)^{1/2} \text{ and } \lambda_2 = \left(\frac{DL_2}{v_{\parallel}} \right)^{1/2}.$$

Here n_0 is the density at $\rho = 0$ (the plasma edge).

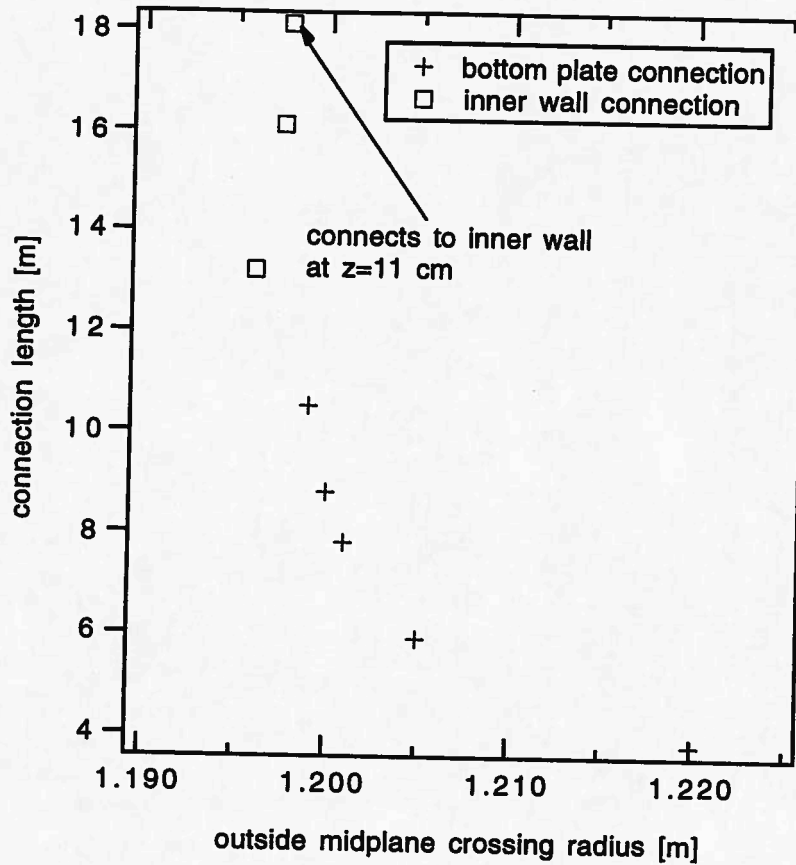


FIG. 9.5. The radial dependence of the parallel connection length

The total parallel flux to the back wall per unit toroidal angle is

$$\begin{aligned} \Gamma_{\parallel,1} &\approx v_{\parallel} \frac{\pi a}{L_1} \int_0^{w_1} n d\rho \\ &\approx n_0 v_{\parallel} \frac{\pi a}{L_1} \frac{\lambda_1 [\lambda_2 \sinh[(w_1 - \rho)/\lambda_1] + \lambda_1 \cosh[(w_1 - \rho)/\lambda_1] - \lambda_1]}{\lambda_1 \sinh(w_1/\lambda_1) + \lambda_2 \cosh(w_1/\lambda_1)}, \end{aligned}$$

where $v_{\parallel} \pi a / L_1$ is the projection of the parallel flow velocity into the toroidal plane and a is an average minor radius for the edge. For region 2, we find

$$n = n_0 \frac{\lambda_2 \exp[(w_1 - \rho)/\lambda_2]}{\lambda_1 \sinh(w_1/\lambda_1) + \lambda_2 \cosh(w_1/\lambda_1)}$$

and the total parallel flux to the top and bottom wall/divertor regions per unit toroidal angle is

$$\Gamma_{\parallel,2} \approx v_{\parallel} \frac{\pi a}{L_2} \int_{w_1}^{\infty} n d\rho \approx v_{\parallel} n_0 \frac{\pi a}{L_2} \frac{\lambda_2^2}{\lambda_1 \sinh(w_1/\lambda_1) + \lambda_2 \cosh(w_1/\lambda_1)}.$$

The ratio of the flux to the divertor regions to the total flux is

$$\Delta = \frac{\Gamma_{\parallel,2}}{\Gamma_{\parallel,1} + \Gamma_{\parallel,2}} = \frac{1}{\cosh(w_1/\lambda_1) + (L_2/L_1)^{1/2} \sinh(w_1/\lambda_1)}$$

For example, consider expected USTX values: $L_1 = 15$ m, $L_2 = 7.5$ m, and $v_{\parallel} = 0.3c_s$ with $T = 40$ eV. The ratio Δ , dependent on D and w_1 , is shown in Figure 9.6 below. For typical calculated USTX equilibria $w_1 \approx 1$ to 2 cm. Using a typical TEXT value of $D = 1$ m²/s we then obtain approximately 60% to 75% of the total outward flux flowing into the diverted SOL. If $D \propto 1/B$ as our TEXT scalings show, then D in USTX will be greater than 5 m²/s, and we will collect > 70% of the outward flux in the diverted part of the SOL, even for a width w_1 as large as 2 cm. Therefore the simple bottom divertor chamber proposed here can collect up to approximately 35% of the outflow.

We note that the low toroidal field at the outer equator makes low-A tokamaks suitable for bundle divertors (see e.g., [19]). Such configurations may allow the flux expansion necessary to investigate possible direct conversion schemes, should these machines ever be considered for D-He³ operation. Our preliminary results show that a simple four-coil system allows extraction of the edge field lines. Figure 9.7 shows a top view of a diverted field line winding around the central OH solenoid and exiting the plasma at the outside equator, and Figure 9.8 shows a poloidal cross section of the same field line. The coils are also indicated. Further expansion can be accomplished with additional coils at larger major radii.

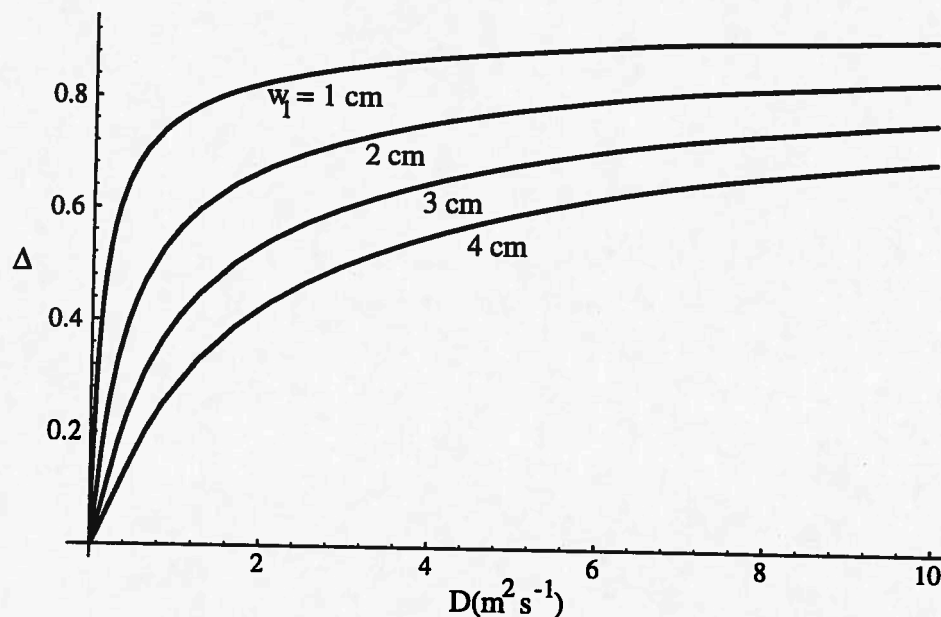


FIG. 9.6. The ratio of particle flux into the diverted part of the SOL to the total outflow across the last closed flux surface, as a function of the assumed radial diffusivity. Other parameters, applicable to USTX, are given in the text. Curves for different innermost SOL width w_1 are shown.

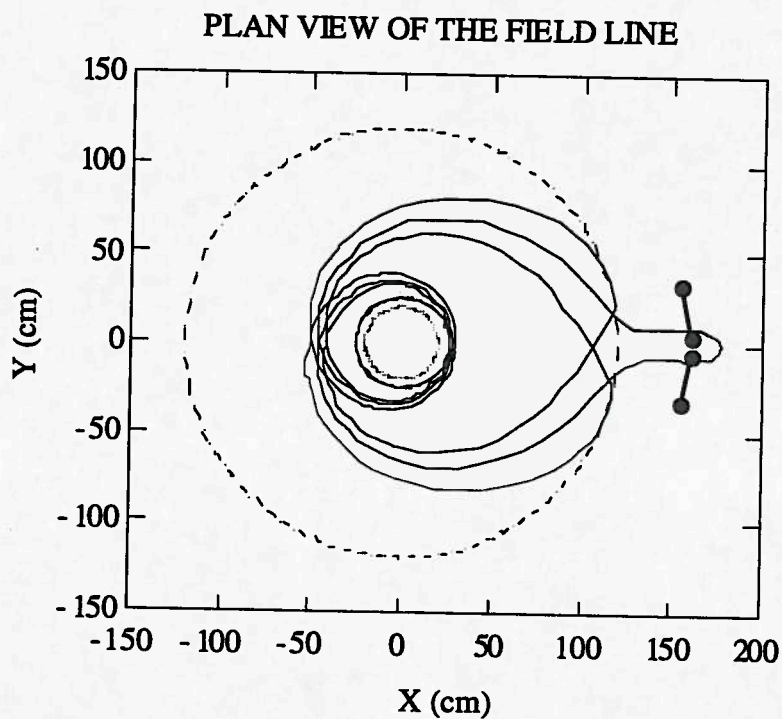


FIG. 9.7. A plan view of a diverted field line. The bundle divertor coils are marked by the joined solid circles; the broken circle is the outermost major radius of the plasma.

POLOIDAL PROJECTION OF FIELD LINE

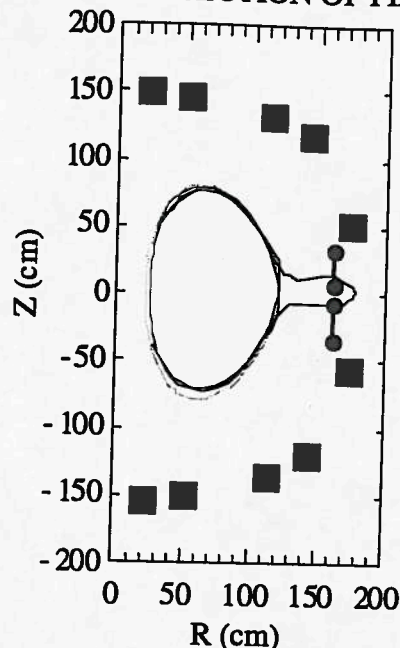


FIG. 9.8. A poloidal projection of the diverted field line shown in figure 9.7. The bundle divertor coils are marked by the joined solid circles.

Impurity-pellet diagnostic and conditioning experiments

The TEXT group has played an active role in advancing the state of the art in pellet-injection both for fueling [20, 21] and diagnostic applications [22]. Much of this work has been carried out in collaboration with ORNL for cryogenic hydrogen pellet injection and General Atomics (GA) for impurity pellet injection. As the recent successful use of lithium pellets in TFTR both for wall conditioning and fast alpha diagnostics [23, 24] indicates, there are many important applications of impurity pellets to fusion research. In view of the fact that USTX will be one of very few university-scale tokamak experiments, it is extremely important to continue to test both new or improved applications of room temperature solid pellets as well as our theoretical understanding of the ablation process in USTX. Hampton University has already submitted a proposal to upgrade the TEXT-U impurity pellet injector and develop several new diagnostic applications of impurity pellets, which could be applied to USTX. We will also continue to collaborate with GA, taking advantage of their strong theoretical and experimental expertise in this field, in testing pellet ablation theory, and developing diagnostics for fusion-grade plasmas. This work will emphasize a comparison between Li and LiH ablation. These are materials which are important for both fueling and diagnostic uses.

9.3 Remote site operations

USTX provides a facility for the use of off-site partners. Traditionally, such arrangements have required that remote collaborators be posted for extended periods of time at the host facility. However, recent experience with the collaborations between the University of Wisconsin at Madison (UWM) and Princeton Plasma Physics Laboratory (PPPL) on TFTR have demonstrated a suite of remote communications and control tools which allow experimenters at the remote site to participate productively in the planning, execution, and analysis of experiments.

Similar tools are being exploited during the collaborative USTX design process. This paradigm for remote collaboration calls for software and hardware tools that allow a remote user to perform as many as possible of the tasks that an on-site user would typically perform. This technology can not only reduce the costs of remote collaborations but also significantly extend the number of remote personnel who can be intimately involved in experiments or other operations. It is proposed that a similar, though more sophisticated, set of tools be implemented for USTX operation. These tools will fall into the following four general categories:

1. General communications: tools to allow remote users to participate (or at least audit) conferences and meetings and give them access to information on machine status and scheduling.
2. Reproduction of the control-room environment: communications with the machine operator, chief experimentalist, and diagnosticians, and access to shot timing information, data wave forms, experimental and operations logs, and PA announcements.
3. Data archive access: software tools to allow users of remote computer platforms to access USTX data directly.
4. Remote operational control of diagnostics as well as the tokamak.

General communications

The general communications requirements call for the fairly straightforward application of increasingly inexpensive video conference technology. For example, video

conferencing over the Internet (running the public domain software CU-SeeMe on Macintosh or IBM-compatible computers) has been used extensively for the UWM/TFTR experiments, for UWM/TEXT BES experiments, and for USTX design conferences. This technology provides for relatively crude but fully functional audio and reduced-frame-rate monochrome video. However, the near-term application of improved compression algorithms (viz., MPEG) is expected to allow high quality color-video conferencing at full frame rate over the Internet.

Reproduction of the control room environment

Access to machine status and scheduling information can also be provided in a straightforward way over the Internet. The tools required to allow the remote user to reproduce the control-room data flow also include video conferencing. Ideally, however, a system more sophisticated than the simple point-to-point video conferencing required for general communications would be implemented. In particular, a system which could be described as a "video-intercom" is envisioned where a remote user could, with the touch of a mouse, immediately open an audio-video channel to the machine operator, the chief experimentalist or one of several diagnostic stations. There is commercially available software which could perform in this manner (e.g., ShareVision by Creative). Alternatively, an Applescript software shell could be written to sit on top of CU-SeeMe to allow multiple CU-SeeMe sessions to be manipulated in the intercom-like manner described. In addition to audio-video links to control room personnel, machine operations logs and the chief experimentalist's log would be kept in the form of an on-line database. This will give remote users access to up-to-date operational information.

Remote users can use the standard USTX graphics package (SUPERPLOT) to plot wave forms. In addition, an automatic data display page, similar to the existing TEXT-USKID page (which automatically displays pertinent data wave forms and discharge parameters) will be made available to remote users via the Internet. Information on the shot cycle timing would be added to the automatic data display.

All public address messages will be digitized and made available to remote users via the Internet (using Maven or equivalent software).

Data archive access

During the analysis phase of experiments, remote users will use specialized software running on remote CPU's. Rather than port all such software to the local USTX computer system, it is preferable to either store USTX data in a machine-independent format or provide file access and translation tools to allow remote access to the USTX archives from these remote platforms (via the Internet). Some work in this direction has already been done for remote access to the TEXT-U archives.

Remote operational control

At the field task proposal meeting in DOE, Washington, March 1995 it was reported that a LLNL group had operated C-MOD by remote control for one day. We intend to investigate whether such a system is cost effective for USTX to enhance the ability of remote experimenters to carry out their work. In summary, the suite of rather inexpensive software and hardware tools briefly described here should allow a remote user to "attend" USTX planning and data meetings, participate in experimental runs and perform productive data analysis from a remote site.

9.4 National facility organization and collaborators.

We propose to operate USTX as a national facility, whereby personnel from other national and international institutions can perform experiments either on-site or by remote access (see above). Such a system has worked well on the TEXT device. Of particular importance is the role of the ASIPP Hefei, PRC (see Chapter 10). In addition, at the present level of planning the following national institutions have expressed an interest in participating:

Auburn University	MHD studies (magnetic islands, locked modes)
-------------------	--

GA	magnetic diagnostics high beta studies current drive scenarios current initiation and ramp-up
----	--

Hampton University	divertor scenarios impurity pellet injection
--------------------	---

ORNL	auxiliary heating hardware and operation confinement studies
RPI	diagnostics (HIBP) turbulence and transport studies improved confinement studies
U. of Washington	current drive hardware and studies (helicity injection)
UWM	diagnostics (BES) confinement, turbulence and transport studies current drive hardware and studies (FWCD, Alfvén waves)
UCLA	diagnostics (interferometry, polarimetry, scattering, reflectometry) current profile studies turbulence and transport studies

The details of how USTX as a National Facility should be operated, which experiments should be undertaken, etc., remain to be worked out. A program advisory committee will assist in these matters.

References to Chapter 9

- [1] S. G. Bespoludennov, V. I. Khripunov, and V. I. Pistunovich, in *Research Trends in Physics: New Ideas in Tokamak Confinement* (La Jolla International School of Physics, The Institute for Advanced Physics Studies), edited by V. Chan, N. Fisch, V. E. Golant, *et al.*, (American Institute of Physics, New York, 1994), p. 431.
- [2] M. Greenwald, J. L. Terry, S. M. Wolfe, *et al.*, Nucl. Fusion **28** (1988) 2199.
- [3] V. J. Simcic, T. P. Crowley, P. M. Schoch, *et al.*, Phys. Fluids B **5** (1993) 1576.
- [4] A. Y. Aydemir, personal communication (1995).
- [5] C. Watts and J. Heard, personal communication (1995).
- [6] F. A. Haas and A. J. Wootton, Nucl. Fusion **20** (1980) 1993.
- [7] W. Houlberg, in *Proceedings of the U. S. - Japan Workshop on Bootstrap Current in Tokamaks and Stellarators*, Lake Lanier Islands, GA, (1994).
- [8] W. A. Houlberg, K. C. Shaing, and S. P. Hirshman, in *Proceedings of the Sherwood Theory Conference*, Lake Tahoe, NV, (1995).
- [9] K. T. Tsang, Phys. Fluids **20** (1977) 1680.

- [10] A. J. Wootton, H. Y. Tsui, and S. Prager, *Plasma Phys. Controlled Fusion* **34** (1992) 2023.
- [11] G. Rewoldt, W. M. Tang, and S. Kaye, *Bull. Am. Phys. Soc.* **39** (1994) 1573.
- [12] A. Wootton, in *Transport, Chaos and Plasma Physics*, edited by S. Benkadda, F. Doveil, and Y. Elskens, (World Scientific, Singapore, 1994), p. 130.
- [13] P. Hurwitz, personal communication (1995).
- [14] C. B. Forest, Y. S. Hwang, M. Ono, *et al.*, *Phys. Rev. Lett.* **68** (1992) 3559.
- [15] D. Reiter, *The EIRENE Code; User's Manual*, Report 1947, KFA Julich (1984).
- [16] D. Reiter, *The EIRENE Code; User's Manual: Jan. 92*, Report 2599, KFA Julich (1992).
- [17] X. Bonnin *et al.*, *Utilisation du Code EIRENE pour simuler le transport des neutres dans TdeV*, Report RI 409f, CCFM (1993).
- [18] A. Punjabi, A. Verma, and A. Boozer, in *Proceedings of the 1992 International Conference on Plasma Physics*, edited by G. Thomas, Innsbruck, (European Physical Society, 1992), Vol. 16c part II, p. 863.
- [19] S. J. Fielding and A. J. Wootton, *Physica Scripta* **23** (1981) 97.
- [20] R. D. Durst, *An Experimental Investigation of the Dynamics of Pellet Ablation on the Texas Experimental Tokamak*, Ph.D. Dissertation, The University of Texas, Austin, TX (1988).
- [21] S. C. McCool, P. H. Edmonds, and G. G. Castle, *Fusion Tech.* **21** (1992) 114.
- [22] G. G. Castle, *The Dynamics of Plasma-Pellet Interaction in TEXT*, Ph.D. Dissertation, The University of Texas, Austin, TX (1994).
- [23] R. K. Fisher, *Bull. Am. Phys. Soc.* **39** (1994) 1544.
- [24] R. K. Fisher *et al.*, submitted to *Phys. Rev. Lett.* (1995).

CHAPTER 10

PROJECT MANAGEMENT, COSTS AND SCHEDULES

Introduction

This section summarizes the project management structure and preliminary costs and schedules for the design and construction of USTX up to and including the first plasma discharges and initial experiments.

An essential element of this project is the collaboration with the Academia Sinica Institute of Plasma Physics (ASIPP), Hefei, P.R.C. As a part of this collaboration, the ASIPP have offered to supply all manpower costs required for the design, fabrication and engineering of the device, incurred in the P.R.C., in exchange for participation in the USTX experimental program. A similar but somewhat smaller collaboration with the ASIPP has given the senior project managers confidence that the program can be successfully completed.

Costs described in this proposal include all materials and components, and assignments of U.S. personnel in the P.R.C. and for P.R.C. personnel assigned to the U.S. A preliminary cost estimate has been made and is attached. Because all engineering and fabrication will be carried out at the ASIPP at no cost to the project, the collaboration has an enormous cost leverage with a total direct project cost to the U.S. estimated at \$3.5M. FRC personnel assigned to the project (FRC base cost) will cost an estimated \$3.7M, distributed over the three year duration of the project, making a total project cost of \$7.2M for the MDF. If the entire project were carried out in the U.S. the cost is estimated at over \$16.5M, an effective saving of at least \$9.3M due to the substantial contribution by the ASIPP. Following completion of the USTX project, the annual U.S. contribution to the operating costs are estimated at \$2.76M. After project approval and initial funding, representatives from the project team will travel to the P.R.C. in order to finalize the protocols and to define the project and costs.

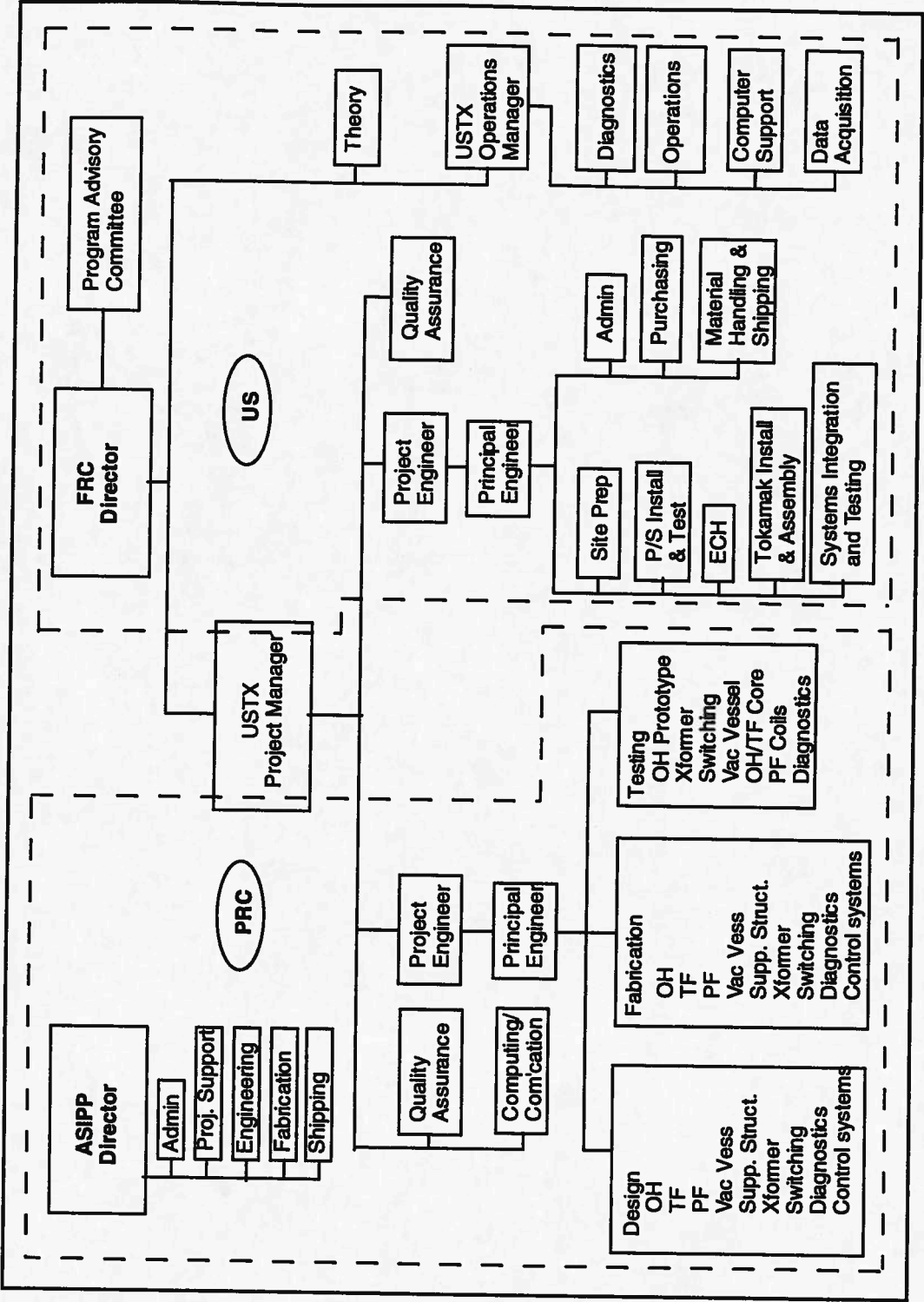
The project will be both designed and fabricated at the ASIPP; this will allow considerable overlap in the design and fabrication phases, resulting in an accelerated schedule with first plasma planned for Spring 1999. Project closeout will be in the summer of 1999 which will be followed by the USTX program physics phase.

Project Management

As a consequence of the international collaboration, a sophisticated multi-national project team will be established in order to support the design, engineering, fabrication and shipping activities. An initial project management structure is shown in Table. 10.1. The Program Directors are responsible for communication with DoE and with the Academia Sinica for establishing the basic mission and schedules, and for direction and supervision of the project. The Project Manager (PM) will be from the FRC and is responsible for the successful completion of the project. During the project development phase the PM will be located in the U.S. Following the start of the project the PM will transfer to the ASIPP and he or his representative will remain at the ASIPP until completion of the fabrication and assembly/test activities. The PM will then return to the U.S. with the majority of the ASIPP branch of the project team for the completion of the project. The project engineers are responsible for the detailed management of the project, personnel assignments, procurements, and schedule and cost monitoring. Two project engineers will be appointed, one in the U.S. and one in the P.R.C. The Principal Engineer is responsible for coordinating the design, fabrication, installation and testing phases of the project. The primary Principal Engineer will be from ASIPP and will be responsible for the design, testing and fabrication of the tokamak, power supply components, control systems, etc. After delivery to the U.S. he will be assigned to work at the FRC in coordination with the U.S. principal engineer and site engineering team.

Crucial to the success of the project is a strict Quality Control and Quality Assurance program. Two Quality Assurance (QA) managers will be appointed. One will be from the U.S. and one will be from the ASIPP. A project requirement will be that QA representatives will monitor all working shifts during the fabrication, assembly and testing phases of the project. The QA program will report directly to the PM. The U.S. QA officer will also be responsible for procurement QA and tracking, and material control and shipment. Communication is a key requirement and Computer/Communications Managers will be appointed; this will be an additional responsibility for one of the U.S. personnel assigned to the P.R.C.

Table 10.1. USTX Project Management Chart.



The project will be managed using a conventional Work Breakdown Structure (WBS). This is shown to the second level in Table 10.2. The depth of this breakdown will be extended to a level such that each activity can be scheduled in detail and resource requirements and costs estimated. It should be noted that the WBS includes activities not actually included in Phase I of the project. They are included to ensure the necessary interfaces are in place.

Table 10.2. Summary Level Work Breakdown Structure.

1. Project support	5. Auxiliary heating and current drive (Phase II)
1.1 Overall Project management	5.1 Neutral beam injection
1.2 Engineering supervision and management	5.2 Current drive
1.3 Drafting & records	5.3 Non-inductive startup
1.4 Safety and quality control	6. Site and facilities preparation
1.5 Procurement, contracts, and shipping	6.1 TEXT removal & cleanup
1.6 Physics	6.2 Water cooling
2. Tokamak mechanical	6.3 Vacuum pumping
2.1 Core assembly integration	6.4 Power distribution
2.2 Solenoid	7. Diagnostics
2.3 TF coils	7.1. Specification/interfaces
2.4 PF coils	7.2. Diagnostic packages
2.5 Vacuum vessel	8. Operations
2.6 Support structure	8.1 Data acquisition
3. Tokamak electrical	8.2 Position control system
3.1 Primary power integration	8.3 Gas handling system
3.2 TF power supplies	8.4 Machine protection
3.3 OH power supplies	8.5 ECH start up
3.4 PF power supplies	8.6 Machine Operation
3.5 NBI power supplies (Phase II)	
3.6 Tokamak control system	
4. Research and development	
4.1 Physics	
4.2 Engineering	

The ASIPP is a division of a large laboratory complex operated by the Academia Sinica, similar to the multi-purpose national laboratories in the U.S. The research and support facilities at the ASIPP include over 100 scientists, 250 engineers and technicians, and 100 technical workers. In addition there are about 100 graduate students of which about a third are working toward their Ph. D. There are seven experimental halls (22,000 m²) and a complete workshop facility (7,500 m²), including a temperature-controlled clean-room facility for precision machine tools. The Institute has designed and fabricated

numerous research devices, including the HT-6B tokamak (now in Azad University, Iran), and the HT-6M mid-size tokamak with 1 MW of ICRH and 100 kW of ECRH. The Kurchatov superconducting tokamak T-7 was transferred to ASIPP and has recently become operational. The laboratory has also been responsible for the design and construction of more than 100 magnets for the transmission line of the Beijing Electron-Positron Collider.

A recent collaboration between the FRC and the ASIPP included the joint design of the vacuum vessel and divertor coil set for the TEXT-Upgrade program. The vacuum vessel itself was fabricated in the P.R.C., and met all performance specifications following final finishing in the U.S. The ASIPP has also contributed to the design activities described in the proposal. These studies include the finite-element stress analysis of the vacuum vessel and of the OH solenoid conductor, design studies of the power supply configurations and high power switching systems, and the effects of eddy current losses in the TF core.

Costs

The unique feature of this project is the cost sharing with the ASIPP which enables a versatile experimental facility to be built for about one third the cost of the facility if built without this collaboration.

Table 10.3 shows a preliminary breakdown of expected costs and resource requirements. Costs are estimated in 1996 dollars. All U.S. labor charges are identified as project costs, including both FRC members and also ASIPP project personnel while on assignment to the U.S. These project costs are separately summed in the cost summary table at the bottom and are not included in the main table. The table columns separate different material and labor costs. The first column is the cost of materials purchased in the U.S. and includes material shipped to the P.R.C. for machining and fabrication. The second column lists the estimated cost to the FRC of materials expected to be available in the P.R.C. and mostly includes tooling and fixtures; also included is material required for the coil winding line. The third column lists the number of full-time-equivalent (FTE) USTX project and technical personnel working on site in the U.S. The fourth column lists the U.S. personnel FTE's while on assignment to the P.R.C. The fifth column lists the number of ASIPP scientists, engineers and technicians (FTE's) on assignment to the U.S. during the assembly and test/startup phase of the project. The sixth column estimates the total number of FTEs for the scientists, engineers, technicians, machinists and other

workers supplied to the project by the ASIPP and working in the P.R.C. The seventh (next from last) column indicates the total cost associated with all personnel paid by the FRC. The eighth (last) column estimates the *effective cost in the U.S.* of the manpower resources supplied by the ASIPP. Although the USTX project will not be charged these costs, equivalent direct costs will be paid by the ASIPP, both for the personnel at ASIPP and also to the families of the ASIPP personnel while on assignment to the U.S.

The manpower requirements to be supplied by the P.R.C. have been extracted from prior estimates and are costed at \$50K per year to indicate the approximate cost benefit associated with this support. All materials are charged to the project; the agreement with the ASIPP is that the FRC will pay all costs other than for ASIPP personnel. It is assumed that all fabrication will be carried out at ASIPP. Material costs are based on estimated component weights and present costs of the appropriate materials. P.R.C. personnel assigned to the U.S. will be paid \$20k/yr. (the project will also be charged fringe benefits and university overhead). Each individual will pay all travel and housing costs out of this allowance and the ASIPP will continue to pay his salary in the P.R.C. All U.S. personnel on assignment to the P.R.C. will be charged a reduced overhead rate. A 30% contingency has been added to the project costs to allow for the significant uncertainties associated with the present scope of the project and material and resource costs.

In summary, the total project cost over the approximately three years to first plasma is \$7.2M. This cost includes all U.S. personnel, including those assigned to the USTX project from the FRC base program. The research and design activities required to advance the project to the present level have not been separately funded. All work has been voluntary by members of the FRC team. A conservative estimate of the value of the ASIPP contribution is \$9.3M. The total effective project cost is thus estimated at over \$16.5M, which is appropriate for an experimental construction project of this size, including existing site benefits.

The cost of USTX has been further minimized by extensive use of the existing site credits, including motor generators, power supplies, diagnostics, laboratory space and the electro-mechanical site facilities previously utilized for the TEXT program.

Table 10.3. Summary of USTX Project Cost Estimate.

USTX Cost Breakdown									
		Mat	Mat	Labor	Labor	Labor	Labor	Cost	Cost
		in US	in PRC	US@US	US@PRC	PRC@US	PRC@PRC	to US	to PRC
		k\$	k\$	FTE	FTE	FTE	FTE	k\$	"k\$"
Project Costs									
				18.25	4.5	2	6	3818	300
Tokamak Core		299	70	0	0	0	100	0	5000
Prototype Core Assy		19	50	0	0	0	4	0	175
								0	0
P/S		350	0	0	0	6	7	229	350
OH Switchgear		125	0	0	0	2	11	76	550
Tok Control System		240	0	0	0	4	4	153	200
Diagnostic		340	0	0	0	5	15	191	750
ECH Breakdown		25	0	0	0	1	3	38	150
Shipp and pack			50					0	0
Installation		50	0	0	0	10	0	381	0
Subtotal		1447	170	0	0	28	144	1068	7175
Contingency		434	51	0	0	8	43	320	2153
								0	0
Total		1881	221	0	0	36	187	1388	9328

Cost summary		
Material (to US)		2102
PRC @ US		1388
Subtotal		3491
FRC base costs		3742
Total US cost		7232
PRC @ PRC (Est.)		9328
Total Value		16560

Table 10.4 presents the projected USTX budget for the three-year USTX design, fabrication, installation, and initial experiment phases. A July 1, 1996 start is assumed. As a result, only three months of costs are incurred in FY 1996 and only nine months in FY 1999. Project management consists of a project manager, project engineer, principal engineer, quality assurance and procurement, computer/communications support, and accounting and administration. Physics support consists of theoretical support, program oversight, and a diagnostics manager. Engineering support consists of engineers and technicians. These will be carried over to operations at the end of the project.

Table 10.4. USTX Project Budget for FY 1996 to 1999
(U.S. MDF costs only, 1996 \$).

Items	FY 1996	FY 1997	FY 1998	FY 1999
Project management	\$144,000	\$576,000	\$618,900	\$382,600
Physics support	\$64,000	\$254,000	\$337,900	\$264,900
Engineering support	\$0	\$0	\$431,800	\$667,300
Total Base Level	\$208,000	\$830,000	\$1,388,600	\$1,314,800
USTX Construction	\$104,500	\$549,200	\$1,462,000	\$1,378,000
Total	\$312,500	\$1,379,200	\$2,850,600	\$2,692,800

Machine Operations

Although not an element of this project, tokamak operations will be included in this chapter to present a complete picture of the program. The project is expected to be closed out after initial tokamak operation is begun. A nominal end of project is proposed as a 200 kA, 100 ms discharge, with power supplies and associated systems run to full design performance.

The USTX operations group will include a significant number of ASIPP engineers and scientists. Table 10.5 presents an initial estimate of this operations and science team. The total annual budget is estimated at \$2.7M.

**Table 10.5. Estimated USTX annual operations budget
(U.S. costs only, 1996 \$).**

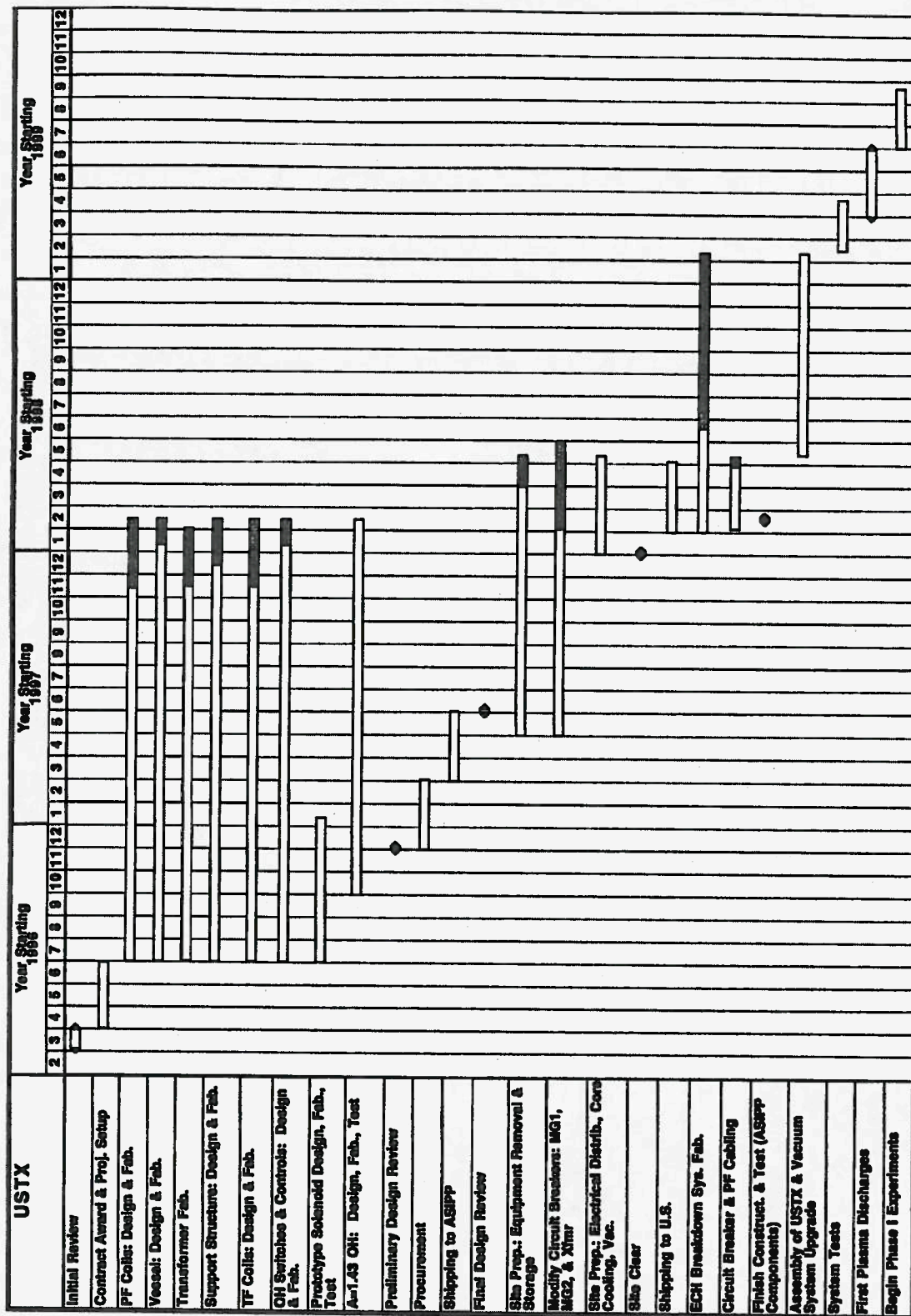
	Category	Source	FTE	cost \$k
Operations				
	Engineers	FRC	2	192
		ASIPP	3	115
	Technicians	FRC	3	230
		ASIPP	3	115
Physics				
	Physicists	FRC	8	1,074
		ASIPP	6	230
	Students	FRC	3	86
		ASIPP	2	38
Admin		FRC	2.5	144
Tokamak				500
Total				2,725

Schedule

The present schedule assumes project approval and start by July 1, 1996 and commits the project to initial plasma operation by April, 1999. A preliminary schedule is shown in Table. 10.6. A more detailed schedule will be developed in conjunction with the ASIPP after project approval. Initial activity will concentrate on the design and construction of the prototype solenoid. Following successful demonstration of the solenoid performance, advanced procurement and material shipping to the P.R.C. will be initiated. As the design and fabrication are to be carried out at the same facility with the same engineering team, considerable advance procurement and fabrication is expected. This should expedite project completion. Before final shipment of the completed facility to the U.S., a trial assembly will be completed at the ASIPP. R&D activities, including the solenoid, power supply components and switching systems construction, will be fully tested before delivery. Shipping is expected to take about three months. This time is included in the schedule. Prior experience with a similar design and fabrication activity, the TEXT-Upgrade vacuum vessel, indicates that this project is not liable for import and custom charges.

Parallel with the design and construction at the ASIPP, the FRC site will be cleared of the TEXT experiment and prepared for installation of the USTX facility. This preparation will include modification to power supplies where needed, advance installation of transformer and switching systems and preliminary installation of machine and plasma control and data acquisition systems.

Table 10.6. Schedule assuming a July, 1996 start. Slack is shaded



Appendix A.

Background and Experience of the Principal Investigator

ALAN J. WOOTTON
Fusion Research Center
The University of Texas at Austin
Austin, TX 78712 U.S.A.
(512)471-5780

EDUCATION

1969 - 1972 **PH.D.** (London University) awarded 1973
1966 - 1969 **B.Sc.** (London University) awarded 1969

EMPLOYMENT

1993 - Present **Director**, Fusion Research Center,
The University of Texas at Austin.
Grants administered at present:
DE FG03 94ER54241
DE FG03 93ER54223
DE FG05 88ER53266
DE FG03 95ER54296
S-03679 - PRINCETON/Edmonds
TAERF (Texas Atomic Energy Research
Foundation)

1990 - Present **Professor**, Physics Department, University of Texas at Austin

1984 - 1993 **Director of TEXT and Associate Director of Experimental Research**,
Fusion Research Center, The University of Texas at Austin

1981 - 1984 **Experimental Physicist**, Oak Ridge National Laboratory (Fusion
Energy Division)

1977 - 1981 **Senior Scientific Officer**, Culham Laboratory

1974 - 1977 **Research Assistant**, Culham Laboratory

1972-1974 **Research Assistant**, Royal Holloway College

COMMITTEES, ETC.

GA (DIII-D) Advisory Committee Member (1994 - present)
Transport Task Force Steering Committee Member (1991 - present)
International Scientific Committee Member for the Transport, Chaos & Plasma
Physics series of workshops (1994 - present)
PPPL (TFTR) Advisory Panel (1991 - present)
Group Leader, DOE Transport Task Force (1994 - 95)
MIT (C-MOD) Experimental Division Advisory Panel (1991 - 94)
Member of DOE Committee "Edge Theory", (1992 - 93)
Scientific Advisory Committee for the International School of Plasma
Physics, "Piero Caldirola", Societa Italiana di Fisica (1992)

ALAN J. WOOTTON'S PUBLICATIONS LIST 1993-95

1. Bravenec, R. V. and A. J. Wootton, "Effects of Limited Spatial Resolution on Fluctuation Measurements," *Rev. Sci Instrum.* 66:802 (1995).
2. Castle, G. G. and A. J. Wootton, "Stochasticity from External Magnetic Field Measurements," *IEEE Trans. on Plasma Sci.* 22:369-375 (1994).
3. Catto, P., J. R. Myra and A. J. Wootton, "Analytic model for the runaway distribution function in the presence of spatial diffusion," *Phys. Plasmas* 1:684-690 (1994).
4. Catto, P. J., J. R. Myra, R. D. Bengtson and A. J. Wootton, "Modeling and simultaneous sawtooth measurements of the thermal and energetic electron diffusivities from the Texas Experimental Tokamak," *Phys. Fluids B* 5:125-137 (1993).
5. Cima, G., R. V. Bravenec, A. J. Wootton, T. D. Rempel, R. F. Gandy, C. Watts and M. Kwon, "Core temperature fluctuations and related heat transport in the Texas Experimental Tokamak-Upgrade," *Phys. Plasmas* 2:720-726 (1995).
6. Foster, M. S., J. L. Craig, A. J. Wootton, P. E. Phillips, J. Uglum, E. R. Solano, D. L. Brower, Y. Jiang, S. C. McCool, J. Lierzer and G. G. Castle, "Vacuum Compatible, Variable Cross Section Magnetic Coil Diagnostic Used in Digital Feedback Control of Plasma Position in TEXT-Upgrade," *Rev. of Sci. Instrum.* 66:461-463 (1995).
7. Foster, M. S., S. C. McCool and A. J. Wootton, "The AC Response of a Tokamak Plasma to Driven Helically Resonant Radial Magnetic Perturbations," *Nucl. Fusion* 35:329-333 (1995).
8. Hidalgo, C., B. Branas, T. Uckan, J. Harris, R. Isler, C. R. Ritz and A. J. Wootton, "On the role of neutral particles on edge turbulence and electric fields in ATF," *Phys. Plasmas* 1:3-5 (1994).
9. Hidalgo, C., J. Harris, T. Uckan, G. Garriss, T. Bell, M. Meier, C. R. Ritz and A. J. Wootton, "Experimental Evidence of Edge Turbulence Driven by Multiple Mechanisms in ATF," *Nuc. Fusion* 33:146-149 (1993).
10. Hidalgo, C., E. Sanchez, T. Estranda, B. Branas, C. R. Ritz, U. Uckan, J. Harris and A. J. Wootton, "Experimental Evidence of 3-Wave Coupling on Plasma Turbulence," *Phys. Rev. Lett.* 71(3):127-130 (1993).
11. Li, G., R. D. Bengtson, H. Lin, M. A. Meier, H. Y. W. Tsui and A. J. Wootton, "The Plasma Potential Asymmetry and Steady State Radial Convection in the TEXT-U Tokamak," *Nucl. Fusion* 34:659-664 (1994).
12. Rempel, T. D., R. F. Gandy and A. J. Wootton, "Density fluctuation effects on electron cyclotron emission correlation measurements in optically gray plasmas," *Rev. Sci. Instrum.* 65(6):2044-2048 (1994).
13. Richards, B., T. Uckan, A. J. Wootton, B. A. Carreras, R. D. Bengtson, P. Hurwitz, G. X. Li, H. Lin, W. L. Rowan, H. Y. W. Tsui, A. K. Sen and J. Uglum, "Modification of tokamak edge turbulence using feedback," *Phys. Plasmas* 1:1606-1611 (1994).

ALAN J. WOOTTON'S CONFERENCE PROCEEDINGS LIST 1993-95

1. Bengtson, R. D., R. Bell, L. Blush, J. A. Boedo, R. W. Conn, D. B. Crockett, E. D. Luna, R. Doerner, I. Garcia-Cortes, K. W. Gentle, C. Hidalgo, S. Kaye, H. Kugel, R. Lehmer, G. X. Li, H. Lin, M. Meier, A. G. Meigs, R. Moyer, M. Okabayashi, B. Richards, W. L. Rowan, J. Sanchez, L. Schmitz, A. Sen, S. Sesnic, Y. Sun, H. Y. W. Tsui, G. R. Tynan, T. Uckan, J. Uglum, D. L. Winslow, A. J. Wootton and V. Zhuravlev, "Control of edge turbulence in PBX-M and TEXT-U," Fifteenth International Conference on Plasma Physics and Controlled Nuclear Fusion Research, Seville, Spain, (1994).
2. Crockett, D.B., P.E. Phillips, W.A. Craven, and A.J. Wootton, "Edge parameters from an energy analyzer and particle transport on TEXT", Proceedings of the Tenth Topical Conference on High Temperature Plasma Diagnostics, Rochester, New York (1994).
3. Estrada, T., J. Sanchez, H. J. Hartfuss, M. Hirsch, T. Geist and A. J. Wootton, "Density Fluctuation Measurements by Broadband Heterodyne Reflectometry on the W7-AS Stellarator", 20th EPS Conference on Controlled Fusion and Plasma Physics, Lisboa, Portugal (1993).
4. Hidalgo, C., B. Branas, T. Uckan, J.H. Harris, R. Isler, Ch.P. Ritz, and A. Wootton, "On the Role of Neutral Particles on Edge Turbulence and Electric Fields in the ATF Torsatron", 20th EPS Conference on Controlled Fusion and Plasma Physics, Lisboa, Portugal (1993).
5. Ouroua, A., A. J. Wootton and The TEXT Group, "A comparison between the measured thermal diffusivity χ_i in TEXT and the Predicted χ_i ," U.S. Japan Workshop on Ion Temperature Gradient-Driven Turbulent Transport, Austin, Texas (1993).
6. Richards, B., T. Uckan, D. L. Winslow, R. D. Bengtson, J. L. Craig, P. E. Phillips, A. K. Sen, J. Uglum and A. J. Wootton, "Edge Diagnostics and Feedback Control Using an Active Probe on TEXT," 21st EPS Conference on Controlled Fusion and Plasma Physics, Montpellier, France (1994).
7. Rowan, W. L., R. D. Bengtson, X. Bonnin, P.H. Edmonds, P.D. Hurwitz, E.R. Solano, H.Y.W. Tsui, J.R. Uglum and A.J. Wootton, "Particle Balance in Diverted Plasmas in TEXT-U" 11th PSI Conference, Mito-shi, Ibaraki-ken, Japan (1994).
8. Solano, E. R., P. H. Edmonds, D. L. Brower, G. Cima, A. Ouroua, P. E. Phillips, D. R. Roberts, W. L. Rowan, A. J. Wootton, R. D. Bengtson, X. Bonnin, R. V. Bravenec, G. Castle, R. Chatterjee, J. Y. Chen, K. Chiang, W. A. Craven, J. Craig, D. B. C. kett, T. P. Crowley, A. Y. Dnestrovskij, A. Darbar, L. Duaiappaah, M. S. Foster, M. R. Freeman, A. Fujisawa, H. Gasquet, K. W. Gentle, G. A. Hallock, J. W. Heard, P. D. Hurwitz, J. W. Jagger, Y. Jiang, Y. Karzhavin, J. R. Lierzer, S. C. McCool, M. A. Meier, D. M. Patterson, D. A. Pavlovsky, S. D. Reedy, B. Richards, P. M. Schoch, K. A. Schroder, S. Shin, D. C. Sing, T. D. Steckler, R. Steimle, D. Storek, D. R. Terry, H. Y. W. Tsui, J. Uglum, Y. Wen, D. L. Winslow, B. Z. Zhang and L. Zeng, "Diverted discharges in TEXT-UPGRADE with Electron Cyclotron Heating," 1994 International Conference on Plasma Physics, Fox Do Iguacu, Brazil (1994).

**ALAN J. WOOTTON'S
PRESENTATIONS LIST
1993-95**

1. Wootton, A.J., "USTX and Latest Results from TEXT", Oak Ridge National Laboratory (1993).
2. Wootton, A. J., "Edge Turbulence," Summer School on Plasma Fluctuation and Transport, University of Wisconsin, Madison, Wisconsin, (1993).
3. Wootton, A. J., "The Effects of Magnetic Perturbations on Plasma Transport or is Magnetic Turbulence important in Tokamaks?," Transport, Chaos and Plasma Physics, Marseille, France, (1993).
4. Wootton, A. J., "Fluctuations and Local Transport-Latest Developments," Local Transport Studies in a Fusion Plasmas, Varenna, Italy, (1993).
5. Wootton, A. J., "Magnetic Fluctuation in Tokamaks," IPP, Garching, Germany, (1993).
6. Wootton, A. J., "Magnetic Islands," Summer School on Plasma Fluctuation and Transport, University of Wisconsin at Madison, Wisconsin, (1993).
7. Wootton, A. J., "Magnetic Perturbations," Summer School on Plasma Fluctuation and Transport, University of Wisconsin at Madison, Wisconsin, (1993).
8. Wootton, A. J., "Sampling Fluctuation Diagnostics," Summer School on Plasma Fluctuation and Transport, University of Wisconsin at Madison, Wisconsin, (1993).
9. Wootton, A. J., "Fluctuation and Transport in Plasmas," The University of California at San Diego, San Diego, California, (1994).
10. Wootton, A. J., "Fusion," Rotary Club/Austin, Austin, Texas, (1994).
11. Wootton, A. J., "Fusion," LAMP, Austin, Texas, (1994).
12. Wootton, A. J., "Magnetic Fluctuations in Tokamaks," R.F. Current Drive and Profile Control for Advanced Tokamaks, Boulder, Colorado, (1994).
13. Wootton, A. J., "Plasma Physics and Fusion," Hampton University, Hampton, Virginia, (1995).
14. Wootton, A. J., "USTX and Latest Results from TEXT", General Atomics (1995).
15. Wootton, A.J., "Plasma Physics and Fusion", University of Texas at Arlington (1995)
16. Wootton, A.J. "Fusion", UT Radio Club (1995).

Appendix B.

Description of Facilities and Resources of the Applicant

Existing Facility Characteristics

1. Building or parts of a larger building, directly associated with the given facility.
 - a. Building name
 - Robert Lee Moore (RLM), Floor 1
 - Robert Lee Moore, Floor 2
 - Robert Lee Moore, Floor 3
 - Robert Lee Moore, Floor 11
 - Robert Lee Moore, Floor 12
 - Engineering Science (ENS) Basement
 - Engineering Science Floor 1
 - b. Size (sq. ft.):

RLM1:	20,000
RLM2:	2,500
RLM3:	2,000
RLM11	9,000
RLM12	7,000
ENS B	9,000
ENS 1	1,000
 - c. When built:
 - RLM: 1972
 - ENS: 1961
 - d. Type of heating: Heated Water
 - e. Peak heating rate: N/A
 - f. Type of air conditioning: Chilled Water
 - g. Air conditioning cap.: N/A
 - h. Significant features: Concrete shielding walls in ENS
2. Switchyard, or part thereof, associated with the given facility
 - a. Number of transformers: None
 - b. Capacity of transformers: -0-
3. Motor Generator Energy Storage System
 - a. Number of units: 3
 - b. Power rating of each generator: 1-100 MVA (Pulsed) 2-18 MVA (continuous)
 - c. Power rating of each motor: 15,000 HP for 100 MVA unit, 400 HP for ea 18 MVA unit
 - d. Deliverable energy of each unit: 90 MJ for 100 MVA unit, 15 MJ for each 18 MVA unit

9. Coil systems	TF	OH	VF	EML	(DIV,BIAS)
a. Number of Coils	16	8	6	8	(3,2)
b. Type of coil:	Cu	Cu	Cu	Cu	Cu
c. Cooling medium:	H ₂ O	Air	Air	Air	H ₂ O
d. Outer dims:	1.5 m	1.7 m	1.7 m	1.5 m	0.65 m
e. Weight of each coil:	2500 kG	(TF only)			700 kG
f. Rated Current:	157 kA	10 kA	10 kA	10 kA	25 kA, 10 kA
g. Rated voltage/coil:	31.25 V	37.5 V	40 V	54 V	167 V
h. Peak field at conductor:	4.3 T	0.2 T	0.2 T	0.1 T	2 T
i. Peak stored energy in each system:	25 MJ	7 MJ	2 MJ	2 MJ	80 kJ

10. Vacuum Vessel

- a. Key dimensions: R=1 m, a=0.3 m
- b. Volume: 2.5 m³
- c. Weight: 2.5 T
- d. Cooling medium: Air
- e. Cooling flow: -0-
- f. Cooling system peak pressure: one atmosphere

11. Vessel Vacuum Pumping:

- a. Base pressure: 1.0×10^{-8} Torr
- b. Number of ultrahigh vac. pumps: 2
- c. type of pumps: turbo-molecular
- d. Speed of each pump: 1500 liter/sec
- e. Cryogenic supply system: -0- Univ. of Texas
- f. Cryopanel area: N/A
- g. Surface pumping panels: N/A
- h. Surface pumping panel area: N/A

17. Tritium Clean-up Systems

a. Floor space occupied None

18. Water Cooling Systems

a. Number of systems: 3

b. flow of each system a) 100 gpm
b) 200 gpm
c) 200 gpm

c. Peak pressure of each system 150 psi

d. Heat rejection of total system 200 MW

e. Method of rejecting heat to
environment water tower and chilled water heat exchange

Appendix C.

Statement of Current and Pending Support

Appendix D.

Assurances and Certifications that Apply

Appendix E.

Annotated FRC Publication List

An annotated bibliography of some of the major physics results from TEXT and TEXT-U

February 1996

1. We completed a survey of interior and edge turbulence characteristics, and compared our results with those from other devices, including stellarators and torsatrons [A. Wootton, H. Tsui and S. Prager, *Plasma Physics and Controlled Fusion*, **34**, 2023 (1992) and references therein; A. Wootton, B. A. Carreras, H. Matsumoto, K. McGuire, et al., *Physics of Fluids* **B2**, 2879 (1990) and references therein].
2. We demonstrated experimentally for the first time the suppression of turbulence by radial electric fields [Ch. Ritz, H. Lin, T. L. Rhodes and A. J. Wootton, *Phys. Rev. Letts.* **65**, 2543 (1990)], and developed a model for the naturally occurring shear layer [H. Tsui, *Phys. Fluids*. **B4**, 4057 (1993)].
3. We identified experimentally a long-time micro turbulence precursor to disruptions [D. Brower, C.X. Yu, R. V. Bravenec, H. Lin, et al., *Phys. Rev. Letts.* **67**, 200 (1991)].
4. We demonstrated experimentally for the first time the applicability of quasilinear test particle theory to fast electron transport [R. Bengtson, M. R. Freeman and A. J. Wootton, *Rev. Sci. Instrum.* **63** 4595 (1992); P. Catto, J. R. Myra, P. W. Wang, A. J. Wootton, et al., *Phys. Fluids* **B8** 2038 (1991)]. We verified analytic quasilinear test particle theory using Monte-Carlo calculations in various collisionality regimes; this was the first verification of "Rechester-Rosenbluth diffusivity". We demonstrated for the first time the applicability of quasi linear theory ("Rechester-Rosenbluth diffusivity") to thermal plasma transport in an externally applied stochastic magnetic field [A. Wootton, S. McCool and S. B. Zhang, *Nucl. Tech.* **19** 473 (1991)].
5. We showed that quasilinear drift wave theory was capable of explaining interior transport at low collisionalities only if the FIR inferred values of wave vector were assumed applicable. This led us to be the first to propose that there are two distinct turbulence features, one long wavelength and one short wavelength (drift wave-like) [R. Bravenec, K. W. Gentle, B. Richards, D. W. Ross, et al., *Phys. Fluids* **B4** 2127 (1992); D. Ross, R. V. Bravenec, Ch. P. Ritz, M. L. Sloan, et al., *Phys. Fluids* **B3** 2251(1991)].
6. We were the first to experimentally verify the effects of charge exchange on rotation in tokamaks [W. Rowan, A. G. Meigs, R. L. Hickok, P.M. Schoch, et al., *Phys. Fluids* **B4** 917 (1992); P. M. Valanju, M. D. Calvin, R. D. Hazeltine, and E. R. Solano, *Phys. Fluids* **B** 4(8), (1992)].

7. We made the first measurements of the magnetic field associated with a tearing mode inside a hot plasma [V. Simcic, K. A. Connor, T. P. Crowley, R. L. Hickok, et al., *Rev. Sci. Instrum.* **61** 3061 (1990), and V. J. Simcic, T. P. Crowley, P. M. Schoch, et al., *Phys. Fluids B* **5** (1993) 1576].
8. We showed theoretically that transport of ripple trapped ions was reduced by ExB rotation [K. Gentle and R. D. Hazeltine, *Phys. Fluids B* **3**, 3198 (1991)].
9. We showed by analysis of gas puff experiments that quasilinear theory of electrostatic drift waves cannot explain particle transport [K. Gentle, B. Richards, M. E. Austin, R. V. Bravenec, et al., *Phys. Rev. Letts.* **68** 2444 (1992), and B. Richards, M. E. Austin, R. Bravenec et al., *Nucl. Fusion* **32** 567 (1992)].
10. We showed by comparing experiment and theory that atomic physics drives might explain some of the measured edge turbulence properties [J. LeBoeuf, D. K. Lee, B. A. Carreras, N. Dominguez, et al., *Phys. Fluids B* **3** 2291 (1991)], but also called into question some of the theoretical work [D. W. Ross, *Phys. Plasmas* **1**, 2630 (1994)].
11. We quantified the effects of resonant magnetic fields on edge parameters, especially particle and impurity transport [S. McCool, A. J. Wootton, M. Kotschenreuther, A. Y. Aydemir, et al., *Nucl Fusion* **30** 167 (1990); S. McCool, J. Y. Chen, A. J. Wootton, M. E. Austin, et al. *J. Nucl. Mater.* **176** 716 (1990); S. Lippmann, M. Finkenthal, H. W. Moos, S. C. McCool, et al., *Nucl. Fusion* **31** 2131 (1991)].
12. We showed experimentally that edge transport and turbulence are enhanced by sawteeth [T. Rhodes, C. P. Ritz, and H. Lin, *Phys. Rev. Letts.* **65** 583 (1990)].
13. We found, using sawtooth propagation experiments, evidence for coupling of particle and heat fluxes [D. Brower, S. K. Kim, K. W. Wenzel, M. E. Austin, et al., *Phys. Rev. Letts.* **65** 337 (1990)].
14. We identified a quasi coherent mode in the plasma edge [H. Tsui, P.M. Schoch, and A. J. Wootton, *Phys. Fluids B* **5** 1274 (1993)] and determined its coupling to the background turbulence [H. Tsui, K. Rypdal, Ch. P. Ritz and A. J. Wootton, *Phys. Rev. Letts.* **70** 2565 (1993)].
15. We verified experimentally a model predicting the radial electric field in stochastic regimes [Y. Yang, B. Z. Zhang, A. J. Wootton, P. M. Schoch, et al., *Phys. Fluids B* **12** 3448 (1991)].
16. We demonstrated for the first time the "Rutherford regime" growth rate of tearing modes [Y. Zhang, R. Denton, S. M. Mahajan, C. Jiaju, et al., *Phys. Rev. Letts* **65** 2877 (1990)], and at the same time identified the effects of tearing modes on micro turbulence [C. Yu, D. L. Brower, S. J. Zhao, W. A. Peebles, et al., *Phys. Fluids B* **4** 381(1992); C. Yu, D. L. Brower, S. J. Zhao, R. V. Bravenec, et al., *Nucl. Fus.* **32** 1545 (1992)].

17. We showed that external sensor coils could be used for plasma position control [A. Wootton and L. Wang, IEEE transactions **18** 6 (1990); E. Solano, G. H. Neilson and L. L. Lao, Nucl. Fus. **30** 1107 (1990); E. Solano, PP and CNFR **32** 759 (1990)].
18. We discovered possible non local turbulence effects by correlating ECH and turbulence measurements [D. Sing, V. Krivenski, M. Austin, J. A. Boedo, et al., Nucl. Fus. **17** 57 (1991)].
19. We provided the first definitive identification of electrostatic turbulence as a major drive mechanism for particle transport in the edge ["Global particle confinement in the Texas experimental tokamak, "W. L. Rowan, C. C. Klepper, Ch. P. Ritz, Roger D. Bengtson, K. W. Gentle, P. E. Phillips, T. L. Rhodes, B. Richards, and A. J. Wootton, Nuclear Fusion **27**], but noted that steady state convection could also be important at low densities [G. X. Li, R. D. Bengtson, H. Lin et al., Nucl. Fusion **34** 659 (1994)]. We then extended this work to show that edge energy fluxes could be explained by the measured turbulence [Ch. Ritz, R. Bravenec, R. Bengtson, et al., Physical Review Letts., **62** (1989) 1844].
20. We provided the first evidence that biasing in tokamaks improves confinement because of reduced fluctuation levels [P. E. Phillips, A. J. Wootton, W. L. Rowan, Ch. P. Ritz, and others, J. Nucl. Mater. **145-147** 807 (1987)].
21. We have confirmed the presence of non local transport effects, using a cold pulse [K. Gentle, K.W. Gentle, et al., Phys. Rev. Lett. **74**, 3620 (1995)].
22. We have developed a technique using ECRH to drive fast electrons, and then infer magnetic fluctuation levels and their importance in determining thermal plasma transport [D. R. Roberts, R. F. Steimle, and G. Giruzzi, Rev. Sci. Instruments, **66** (1995) 427].
23. We have used fast and runaway electrons to infer that magnetic fluctuations do not explain thermal transport either in TEXT, or most other machines [A. Wootton, in Transport, Chaos and Plasma Physics, Ed S. Benkadda, F. Doveil and Y. Elsken, World Scientific, (1994), P. J. Catto et al, Phys Fluids **B5** 125 (1993), P. J. Catto et al, Phys. Plasma **1** 684 (1994)].
24. We have provided detailed scaling studies of edge turbulence properties [T. L. Rhodes and others, Nucl. Fusion **33** 1147 (1993)].
25. We have demonstrated for the first time that a turbulent medium can be partially controlled using feedback [B. Richards et al., Phys. Plasma **1** 1606 (1994)].
26. We have made the first measurements of temperature fluctuations in a hot tokamak, and concluded that low k electrostatic modes do not explain thermal transport [G. Cima, R. V. Bravenec, A. J. Wootton et al., Phys. Plasmas **2** 720 (1995), T. Rempel and others, Rev. Sci. Instrum. **65** 2044 (1994)].

27. We have identified and quantified the effects of finite sample volumes on various fluctuation diagnostic measurements [R. Bravenec and A. J. Wootton, *Rev. Sci. Instrum.* **66** 802 (1994)].

28 We have developed various new diagnostics and analysis techniques [a novel safety factor diagnostic, a time domain Langmuir probe, an ultra fast bolometer, a correlation radiometer, a neutral spectral analysis technique, a wave launching technique for edge plasma probing, an infra-red interface for automatic heat flux measurements, and an optical technique for measuring density fluctuations in otherwise inaccessible regions].

29. We have provided TEXT as a facility for spectroscopic studies [Sugar and others, *J. Op. Soc. Am.* 799 (1993), and *J. Op. Soc. Am.* **B10** 1321 (1993)].

30. We have demonstrated that the plasma edge turbulence is well approximated by Gaussian statistics [A. V. Filippas, R. D. Bengtson , G. X. Li et al, *Phys. Plasmas* **2** 839 (1995)], i.e. that if any coherent structures exist they must themselves have a Gaussian distribution.

31. First observation of an ion feature in the turbulence spectrum were made, having many of the features expected for ion temperature gradient modes [D. L. Brower, W. A. Peebles, S. K. Kim, N. C. Luhmann, Jr., W. M. Tang, and P. E. Phillips, *Phys. Rev. Lett.* **59**, 48 (1987)].

32. We have demonstrated that the plasma 'healing' of magnetic islands is approximately consistent with a published model [M. S. Foster, S. C. McCool and A. J. Wootton. *Nucl. Fusion* **35** 329 (1995)].

Appendix F.

Letter from ASIPP

Dr. Alan J Wootton, Director
Fusion Research Center
University of Texas at Austin
RLM 12.202
Austin TX 78712
USA

February 21, 1996

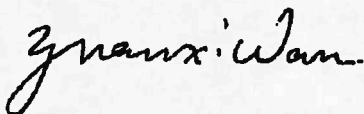
Dear Dr. Alan J Wootton

This letter of agreement between ASIPP and FRC describes a collaboration for the University Spherical Tokamak Experiment(USTX), to be located and operated at the University of Texas, Austin, TX, USA.

In summary, the agreement is that the entire engineering design and the fabrication of the USTX, if which is not exceeded the ability of ASIPP, will be carried out at ASIPP and that the ASIPP will supply all internal engineering and labor costs at no charge to the project. The FRC will be responsible for all material and other actual costs beyond the ASIPP personnel costs and will supply project related support to the ASIPP during the design and fabrication phases of the project. The FRC will also support a team of engineers and technicians in the U.S. during the installation and startup phase of the project. When the tokamak becomes operational the FRC will support a research team of ASIPP for the significant joint research program in U.S. Initial estimates are that this team will consist of about 12 visiting scientists and engineers.

Following approval and funding of the project by the US DoE, I hope the senior project members of the U.S. will visit ASIPP in order to develop the detail of the project and to finalize the relative responsibilities of the two partners.

Your sincerely,



Dr. Yuan xi Wan
Director
Institute of Plasma Physics, Academia Sinica(ASIPP)
P.O.Box 1126
Hefei Anhui 230031
P.R. China

Appendix G.

Magnetic Island Research on USTX Auburn University

MAGNETIC ISLAND RESEARCH on USTX

***A Joint Research Proposal between Auburn University
and the University of Texas***

May, 1995

Auburn University fusion scientists (Rex Gandy and Jim Hanson) propose a collaborative research program on the University Spherical Tokamak Experiment (USTX) centered around the study of magnetic islands. The basic physics goal of this research will be to understand the role of magnetic islands in toroidal fusion plasmas. Specifically, we propose to study MHD instability on USTX with particular focus on tearing mode and locked mode physics. Techniques of active control of magnetic islands will be studied. Control of magnetic islands have important applications with regard to optimized operation of a fusion reactor. For example, energy-selective transport is possible by tailoring the size and distribution of magnetic islands in the device.

The hardware component of this work will be the Auburn Resonant Coil Set (ARCS). The coil set would be highly flexible to allow interaction with a wide-range of magnetic surfaces (i.e. varying safety factor). Control of specific magnetic island(s) size and phase would be possible. Sets of magnetic island detection coils will be utilized. This will consist of the standard B-dot loops and a novel set of saddle-type coils to detect locked modes. The personnel involvement would consist of partial summer support for the principal investigators, an on-site post doctoral research scientist and student assistance. The following physics studies will be addressed:

(1) **Inherent Error Field Minimization.** Due the relatively small magnitude of the magnetic field on USTX, inherent static magnetic field errors(e.g. iron in building materials) could lead to large error fields. Of course, the standard errors from winding feeds, coil misalignments, etc. can also lead to magnetic islands. A set of resonant coils can be used to

